

Cronin effect and high- p_{\perp} suppression in the nuclear gluon distribution at small x

E. Iancu, K. Itakura, and D. N. Triantafyllopoulos

*Service de Physique Théorique, CEA/DSM/SPhT, 91191 Gif-sur-Yvette Cedex,
France*

Abstract

We present a systematic, and fully analytic, study of the ratio \mathcal{R}_{pA} between the gluon distribution in a nucleus and that in a proton scaled up by the atomic number A . We consider initial conditions of the McLerran–Venugopalan type, and quantum evolution in the Color Glass Condensate, with both fixed and running coupling. We perform an analytic study of the Cronin effect in the initial conditions and point out an interesting difference between saturating effects and twist effects in the nuclear gluon distribution. We show that the distribution of the gluons which make up the condensate in the initial conditions is localized at low momenta, but this particularity does not survive after the quantum evolution. We demonstrate that the rapid suppression of the ratio \mathcal{R}_{pA} in the early stages of the evolution is due to the DGLAP-like evolution of the proton, whose gluon distribution grows much faster than that in the nucleus because of the large separation between the respective saturation momenta. The flattening of the Cronin peak, on the other hand, is due to the evolution of the nucleus. We emphasize interesting differences between the fixed coupling and the running coupling scenarios, which are particularly important in the late stages of the evolution.

Contents

1	Introduction	3
2	Cronin effect in the initial conditions	11
2.1	Generalities	11
2.2	The McLerran–Venugopalan model: Fixed & running coupling	14
2.3	Cronin effect in the McLerran–Venugopalan model	20
2.4	A sum rule in the MV model and its consequences	25
3	Non-linear gluon evolution in the Color Glass Condensate	32
3.1	Non-linear evolution at low k_{\perp} : Saturation and universality	33
3.2	Linear evolution at high k_{\perp} : Fixed coupling	34
3.3	Linear evolution at high k_{\perp} : Running coupling	41
4	High- k_{\perp} suppression from quantum evolution: The general argument	44
4.1	Nucleus in the linear regime ($k_{\perp} \gg Q_s(A, y)$)	44
4.2	Nucleus in the saturation regime ($k_{\perp} \leq Q_s(A, y)$)	46
4.3	A general argument on the k_{\perp} -dependence	47
5	The evolution of the Cronin peak with increasing y	48
5.1	The suppression of the peak: Fixed coupling	49
5.2	The suppression of the peak: Running coupling	53
5.3	The flattening of the Cronin peak	55
6	High- k_{\perp} suppression in the nuclear gluon distribution at small x	61
6.1	Fixed coupling	62
6.2	Running coupling	68
A	Appendix	72
	References	77

1 Introduction

Motivated especially by the recent experimental results for gold–gold (Au–Au) [1, 2] and deuteron–gold (d–Au) collisions at RHIC [3–6], there is currently a large interest in the physics of collective phenomena in the wavefunction of an energetic nucleus, which could explain, for instance, why the gluon distribution of a large nucleus (with atomic number $A \gg 1$) is not simply the incoherent sum of the gluon distributions of the A constituent nucleons. For sufficiently high energies (and, marginally at least, also for the energies at RHIC), one expects these collective phenomena to be associated with non–linear effects favored by the high gluon density, which rises rapidly with the energy, and also with A [7–12]. Thus, these effects are expected to be more pronounced in a (large) nucleus as compared to a proton, and this difference should be particularly important at not so high energies, where the proton is still in a linear regime.

This difference could explain some of the remarkable regularities observed in the results for d–Au collisions at RHIC, like the Cronin enhancement in particle production at central rapidity ($y = 0$) [3], and the ‘high- k_\perp suppression’ in the particle yield at ‘forward rapidities’ ($y = 2 - 3$ in the deuteron fragmentation region) [4–6]. Specifically, the Cronin peak [13] can be understood as the result of Glauber–like multiple scattering off the gluon distribution produced by uncorrelated “valence quarks” [14] (as described, e.g., by the McLerran–Venugopalan model [10], see also [15]), whereas the high- k_\perp suppression can result from non–linear effects in the quantum evolution with increasing energy [16]. (See also [17] for alternative interpretations of these results.) On the other hand it is most likely that a similar suppression seen in Au–Au collisions at central rapidity [2] is due to jet quenching through final state interactions [18].

More precisely, the experimental results are used to construct the ratio $R_{dA}(k_\perp, y)$ between the number of particles produced in a d–Au collision (with a given transverse momentum k_\perp and at a given rapidity y) and the corresponding number for a proton–proton collision scaled up by the number of collisions. The deviation of this ratio from one — like a Cronin peak ($R_{pA} > 1$ at intermediate momenta), or the high- k_\perp suppression ($R_{pA} < 1$ at generic, hard, momenta) — can be attributed to the difference between the gluon spectrum (or “unintegrated gluon distribution”) in the nucleus, and that in the proton scaled up by A . In turn, this difference is measured by the ratio :

$$\mathcal{R}_{pA}(k_\perp, y) \equiv \frac{\varphi_A(k_\perp, y)}{A^{1/3} \varphi_p(k_\perp, y)}, \quad (1.1)$$

between the gluon occupation factors (see Eq. (2.1)) in the nucleus and the proton¹.

¹ Our conventions are such that the more standard “unintegrated gluon distribution” is equal

Previous studies in the literature show that it is indeed possible to compute the cross-section for particle production in terms of the gluon distributions in the target and the projectile [7, 14, 19–21], and, moreover, any qualitative trend seen in the ratio (1.1) of the gluon distributions gets transmitted to the corresponding ratio for the cross-sections [16, 22, 23], which is the quantity relevant for RHIC.

Motivated by this observation, and also by the conceptual importance of the ratio (1.1) as a direct measure of collective effects in the nuclear wavefunction, we shall devote this work to a systematic analysis of this quantity within the effective theory for the Color Glass Condensate (CGC) [24], which is the appropriate framework to describe non-linear effects in the gluon distribution within QCD.

Although inspired by the RHIC phenomenology, our analysis does not aim to the description of the data (for such attempts, see e.g. [25, 26]), but is rather oriented towards the fundamental understanding of phenomena like the emergence of the Cronin peak in the ratio \mathcal{R}_{pA} and the suppression of this peak with increasing energy. Our main objective is to present a calculation for such phenomena from **first principles**, and which is **fully analytic**. These requirements entail strong constraints on the kinematical range which is accessible to our analysis, and also a significant loss of accuracy, due on one hand to the limited accuracy of the perturbative framework that we shall use, and on the other hand to the additional approximations that we shall perform within this framework, to allow for analytic calculations. In particular, our focus on the gluon distribution, rather than on the cross-section for multiparticle production, is also motivated by the requirement of (analytic) calculability, together with our concern to avoid theoretical uncertainties as much as possible.

As already mentioned, our theoretical framework will be the CGC effective theory [10, 24, 27–34] (see also [11, 12] for recent review papers), which is a lowest-order (in α_s) formalism in QCD, although obtained after elaborate resummations: These resummations include only those diagrams of perturbative QCD in which the powers of α_s are enhanced by either large logarithms of the energy (i.e., by powers of $y \sim \ln s$), or by high density effects (e.g., by the gluon occupation factor, which at saturation is of order $1/\alpha_s$). Still, it should be emphasized that this formalism becomes more and more accurate with increasing energy because, first, it does include the leading effects at large y , and, second, the saturation momentum $Q_s(y)$ which sets the scale for the running of the coupling increases very fast with y [7, 35–40], and therefore α_s decreases (like $1/\sqrt{y}$) at high energy. Thus, the results that we shall obtain here represent the actual prediction of QCD for sufficiently large y .

to $S_A \varphi_A(k_\perp, y)$, with S_A the area of the nuclear disk (assumed to be homogeneous in transverse space, for simplicity). Thus, a factor of $A^{2/3}$ has cancelled in the ratio S_A/S_p between the nucleus and proton transverse areas.

The argument above also shows that the inclusion of running coupling effects in the formalism is crucial in order for the asymptotic freedom of QCD to become operative at high energies. The running of the coupling is a higher order effect in α_s , so its inclusion in a leading order formalism is by definition ambiguous. But physical intuition about the typical scales involved in the interactions, and also the experience with the next-to-leading-order BFKL equation [41–43] — which in the context of the CGC formalism is the linear equation describing the approach towards saturation — will permit us to effectively use a one-loop running coupling, with the scale for the running set either by the gluon transverse momentum k_\perp , or by the saturation momentum.

As mentioned above, another source of accuracy loss are the further approximations needed to make the CGC formalism tractable via analytic calculations. Whereas the initial conditions that we shall use at low energy — namely, the McLerran–Venugopalan model [10] — are sufficiently simple to allow for exact (analytic) calculations, the subsequent evolution with increasing y is described by complicated non-linear equations which couple n -point correlations with any number of points n [24, 30, 32]. This is similar to the infinite hierarchy of Schwinger–Dyson equations, and within the CGC theory it can be summarized into a closed functional equation for the generating functional of the correlations [24, 29, 32], also known as the JIMWLK equation. Exact numerical solutions to this functional equation have recently become available [44], but these are still difficult to handle, so most numerical analyses (including that of the \mathcal{R}_{pA} -ratio in Ref. [23]) have instead focused on a simpler non-linear equation, the Kovchegov equation [31], which is a kind of mean field approximation to the general JIMWLK equation [45, 46], and is expected to work reasonably well for a large nucleus at not so high energies.

But whereas the numerical calculations are undoubtedly important, they cannot fully supplant the analytic studies as far as our physical insight and fundamental understanding are concerned. The numerical results in Ref. [23] have revealed very interesting features — notably, an extremely fast suppression of the ratio $\mathcal{R}_{pA}(k_\perp, y)$ at generic momenta with increasing y , and also the complete disappearance of the Cronin peak after only a short evolution —, but these observations have also raised new questions, since the precise mechanism behind such a rapid evolution has remained unclear. In particular, it was not clear whether the two effects alluded to above (the high- k_\perp suppression and the flattening of the Cronin peak) were caused by the same mechanism, or not. Also, the specific roles played by the proton and by the nucleus during evolution have not been elucidated.

All the previous analytic investigations in the literature appeared before the numerical results in Ref. [23], and cannot fully explain the latter: For instance, while the arguments in Refs. [16, 22] do explain the suppression at relatively large y and for high k_\perp , they cannot explain why this suppression is so rapid in the early stages of the evolution, or why the Cronin peak flattens out so fast. Indeed, the approximations used in these previous studies do not apply for transverse momenta in, or near, the nuclear saturation region, nor for

very small values of y . Besides, running coupling effects have never been considered in the previous studies, either analytic or numerical. As we shall see, these effects lead to important changes, especially for the evolution at late stages. More generally, what seems to be still missing is a coherent, qualitative and quantitative, picture explaining what are the specific features of the MV model which imply the emergence of a well pronounced peak at low energies, and also what are the generic features of the quantum evolution which lead to the rapid flattening of this peak, and to a general suppression in the ratio \mathcal{R}_{pA} at all non-asymptotic momenta.

Our subsequent analysis is intended to fill this gap, through a systematic study of the ratio \mathcal{R}_{pA} in the MV model and of its evolution with y , for both fixed and running coupling. Being systematic, our analysis has necessarily some overlap with previous studies in the literature, especially with Ref. [22], with which we share some results and conclusions, notably about the high- k_\perp suppression. In our opinion, what distinguishes the present analysis from such previous investigations, in addition to its aim to completeness and the treatment of the running coupling case, is the constant effort towards elucidating the fundamental reasons for the observed behavior, and also the use of a coherent scheme of approximations, which will be carefully justified, and whose limitations will be discussed.

In what follows, we shall briefly describe the picture which emerges from these calculations when increasing y from $y = 0$, and at the same time describe the structure of the paper :

i) Initial conditions at $y = 0$: Cronin peak in the MV model (cf. Sect. 2)

Although a Cronin peak in the ratio $\mathcal{R}_{pA}(k_\perp)$ has been clearly seen in numerical simulations of the MV model [21, 23, 47, 48], its analytic study has been hindered so far by the non-linear aspects of the problem, which must be treated exactly. In Sect. 2, we shall present a complete, analytic, study of the nuclear gluon distribution in this model, which will enable us to compute the magnitude and the location of the peak, and clarify the conditions for its existence: The emergence of a well pronounced peak in the MV model reflects the peculiar redistribution of gluons in transverse phase space, under the influence of the non-linear effects responsible for saturation. In turn, this issue has two aspects:

The very existence of a peak can be anticipated on the basis of very general arguments (like the sum rule introduced in Ref. [22]; see also Sect. 2.4 below), which reflect two basic properties of the MV model: (a) the fact that the gluon distribution saturates, at a value of order $1/\alpha_s$, for low momenta $k_\perp \leq Q_s(A)$, and (b) the fact that, at large momenta $k_\perp \gg Q_s(A)$, the nuclear gluon distribution is simply the incoherent sum of the individual distributions of the A nucleons (so that $\mathcal{R}_{pA}(k_\perp) \rightarrow 1$ when $k_\perp \rightarrow \infty$). As we shall see in Sect. 2.3, these two properties alone imply the existence of a peak at intermediate momenta. The height of the peak is of order $\rho_A \equiv \ln Q_s^2(A)/\Lambda_{\text{QCD}}^2 \sim \ln A^{1/3}$, and thus is parametrically enhanced at large A .

Moreover, the fact that the peak is so pronounced, and located in the vicinity of the saturation momentum $Q_s(A)$, is the consequence of the fact that the distribution of the saturated gluons which make up the condensate is **compact**, in the sense that it **vanishes exponentially at momenta above the saturation scale**. This feature has not been recognized in previous studies of the MV model. Of course, on top of this compact distribution there is also a **power-law tail**, which represents the sum of the ‘twist’ contributions usually mentioned when discussing the high- k_\perp behavior of the distribution. But as we shall see, for momenta $k_\perp \lesssim Q_s(A)$, the sum of the twist terms is **parametrically suppressed at large A** as compared to the compact distribution which represents the condensate. Because of that, the overall distribution has a rapid, exponential, fall-off at momenta just above $Q_s(A)$, leading to the pronounced peak seen in numerical simulations [21, 23, 47, 48].

ii) $y > 0$: Non-linear quantum evolution in the CGC (cf. Sect. 3)

In Sect. 3 we shall present our approximations to the solution to the non-linear equations which describe the evolution of the gluon distribution with y .

In the saturation region at low momenta, physics is fully non-linear, but for $k_\perp \ll Q_s(A, y)$ the solution can be constructed in a mean field approximation [33, 34]. The result is an universal, and slowly varying, function of $z \equiv k_\perp^2/Q_s^2(A, y) : \varphi_A \propto (1/\alpha_s) \ln 1/z$ for $z \ll 1$ [33–35]. The solution in the transition region around $Q_s(A, y)$ is not known in general (see however Sect. 5.3), but we do know that, along the **saturation line** $k_\perp = Q_s(A, y)$, φ_A is constant and of order $1/\alpha_s$.

At high momenta $k_\perp \gg Q_s(A, y)$, physics is linear, and the general evolution equations reduce to BFKL equation [41], for which we shall construct solutions in the saddle point approximation (with saturation boundary conditions) [36, 37, 39]. We shall distinguish between two physical regimes, which are controlled by different saddle points: (I) a “DLA” (“double-log accuracy”) regime at very large momenta $k_\perp \gg Q_g(A, y)$, in which the evolution is dominated by the transverse phase-space $\rho(k_\perp) \equiv \ln(k_\perp^2/Q_s^2)$, and (II) a “BFKL regime” within the range $Q_s(A, y) \ll k_\perp \ll Q_g(A, y)$, where physics is linear but influenced by saturation, and the BFKL solution preserves the **geometric scaling** [49] property characteristic of saturation: it depends upon the kinematical variables k_\perp and y only through the ratio $z = k_\perp^2/Q_s^2(A, y)$ [36, 37]. Here, $Q_g(A, y)$ is the “geometric scaling momentum”, which grows faster than the saturation momentum with y , and marks the upper bound of the geometric scaling region [36] (see also [37–39, 46]).

The approximations described in this section will be sufficient to study the suppression in the ratio $\mathcal{R}_{pA}(k_\perp, y)$ with increasing y at generic momenta. On the other hand, they are not sufficient to describe the flattening of the Cronin peak (see below).

iii) $y > 0$: The general argument for high- k_\perp suppression (cf. Sect. 4)

In Sect. 4 we shall identify and characterize the general features of the quantum evolution which are responsible for the suppression of the ratio \mathcal{R}_{pA} at generic momenta.

The rapid suppression of the ratio $\mathcal{R}_{pA}(k_\perp, y)$ with increasing y is shown to be the consequence of the strong dissymmetry between the quantum evolution of the nucleus and that of the proton, which in turn reflects the large separation of scales between the respective saturation momenta. Physically, it is so because, for the same values of y and k_\perp , the transverse phase-space available for the evolution, namely $\rho(A, k_\perp) \equiv \ln(k_\perp^2/Q_s^2(A))$, is larger for the proton than for the nucleus (since $Q_s(A) \gg Q_s(p)$). In more technical terms, the proton evolves faster because of general properties of the kernel of the BFKL equation, like the convexity of its eigenvalue $\chi(\gamma)$, which accelerate the evolution with increasing ρ .

Moreover, the **suppression rate** $d \ln \mathcal{R}_{pA}/dy$ is largest at small y and for not so large transverse momenta (as compared to the nuclear saturation momentum), since in this regime the difference between the evolution of the proton and that of the nucleus is most pronounced. This explains the rapid suppression observed in the early stages of the evolution in the numerical results in Ref. [23]: This is the consequence of the DGLAP [57] evolution of the proton (as described here by DLA), while the nucleus evolves comparatively little (except at extremely large momenta).

The general properties of the evolution equations can also be used to show that, for fixed and sufficiently large y (such that $\alpha_s y \gtrsim 1$), the ratio $\mathcal{R}_{pA}(k_\perp, y)$ is a **monotonously increasing function** of k_\perp . Thus, for such a large y , there is no Cronin peak anymore.

iv) The flattening of the Cronin peak (cf. Sect. 5)

The evolution of the proton **alone** produces a rather uniform suppression in the \mathcal{R}_{pA} -ratio at all momenta. Thus, by itself, this cannot wash out any structure present in the initial conditions, like the Cronin peak. Therefore, the disappearance of the peak is necessarily related to the evolution of the nucleus.

In order to study this phenomenon, we shall use the Kovchegov equation to compute the evolution of the nuclear gluon distribution in the first step Δy in rapidity, with $\alpha_s \Delta y \ll 1$. This calculation allows us to follow the evolution of the peak at least up to the rapidity y_0 , with $\alpha_s y_0 \sim (\ln^2 \rho_A)/\rho_A \ll 1$, where the height of the peak becomes of order one. As the calculation shows, the effect of the evolution is to **generate power law tails which progressively replace the original exponential tail of the gluon distribution at saturation**. Because of that, the peak flattens out, and moves up to larger momenta.

The flattening is related to the difference in the nuclear evolution at momenta below and, respectively, above the saturation momentum $Q_s(A, y)$. For $k_\perp < Q_s(A, y)$, the gluons in the nucleus are saturated, and evolve only slowly. For $k_\perp > Q_s(A, y)$, the nucleus is

in the linear, BFKL, regime, and the corresponding gluon distribution increases much faster (although not so fast as the proton distribution at the same k_\perp). Because of this dissymmetry, the Cronin peak gets tilted up, and flattens out very fast. Although we cannot control analytically this evolution until the complete disappearance of the peak, we shall check that the peak has flattened out when $\alpha_s y \sim 1$.

v) High- k_\perp suppression: the detailed picture (cf. Sect. 6)

In Sect. 6, we shall give the detailed picture of the phenomenon of “high- k_\perp suppression” in the kinematic plane $y - \ln k_\perp^2$. (Previously, a similar analysis will be presented in Sect. 5, but only for the evolution along the nuclear saturation line $k_\perp = Q_s(A, y)$.) In fact, the suppression will be seen to occur at all momenta, and not only at those which are “high” in the sense of the present analysis (and which are such that $k_\perp \gg Q_s(A, y)$). Still, the suppression is stronger for momenta above the proton saturation scale $Q_s(p, y)$ — since this is where the proton evolves faster — but below the nuclear geometric scale $Q_g(A, y)$, since for even larger momenta ($k_\perp \gg Q_g(A, y)$), both the proton and the nucleus are in the DLA regime, and their respective evolutions almost compensate in the ratio $\mathcal{R}_{pA}(k_\perp, y)$. Thus, not surprisingly, this ratio will be found to asymptotically approach one from the below when increasing k_\perp at fixed y . But since $Q_g(A, y)$ increases rapidly with y , it is clear that, for $\alpha_s y \gtrsim 1$, a strong suppression will be visible at all non-asymptotic momenta.

The explicit analysis in Sect. 6 will confirm the general trend of the evolution anticipated in Sect. 4: For generic momenta k_\perp (such that the nucleus is either at saturation, or in the BFKL regime), the suppression in the ratio $\mathcal{R}_{pA}(k_\perp, y)$ is very fast in the early stages of the evolution, when the proton is in the DLA regime, but with increasing y it slows down, and eventually \mathcal{R}_{pA} stabilizes at a very small value, proportional to an inverse power of $A^{1/3}$. Besides, for fixed y (with $\alpha_s y \gtrsim 1$), the ratio is monotonously increasing with k_\perp , from a very small value $\sim 1/A^{1/3}$ for $k_\perp \sim \Lambda_{\text{QCD}}$ to $\mathcal{R}_{pA} \simeq 1$ when $k_\perp \rightarrow \infty$.

In order to describe this evolution, it is convenient to follow a line which is parallel to the saturation line in the kinematic plane $y - \ln k_\perp^2$ (see Fig. 1). That is, we simultaneously increase y and k_\perp in such a way to keep the ratio $z \equiv k_\perp^2/Q_s^2(A, y)$ fixed. If $z = \mathcal{O}(1)$, then when increasing y from zero, the proton starts in the DLA regime, because $Q_g(p, y) \ll Q_s(A, y)$ at sufficiently small y . But with increasing y , $Q_g(p, y)$ grows faster than $Q_s(A, y)$, so at some ‘critical’ value y_c the proton changes from DLA to BFKL regime. The value of y_c is more or less the same (when expressed in units of $1/\alpha_s$) for both fixed and running coupling: $\alpha_s y_c \sim \rho_A$, where in the case of a running coupling, $\alpha_s \equiv \alpha_s(Q_s^2(A, y)) \sim 1/\sqrt{y}$. However, the evolution for larger $y > y_c$ turns out to be quite different for fixed and running coupling, as we explain now:

(a) With fixed coupling, the suppression slows down significantly at $y > y_c$, because the BFKL evolution of the proton and that of the nucleus almost cancel in the ratio (1.1). This is so because, in this regime, the dominant energy dependence in both distributions (φ_A

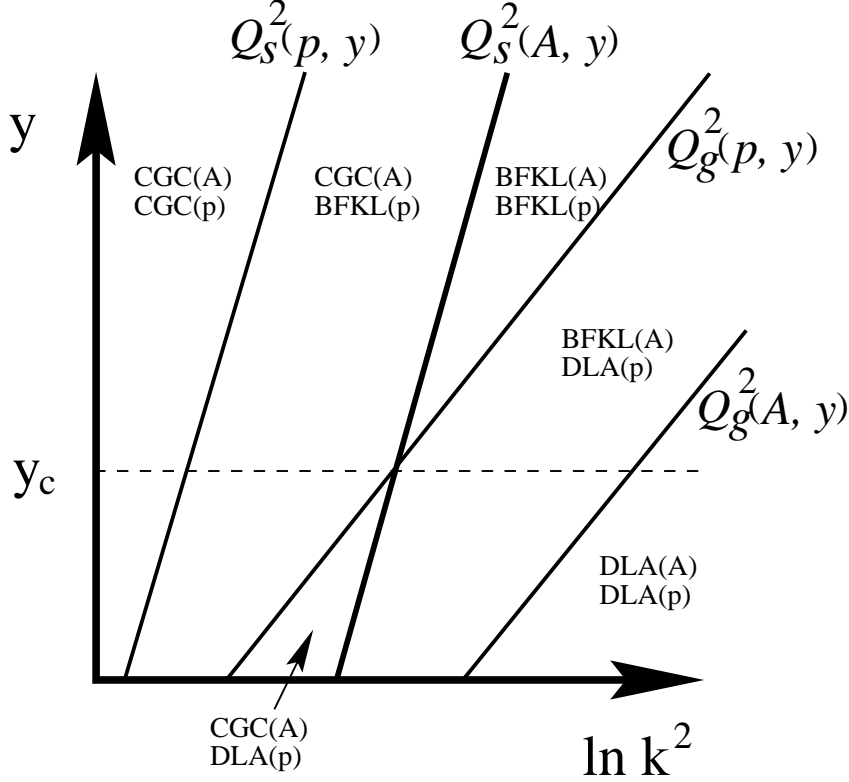


Fig. 1. Physical regimes for evolution in the kinematic plane $y - \ln k_{\perp}^2$ (for fixed coupling, for definiteness; see Fig. 10 for the corresponding picture with a running coupling). Both the saturation momentum $Q_s(A)$ and the ‘geometric scale’ momentum $Q_g(y)$ rise exponentially with y (for both the proton and the nucleus), and thus are represented by straight lines in the logarithmic scale of the plot. As visible on this plot, the geometric scale rises faster (its logarithmic slope is roughly twice as large as for the saturation momentum).

and φ_p) is carried by the respective saturation momenta, which for fixed coupling evolve in the same way with y [40]. Then, the ratio \mathcal{R}_{pA} decreases only slowly, and eventually stabilizes, when $\alpha_s y \gtrsim \rho_A^2$, to a small value $\mathcal{R}_{pA} \sim 1/(A^{1/3}\rho_A)^{1-\gamma}$. Here, $\gamma \approx 0.63$ is the BFKL saddle point (or ‘anomalous dimension’) near saturation [36, 37].

(b) With **running coupling**, the rapid suppression is pursued within a large range of y above y_c , because in that range the proton and nuclear saturation momenta evolve differently with y [40]. Specifically, the proton saturation momentum $Q_s(p, y)$ grows initially faster, and catches up with that of the nucleus when $y \sim \rho_A^4$. For larger y , $Q_s(A, y) \approx Q_s(p, y)$, and the ratio stabilizes at the even smaller value $\mathcal{R}_{pA} \simeq 1/A^{1/3}$. Note that this limiting value is simply the factor of $A^{-1/3}$ introduced by hand in Eq. (1.1). Thus, this limit is achieved in the regime where the proton and nuclear occupation factor become equal with each other. With a running coupling, this eventually happens everywhere except at asymptotically large momenta.

To conclude this introductory discussion, let us emphasize that all the phenomena discussed so far — the Cronin peak in the initial condition, its disappearance with increasing y , and the high- k_\perp suppression — are hallmarks of saturation, which however reflect different aspects of saturation, and of the quantum evolution towards saturation : The Cronin peak reflects classical saturation, i.e., the saturation via non-linearities in the classical field equations, whereas the Color sources in these equations (the ‘valence quarks’) are uncorrelated. This is, of course, the content of the MV model, but it could also be a reasonable approximation for a large nucleus at not so high energies, where the effects of quantum evolution are negligible. The driving force towards both high- k_\perp suppression and the flattening of the Cronin peak is the linear evolution (either DGLAP, or BFKL), but notwithstanding this, these phenomena are still a signal of saturation, since they occur only because of the mismatch between various regimes of evolution, which is made possible by saturation : For the flattening of the peak, this is the mismatch between the nuclear evolution below and above the saturation scale, whereas for the high- k_\perp suppression, this is the mismatch between the (linear) evolutions of the proton and of the nucleus, which originates in the difference between the respective saturation momenta.

2 Cronin effect in the initial conditions

2.1 Generalities

By the “unintegrated gluon distribution” we shall more precisely understand in what follows the **gluon occupation factor**, i.e., the number of gluons of given spin and color per unit phase-space in a nucleus with atomic number A :

$$\varphi_A(k_\perp, y) \equiv \frac{(2\pi)^3}{2(N_c^2 - 1)} \frac{dN_A}{dy d^2k_\perp d^2b_\perp}. \quad (2.1)$$

Here, y denotes the rapidity (related to the longitudinal momentum fraction x of the gluons via $y = \ln(1/x)$), k_\perp is the transverse momentum, and b_\perp is the gluon position in transverse space. For simplicity, we shall consider a hadron which is homogeneous in the transverse plane, and we shall suppress the b_\perp -dependence in all the formulae. Within light-cone quantized QCD, the gluon occupation factor (2.1) is related to a gauge-invariant 2-point function of the color fields, which can be computed within the CGC effective theory [12, 24]. More precisely, the evolution of this quantity with y can be computed within perturbative QCD (to the accuracy of the effective theory), but the initial conditions at $y = 0$ remain non-perturbative, and require a model. It turns out that the choice of this model has a strong influence on the physical problems that we would like to address, especially as far as the existence of a Cronin peak [13] is concerned.

Physically, the initial conditions that we are interested in correspond to a large nucleus ($A \gg 1$) in a regime at intermediate energies. The initial energy should be high enough for the gluons with the smallest values of x to be coherent with each other, but low enough for the quantum effects in the gluon distribution to be negligible. These conditions require $x_0 \lesssim 1/A^{1/3}$, but at the same time $\alpha_s \ln 1/x_0 \ll 1$, where x_0 denotes the longitudinal fraction of the slowest gluons within the nucleus at the initial energy. For instance, for a gold nucleus and with $\alpha_s \approx 0.2$, these requirements can be satisfied by choosing $x_0 \sim 10^{-1}$. (From now on, the rapidity variable will be understood to represent the difference from this original rapidity: $y = \ln(x_0/x)$.) Under these conditions, the gluon distribution in the nucleus is simply the result of classical radiation from the valence quarks. But if A is large enough — which is what we assume here —, the resulting gluon density can be still very high, and thus favor non-linear effects which lead to **gluon saturation** at sufficiently low k_\perp , below some characteristic scale $Q_s(A)$.

A simple model which encompasses these physical conditions is the McLerran–Venugopalan (MV) model [10, 12], in which the total color charge in the nucleus is the incoherent sum of the individual color charges of the valence quarks, and the corresponding saturation momentum scales like $Q_s(A) \sim A^{1/6}$ (since $Q_s^2(A)$ is proportional to the color charge squared per unit transverse area). If A is large enough, this scale is hard ($Q_s^2(A) \gg \Lambda_{\text{QCD}}^2$), and the matter made of the gluons (the CGC) is weakly coupled.

In what follows we shall adopt the MV model as our initial condition at $y = 0$. The remaining part of this section is devoted to a study of the gluon distribution in this model, with emphasis on the Cronin peak, and, more generally, on the role of non-linear effects in rearranging the gluons in momentum space. Although this model has been extensively studied in the literature [10, 12, 14, 27, 28] (in particular, in relation with the Cronin peak [22, 23, 47, 48]), our analysis below will bring some new results and conceptual clarifications, and will reveal some novel, and perhaps surprising, features, which to our knowledge have escaped to previous investigations.

Specifically, in Sect. 2.2, we shall provide a complete, analytic, study of the gluon distribution in the MV model, that we shall generalize on this occasion to include running coupling effects, in such a way to be compatible with the quantum evolution to be discussed later. The results obtained in this analysis will permit us to clarify the conditions for the emergence of the peak, and explicitly compute properties like the location of the peak and its magnitude (in Sect. 2.3). Then, in Sect. 2.4, we shall reexamine a global argument in favor of the Cronin peak, based on a sum-rule [22], that we shall use in order to better understand the origin of the gluons which make up the condensate.

A rather surprising feature which will emerge from this analysis refers to the redistribution of gluons in momentum space under the influence of the non-linear effects : Whereas it has been since long appreciated that the effect of the repulsive interactions is to push

the gluons towards the modes at larger momenta, and thus provide a spectrum which is infrared–safe [12, 14, 28], it has not been recognized so far that the dominant part of this spectrum — the one which is parametrically enhanced for large A , and provides a plateau of order $1/\alpha_s$ at saturation ($k_\perp \lesssim Q_s(A)$) — is actually **compact**, i.e., it falls off exponentially with increasing k_\perp above $Q_s(A)$. In fact, as we shall see, it is precisely this exponential decrease in $\varphi_A(k_\perp)$ for momenta just above $Q_s(A)$ which explains why a pronounced peak appears in the ratio \mathcal{R}_{pA} when computed in the MV model.

To conclude this general discussion, let us mention two alternative definitions for the unintegrated gluon distribution which are used in the literature. These definitions have in common the fact that they relate the gluon distribution to a scattering operator: the scattering amplitude $\mathcal{N}_A(r_\perp, y)$ for a color dipole with transverse size r_\perp which scatters of a hadronic target with atomic number A at relative rapidity y . Under suitable approximations, this quantity obeys a closed, non–linear, evolution equation (a generalization of the BFKL equation), originally derived by Kovchegov [31].

Specifically, in Ref. [36], the following definition has been proposed (the color dipole is taken to be made off two gluons):

$$\varphi_A(k_\perp, y) \equiv \int \frac{d^2 r_\perp}{\pi r_\perp^2} e^{-ik_\perp \cdot r_\perp} \frac{\mathcal{N}_A(r_\perp, y)}{\alpha_s N_c}. \quad (2.2)$$

This definition has no deep motivation, but is simply based on the analogy with a formula for the true occupation factor (2.1) which holds within the MV model (see Sect. 2.2 below). In fact, the quantities in Eqs. (2.2) and (2.1) are very similar to each other: They coincide with each other in the linear regime at high momenta $k_\perp \gg Q_s(A, y)$, where they both obey the BFKL equation, and they also show a similar behavior at low momenta $k_\perp \ll Q_s(A, y)$, so they differ, at most, in the transition region towards saturation. The approximations that we shall develop in this paper are not sensitive to the details of this transition region, nor to the differences [45, 46] between the Kovchegov equation and the general, functional, evolution equation for the CGC, so all the results that we shall obtain apply literally to both definitions. Thus, our results are directly comparable to the numerical calculations in Ref. [23], which are based on Eq. (2.2) together with the Kovchegov equation.

A different definition, with a deeper physical motivation, has been introduced in Ref. [19], and reads

$$h_A(k_\perp, y) \equiv \frac{1}{4} k_\perp^2 \nabla_k^2 \varphi_A(k_\perp, y) = k_\perp^2 \int \frac{d^2 r_\perp}{4\pi} e^{-ik_\perp \cdot r_\perp} \frac{\mathcal{S}_A(r_\perp, y)}{\alpha_s N_c}, \quad (2.3)$$

where in this context $\varphi_A(k_\perp, y)$ is the function defined in Eq. (2.2), and $\mathcal{S}_A(r_\perp, y) \equiv$

$1 - \mathcal{N}_A(r_\perp, y)$ is the S -matrix element for dipole-hadron scattering. The quantity (2.3) enters a factorized formula for the cross-section for gluon production in proton-nucleus collisions [14, 21, 53], and as such it is directly relevant for the phenomenology of dA collisions at RHIC. Note that its interpretation as a ‘gluon distribution’ is only conventional (this is based on an analogy with the k_\perp -factorization which holds in the linear regime at not so high energies), and should not give rise to confusion: There is a priori no reason why the (canonical) gluon distribution should enter the calculation of observables for high energy scattering. Indeed, in the high-density environment at high energy, the scattering operators are non-linear in the color field in the target (the non-linear effects describe multiple scattering), so, unlike what happens at low energy, they are not simply proportional to the 2-point function which defines the gluon distribution.

The results that we shall obtain for φ_A later in this paper do not directly apply to h_A , although they could be easily translated for it (at least, in the case of a fixed coupling), by using $h_A \propto k^2 \nabla_k^2 \varphi_A$. The numerical analysis in Ref. [23], which considers both definitions (2.2) and (2.3), shows that the ratio \mathcal{R}_{pA} is qualitatively the same when computed with any of these two definitions. But important quantitative differences persist, especially at low momenta, where the functions φ_A and h_A are very different. In view of this, it would be interesting to repeat for h_A , and also for the convolution yielding the cross-section for gluon production, the analysis that we shall give below in this paper for φ_A . A potential difficulty that we foresee with such an analysis is the fact that the generalization of Eq. (2.3) to the case of a running coupling is ambiguous (unlike for the other definitions, Eqs. (2.1) and (2.2), for which a natural generalization exists; see below).

2.2 The McLerran-Venugopalan model: Fixed & running coupling

The color sources which generate the small- x gluons in the McLerran-Venugopalan (MV) model [10, 12] are the $3A$ valence quarks (from the A nucleons), which are assumed to be uncorrelated with each other except for the long-range correlations associated with confinement. The gluon occupation factor $\varphi_A(k_\perp) \equiv \varphi_A(k_\perp, y = 0)$ at momenta $k_\perp \gg \Lambda_{\text{QCD}}$ is then obtained as [14, 28]

$$\varphi_A(k_\perp) = \int d^2 r_\perp e^{-ik_\perp \cdot r_\perp} \frac{1 - \exp\left\{-\frac{1}{4} r_\perp^2 Q_A^2 \ln \frac{4}{r_\perp^2 \Lambda^2}\right\}}{\pi \alpha_s N_c r_\perp^2}, \quad (2.4)$$

where Λ is a non-perturbative scale of order Λ_{QCD} (the only trace of confinement), $N_c = 3$ is the number of colors, and $Q_A^2 = \alpha_s N_c \mu_A \propto A^{1/3}$ is proportional to the color charge squared μ_A of the valence quarks per unit transverse area. The integration in Eq. (2.4) must be restricted to $r_\perp < 2/\Lambda$, for consistency with the approximations leading to this

formula [12], and also to avoid that the logarithm in the exponent changes sign. But as long as $k_\perp \gg \Lambda$, the value of the integral is very little sensitive to the precise value of the upper cutoff.

Since the MV model is a classical approximation, Eq. (2.4) is a priori written for a fixed coupling α_s . Later, we shall consider quantum evolution with a running coupling, and at that stage we shall also need a generalization of Eq. (2.4) which includes running coupling effects to one-loop order (i.e., for a running coupling $\alpha_s(Q^2) \equiv b_0/\ln(Q^2/\Lambda_{QCD}^2)$). The generalization that we shall consider reads (from now on, we shall not distinguish between the scales Λ and Λ_{QCD})

$$\varphi_A(k_\perp) = \int d^2 r_\perp e^{-ik_\perp \cdot r_\perp} \frac{1 - e^{-\frac{1}{4} r_\perp^2 Q_A^2}}{\pi b_0 N_c r_\perp^2} \ln \frac{4}{r_\perp^2 \Lambda^2}, \quad (2.5)$$

where $Q_A^2 \equiv b_0 N_c \mu_A$ has now a slightly different meaning as compared to the fixed coupling case, but is still proportional to $A^{1/3}$. Formally, Eq. (2.5) is obtained from Eq. (2.4) by replacing in the latter $\alpha_s \rightarrow \alpha_s(4/r_\perp^2)$ within the denominator of the integrand, and also within Q_A^2 . In contrast to Eq. (2.4), there is no need for an upper cutoff in Eq. (2.5): the integral is convergent as written, and for any $k_\perp \gg \Lambda$ it is dominated by perturbative sizes $r_\perp \ll 1/\Lambda$.

Since the choice of a running in the absence of a complete one-loop quantum calculation is a priori ambiguous (especially in the presence of several scales, like in Eq. (2.4)), it is important to justify in more detail our choice leading to Eq. (2.5). Note first that (a) the coupling α_s which is explicit in Eq. (2.4) (in the denominator) and the one which is implicit in the definition of Q_A^2 have the same origin [12, 28], and thus need to be renormalized in the same way, and (b) the quantity $1 - \exp\left\{-\frac{1}{4} r_\perp^2 Q_A^2 \ln \frac{4}{r_\perp^2 \Lambda^2}\right\}$ in the numerator of Eq. (2.4) can be recognized as the scattering amplitude for a color dipole of size r_\perp which scatters of the nucleus. More precisely, this is the dipole made of the two primary gluons radiated by the valence quarks (the gluons which define the distribution), and the scattering amplitude describes the color precession of these primary gluons when propagating through the color field of the nucleus (see [12] for details). As well known, a small dipole couples predominantly to gluons with momenta $k_\perp^2 \lesssim 1/r_\perp^2$, so it is indeed natural to choose the size of the dipole as the argument for the running of the corresponding coupling constant; this is also the choice made in other studies of the evolution of the dipole scattering amplitude with increasing energy [37, 38, 44, 51, 52].

There is one more subtle point about our choice in Eq. (2.5) : as a density of color charge, the quantity μ_A involves itself a factor of α_s , that we have implicitly treated as a constant in our arguments above. Specifically, for $A \times N_c$ valence quarks which are homogeneously distributed within the nuclear disk with radius R_A , one obtains [12]

$$\mu_A = \frac{2\alpha_s A}{R_A^2}. \quad (2.6)$$

Treating α_s in Eq. (2.6) as a constant amounts to neglecting quantum corrections to the distribution of the valence quarks, which is in the spirit of the MV model. One sees that, in writing Eq. (2.5), we have treated differently the vertices describing the radiation of classical color fields from the valence quarks, and those describing the scattering of the color dipole off these classical fields. This is justified for the present purposes because these vertices play different roles in the subsequent evolution with increasing y : Whereas the valence quarks act simply as sources for the primary gluons at $y = 0$, and as such they can be viewed as classical colored particles, the quantum evolution proceeds via gluon radiation from the primary gluons, and the vertices describing this radiation are of the same type as those describing the scattering of the color dipole in Eq. (2.4). Thus dressing **just** these vertices is the minimal way to render Eq. (2.4) consistent with the quantum evolution which includes running coupling effects.

The emergence of the dipole scattering amplitude in Eqs. (2.4) and (2.5) illustrates the deep connection between **unitarization** effects in scattering processes at high energy and **saturation** effects in the nuclear gluon distribution: Both types of effects arise from non-linearities associated with strong gluon fields, which here are encoded in the exponential terms² in the integrands of Eqs. (2.4) and (2.5). The transition from the linear regime to the non-linear one takes place when the exponent is of order one. More precisely, we shall define the **saturation momentum** $Q_s(A)$ such that the exponent is equal to one when $r = 2/Q_s(A)$. For running coupling, Eq. (2.5) immediately implies $Q_s(A) = Q_A \sim A^{1/3}$. For fixed coupling, the saturation scale turns out to be larger than the scale Q_A introduced by the color sources

$$Q_s^2(A) = Q_A^2 \ln \frac{Q_s^2(A)}{\Lambda^2} \sim A^{1/3} \ln A^{1/3}, \quad (2.7)$$

and this difference will be seen to have important consequences. Loosely speaking, the ratio

$$\rho_A \equiv \frac{Q_s^2(A)}{Q_A^2} = \ln \frac{Q_s^2(A)}{\Lambda^2} \sim \ln A^{1/3}, \quad (2.8)$$

will play the same role in the fixed coupling case as the inverse of the coupling constant in the case of a running coupling. In fact, for a running coupling, we shall define similarly $\rho_A \equiv \ln(Q_A^2/\Lambda^2)$, and then it is clear that $1/\rho_A$ is essentially the same as the coupling evaluated at the saturation momentum : $\alpha_s(Q_A^2) = b_0/\rho_A$. Since the MV model makes

² Physically, these exponentials represent the S -matrix for dipole-nucleus scattering.

sense only for weak coupling, it is justified to treat ρ_A as a large parameter, $\rho_A \gg 1$, which we shall do in what follows. It is interesting to note in this context that, for a gold nucleus at typical RHIC energies one expects $Q_s^2(A) \simeq 2 \text{ GeV}^2$, which together with $\Lambda \simeq 200 \text{ MeV}$, yields $\rho_A \simeq \ln 50 \simeq 4$.

It is straightforward to compute the dominant behavior of the gluon distribution at asymptotically large ($k_\perp \gg Q_s(A)$) or small ($k_\perp \ll Q_s(A)$, with $k_\perp \gg \Lambda$ though) momenta. One finds :

(a) Fixed coupling:

$$\varphi_A(k_\perp) \approx \begin{cases} \frac{1}{\alpha_s N_c} \frac{Q_A^2}{k_\perp^2}, & \text{for } k_\perp \gg Q_s(A) \\ \frac{1}{\alpha_s N_c} \ln \frac{Q_s^2(A)}{k_\perp^2}, & \text{for } k_\perp \ll Q_s(A) \end{cases} \quad (2.9)$$

(a) Running coupling:

$$\varphi_A(k_\perp) \approx \begin{cases} \frac{1}{b_0 N_c} \frac{Q_A^2}{k_\perp^2}, & \text{for } k_\perp \gg Q_A \\ \frac{1}{N_c} \left\langle \frac{1}{\alpha_s} \right\rangle \ln \frac{Q_A^2}{k_\perp^2}, & \text{for } k_\perp \ll Q_A \end{cases} \quad (2.10)$$

The average inverse coupling constant which enters the last equation is defined as

$$\left\langle \frac{1}{\alpha_s} \right\rangle \equiv \frac{1}{2b_0} \left(\ln \frac{Q_A^2}{\Lambda^2} + \ln \frac{k_\perp^2}{\Lambda^2} \right) = \frac{1}{b_0} \ln \frac{k_\perp Q_A}{\Lambda^2}. \quad (2.11)$$

The high-momentum behavior in these equations, which is obtained after linearizing the exponential terms Eqs. (2.4) and (2.5), is recognized as the bremsstrahlung spectrum due to radiation from independent color sources. This would be the spectrum at any k_\perp in the absence of non-linear effects in the dynamics of the radiated gluons. But already at high- k_\perp , this spectrum receives non-linear corrections which are suppressed by powers of $Q_s^2(A)/k_\perp^2$ ('higher-twist' effects; see below). The dominant behavior at low momenta is obtained after neglecting the exponential terms Eqs. (2.4) and (2.5), and is correct to leading logarithmic accuracy; that is, the first corrective term would be a constant term under the logarithm.

As we shall see in Sect. 2.3, the asymptotic expressions above are already sufficient to demonstrate the existence of a peak in the ratio \mathcal{R}_{pA} . But in order to study the properties of this peak, we also need the gluon occupation factor at generic (intermediate) momenta, which given the simplicity of the MV model can be computed analytically.

In fact, in the case of a running coupling, we have been able to evaluate the integral in Eq. (2.5) in analytic form, with a result which is displayed in the Appendix, and which will be also discussed below. For fixed coupling, we do not have such an exact result, but we have found a convenient series representation of the integral in Eq. (2.4), which converges very fast, and renders the physical interpretation of the result transparent.

Let us consider the fixed coupling case first. After rewriting the exponent in the integrand of Eq. (2.4) as (cf. Eq. (2.7) and (2.8))

$$\frac{1}{4} r_{\perp}^2 Q_A^2 \ln \frac{4}{r_{\perp}^2 \Lambda^2} = t \left(1 + \frac{\ln 1/t}{\rho_A} \right), \quad t \equiv \frac{r_{\perp}^2 Q_s^2(A)}{4}, \quad (2.12)$$

one can decompose the integral into two pieces as

$$\begin{aligned} \varphi_A(k_{\perp}) &= \int d^2 r_{\perp} e^{-i k_{\perp} \cdot r_{\perp}} \left\{ \frac{1 - e^{-\frac{1}{4} r_{\perp}^2 Q_s^2(A)}}{\pi \alpha_s N_c r_{\perp}^2} + \frac{e^{-\frac{1}{4} r_{\perp}^2 Q_s^2(A)}}{\pi \alpha_s N_c r_{\perp}^2} \left[1 - \exp \left(-t \frac{\ln 1/t}{\rho_A} \right) \right] \right\} \\ &= \varphi_A^{\text{sat}}(k_{\perp}) + \varphi_A^{\text{twist}}(k_{\perp}), \end{aligned} \quad (2.13)$$

where the first, ‘saturating’, piece can be explicitly evaluated, and reads

$$\varphi_A^{\text{sat}}(k_{\perp}) = \frac{1}{\alpha_s N_c} \Gamma(0, z), \quad (2.14)$$

while the second piece — the sum of all-‘twist’ contributions (see below) — can be evaluated as a series expansion, obtained by expanding the exponential within the square brackets in powers of $(t \ln 1/t)/\rho_A$ as

$$\varphi_A^{\text{twist}}(k_{\perp}) = -\frac{1}{\alpha_s N_c \rho_A} \int dt J_0(\sqrt{4zt}) e^{-t} \sum_{n=1}^{n_{\text{max}}} \left(\frac{t}{\rho_A} \right)^{n-1} \frac{\ln^n t}{n!}. \quad (2.15)$$

In these equations, $z \equiv k_{\perp}^2/Q_s^2(A)$, $\Gamma(0, z)$ is the incomplete Gamma function:

$$\Gamma(0, z) = \int_z^{\infty} \frac{e^{-t}}{t} dt, \quad (2.16)$$

$n_{\text{max}} \sim e^{\rho_A} = Q_s^2(A)/\Lambda^2 \gg 1$, and the truncation of the series in Eq. (2.15) at $n \leq n_{\text{max}}$ reflects the upper cutoff $r_{\text{max}} = 2/\Lambda$ which is implicit in the integral over r_{\perp} in the first line of Eq. (2.13). (The corresponding integral giving φ_A^{sat} , Eq. (2.14), has been extended up to infinity, since rapidly convergent.) Without a truncation, the series would

be asymptotically divergent, but the divergent behavior would start to manifest itself only at very large orders, beyond n_{\max} . On the other hand, when $\rho_A \gg 1$ the truncated series is rapidly convergent for any z , and therefore $\varphi_A(k_\perp)$ can be computed even analytically with high accuracy (see the Appendix for details).

The first important observation about the decomposition in Eq. (2.13) is that the second piece, φ_A^{twist} , is multiplied by an overall factor $1/\rho_A$ (this is manifest on Eq. (2.15)), and thus is parametrically suppressed at large A . This implies that, in the saturation region at $z \lesssim 1$ (where both the Γ -function and the sum of the truncated series in Eq. (2.15) are generically of order one), the gluon distribution is dominated by the first piece, φ_A^{sat} . In particular, φ_A^{sat} captures the leading behavior at low momenta $k_\perp \ll Q_s(A)$, cf. Eq. (2.9): indeed, $\Gamma(0, z) \approx \ln 1/z$ for $z \ll 1$, whereas φ_A^{twist} is analytic near $z = 0$. In fact, if one remembers that $1/\rho_A$ can be effectively identified with α_s (cf. the discussion after Eq. (2.8)), it becomes clear that the $1/\alpha_s$ -enhancement of the gluon distribution, which is the hallmark of saturation, is associated solely with φ_A^{sat} : For $z \lesssim 1$, the latter provides a plateau with a height of $\mathcal{O}(1/\alpha_s)$, whereas φ_A^{twist} brings only a small correction, of $\mathcal{O}(1)$.

The second important observation is that the saturating piece φ_A^{sat} is **compact**, in the sense that it vanishes exponentially at momenta outside the saturation region (since $\Gamma(0, z) \approx e^{-z}/z$ for $z \gg 1$). By contrast, it can be checked that, for $z \gg 1$, the function φ_A^{twist} can be expanded in powers of $1/z$ (up to logarithmic corrections), thus generating the ‘twist expansion’ of the MV model. It should be stressed that each of the terms in the truncated series in Eq. (2.15) contains terms to all orders in the twist expansion: the first term ($n = 1$) includes the bremsstrahlung spectrum $\propto 1/z$, together with an infinite series of ‘higher-twist’ terms (i.e., terms of order $1/z^2$, or higher), the second term ($n = 2$) starts at order $1/z^2$, etc. The first few terms in the twist expansion are exhibited in the Appendix.

We see that the gluon distribution of a large nucleus in the MV model naturally decouples into two pieces, one which controls the spectrum at saturation, and another one which controls the tail of the distribution at high momenta. It is natural to interpret the first piece, φ_A^{sat} , as the **occupation factor in the color glass condensate**. The fact that this distribution appears to be compact is probably just specific to the MV model, since, as we shall see, this feature is washed out by the quantum evolution (cf. Sect. 5.3). The previous considerations also suggest that the higher-twist terms contribute only little to the physics of the Cronin peak in the MV model. This will be confirmed by the analysis in the next subsection.

The corresponding discussion in the case of a running coupling is even simpler, since the corresponding ‘twist’ piece involves only one term, instead of a series of terms. Also, some arguments become more transparent since, with a running coupling, $1/\alpha_s(Q_s^2(A))$ and ρ_A are explicitly identified. Specifically, Eq. (2.5) can be decomposed as:

$$\begin{aligned}\varphi_A(k_\perp) &= \varphi_A^{\text{sat}}(k_\perp) + \varphi_A^{\text{twist}}(k_\perp), \\ \varphi_A^{\text{sat}}(z) &= \frac{1}{b_0 N_c} \rho_A \Gamma(0, z), \quad \varphi_A^{\text{twist}}(z) = \int dt J_0(\sqrt{4zt}) \frac{1 - e^{-t}}{b_0 N_c t} \ln \frac{1}{t},\end{aligned}\tag{2.17}$$

where the saturating piece is explicitly enhanced by the factor ρ_A (that is, it is of $\mathcal{O}(1/\alpha_s)$), while φ_A^{twist} is of $\mathcal{O}(1)$ for $z \sim 1$, and can be expanded in powers of $1/z$ for $z \gg 1$ (thus generating the twist expansion). The only noticeable difference with respect to the fixed coupling case is that, now, $\varphi_A^{\text{twist}}(z)$ is not analytic near $z \rightarrow 0$, but rather yields a large **negative** contribution $-(1/2b_0 N_c) \ln^2 z$ in that limit, which contributes to the dominant low-momentum behavior exhibited in Eq. (2.10). Since, however, the overall contribution remains **positive** for any $k_\perp \geq \Lambda$, it is clear that $\varphi_A^{\text{sat}}(k_\perp)$ is still the dominant contribution at any $\Lambda \leq k_\perp \leq Q_A$. The integral giving φ_A^{twist} is explicitly evaluated in the Appendix, where its twist expansion will be also considered.

The previous considerations are illustrated in Figs. 2 and 3, which exhibit the gluon occupation factor $\varphi_A(k_\perp)$, and its various contributions $\varphi_A^{\text{sat}}(k_\perp)$ and $\varphi_A^{\text{twist}}(k_\perp)$, in the MV model with fixed and running coupling, in either linear scale (Fig. 2), or log-log scale in a wider range of momenta (Fig. 3).

2.3 Cronin effect in the McLerran-Venugopalan model

To form the ratio \mathcal{R}_{pA} , Eq. (1.1), one also needs the gluon distribution in the proton, $\varphi_p(k_\perp, y)$. For $y = 0$ and $k_\perp \gg \Lambda$, the proton is in the perturbative (i.e., linear) region, and will be described by the bremsstrahlung spectrum in Eqs. (2.9) or (2.10) (for fixed and running coupling, respectively) with $Q_A^2 \rightarrow Q_p^2$, and $Q_p = \mathcal{O}(\Lambda)$. For instance,

$$\varphi_p(k_\perp) = \frac{1}{\alpha_s N_c} \frac{Q_p^2}{k_\perp^2} \Theta(k_\perp - Q_p) \quad (\text{fixed coupling}).\tag{2.18}$$

We shall assume the following relation between the two scales:

$$Q_A^2 = A^{1/3} Q_p^2,\tag{2.19}$$

which holds formally if one extrapolates the MV model (a priori valid for a large nucleus) down to $A = 1$.

Note that the quantity in the denominator of Eq. (1.1), namely $A^{1/3} \varphi_p(k_\perp)$, coincides with the nuclear gluon distribution in the high momentum limit (i.e., the bremsstrahlung spectrum in Eqs. (2.9) or (2.10)). Thus, within the MV model at least, the ratio $\mathcal{R}_{pA}(k_\perp)$

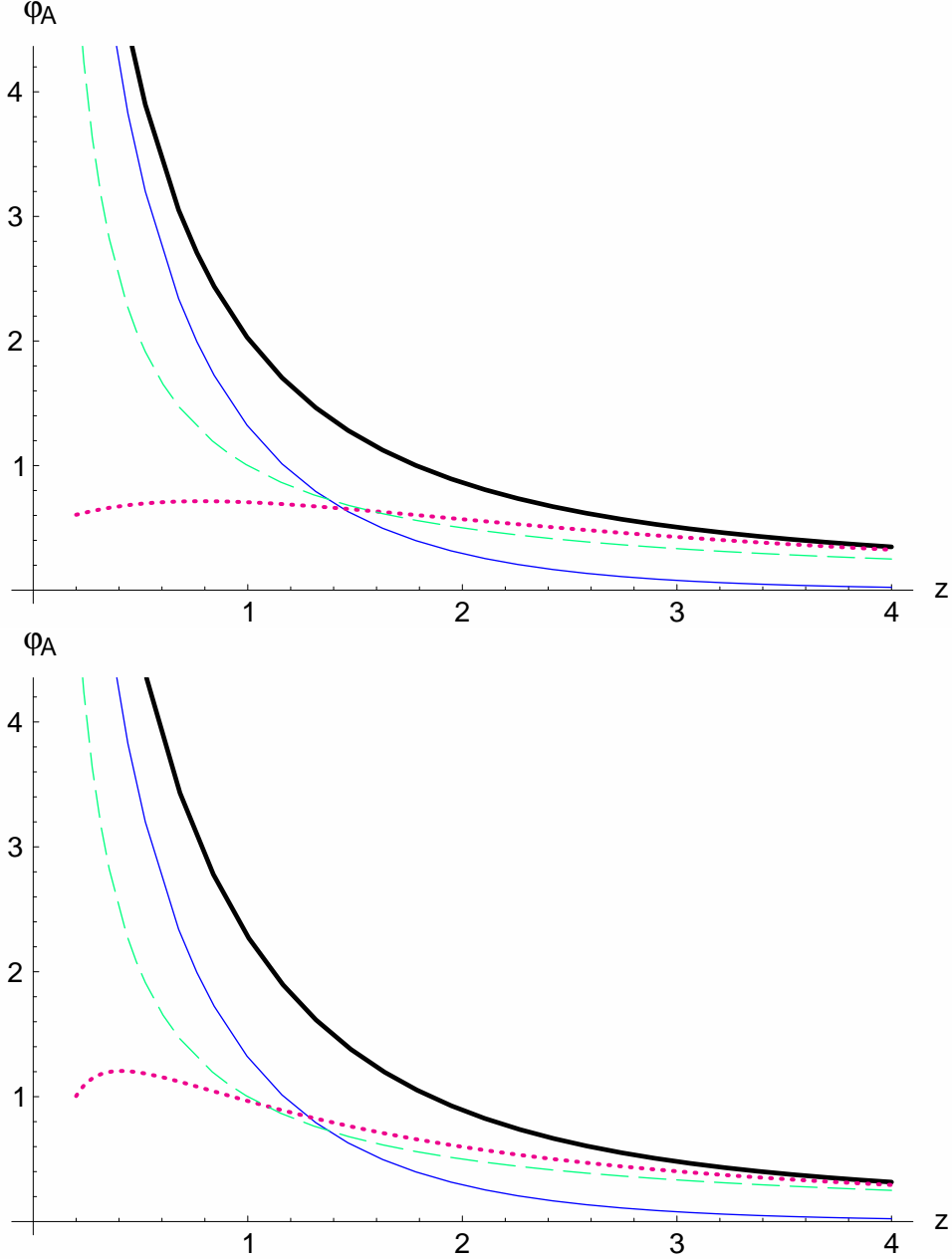


Fig. 2. The gluon occupation factor $\varphi_A(z)$ as a function of the scaled momentum variable $z = k^2/Q_s^2(A)$ in the MV model with either fixed (figure above) or running (below) coupling and $\rho_A = 6$. The black (thick) line corresponds to the gluon occupation factor $\varphi_A(z)$; the blue (solid) line shows the saturation contribution $\varphi_A^{\text{sat}}(z)$; the magenta (dotted) line shows the twist contribution $\varphi_A^{\text{twist}}(z)$; the green (dashed) line represents the bremsstrahlung spectrum

is also a measure of the deviation of the actual nuclear gluon distribution from the corresponding prediction of linear perturbation theory. As already discussed, this deviation is associated with non-linear effects in the gluon dynamics, in particular with saturation.

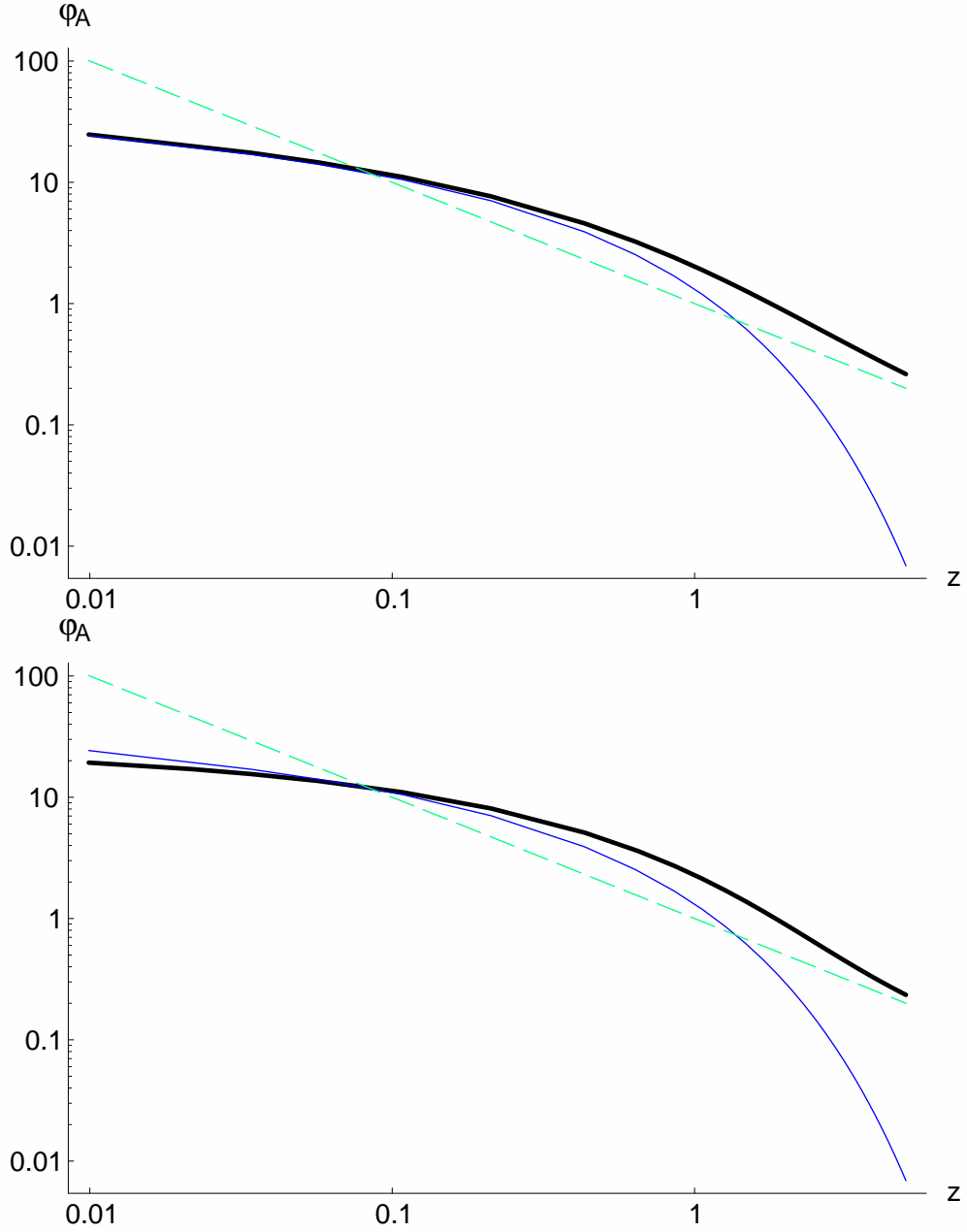


Fig. 3. Logarithmic plot of the gluon occupation factor $\varphi_A(z)$ as a function of the scaled momentum variable $z = k^2/Q_s^2(A)$ in the MV model with either fixed (figure above) or running (below) coupling and $\rho_A = 6$. The black (thick) line corresponds to the gluon occupation factor $\varphi_A(z)$; the blue (solid) line shows the saturation contribution $\varphi_A^{\text{sat}}(z)$; the green (dashed) line represents the bremsstrahlung spectrum

We immediately conclude that $\mathcal{R}_{pA}(k_\perp)$ must approach one at high k_\perp :

$$\mathcal{R}_{pA}(k_\perp) \simeq 1 \quad \text{for} \quad k_\perp \gg Q_s(A). \quad (2.20)$$

By using this condition together with very general properties of saturation, we can deduce the existence of a Cronin peak without any detailed calculation:

Consider the fixed coupling case, for definiteness. The basic consequence of saturation is that, for momenta $k_\perp \lesssim Q_s(A)$, the nuclear occupation factor develops a plateau with the height of $\mathcal{O}(1/\alpha_s)$; that is, $\varphi_A(k_\perp) \approx (1/\alpha_s N_c) \bar{\varphi}(z)$, where $z \equiv k_\perp^2/Q_s^2(A)$, and the function $\bar{\varphi}(z)$ is slowly varying when $z < 1$, and is of $\mathcal{O}(1)$ when $z \sim 1$. The fact³ that this function depends upon k_\perp and A only through z is because $\bar{\varphi}$ is dimensionless, and $Q_s(A)$ is the only scale in the problem other than k_\perp (since at saturation the spectrum cannot be sensitive to the non-perturbative scale Λ). We deduce that:

$$\mathcal{R}_{pA}(k_\perp) \approx \frac{k_\perp^2}{Q_A^2} \bar{\varphi}(z) = \rho_A z \bar{\varphi}(z), \quad \text{for} \quad k_\perp \lesssim Q_s(A). \quad (2.21)$$

Since $\bar{\varphi}(z)$ is only logarithmically divergent as $z \rightarrow 0$, it is clear that the ratio $\mathcal{R}_{pA}(k_\perp)$ is much smaller than one for k_\perp small enough (e.g., it is of $\mathcal{O}(A^{-1/3})$ when $k_\perp \sim Q_p$), but it is of $\mathcal{O}(\rho_A)$, and thus strictly larger than one, for $k_\perp = Q_s(A)$. This behavior at small k_\perp , together with the asymptotic behavior (2.20) at large k_\perp , immediately imply that the ratio \mathcal{R}_{pA} must have a maximum at some intermediate value of k_\perp .

This general argument does not tell us where is the maximum actually located, and not even whether there is a single maximum, or several. But it is highly probable, and will be confirmed by the explicit calculations below, that there is indeed only one maximum, which is located near $Q_s(A)$ and has a height of $\mathcal{O}(\rho_A)$: Indeed, there is no intrinsic scale larger than $Q_s(A)$ in the problem, and for $k_\perp < Q_s(A)$ the ratio is still increasing with k_\perp , as manifest on Eq. (2.21).

Note the specific way how the large factor ρ_A has entered the calculation in Eq. (2.21): this is due to the mismatch (2.7) between the scale Q_A^2 associated with the color sources and the saturation scale $Q_s^2(A)$ generated by the non-linear gluon dynamics. It is easy to check that a similar enhancement occurs also for a running coupling, although in that case the argument is more direct: the factor ρ_A is introduced by the inverse coupling in the saturation condition $\varphi_A(k_\perp = Q_A) \approx \kappa/\alpha_s(Q_A^2)N_c$, with $\kappa \sim \mathcal{O}(1)$.

³ Of course, all these properties are manifest on the expressions (2.14) and (2.17) for $\varphi_A^{\text{sat}}(k_\perp)$, but here we would like to construct our argument without relying on the explicit formulae for φ_A that we have obtained previously, in order to emphasize the general conditions required by the existence of the peak.

We conclude that the existence of the Cronin peak is a consequence of the fact that the gluon distribution at saturation is larger, by a factor of $\rho_A \sim \ln A^{1/3}$, than the naïve extrapolation of the bremsstrahlung spectrum down to $k_\perp \sim Q_s(A)$. This logarithmic enhancement is due to non-linear effects which cause the gluon occupation factor to increase faster with $1/k_\perp^2$ than predicted by linear perturbation theory, before eventually saturating to a value of order $1/\alpha_s$ at $k_\perp \lesssim Q_s(A)$.

We now rely on the explicit formulae for φ_A established in the previous subsection to give a complete description of the peak. For more clarity, we start by considering the large- A limit, in which the gluon occupation factor for momenta around $Q_s(A)$ reduces to the saturating piece φ_A^{sat} . (The corresponding contribution of φ_A^{twist} is suppressed by a factor $1/\rho_A$.) Using $\varphi_A^{\text{sat}}(k_\perp)$ from either Eq. (2.14) or Eq. (2.17), one finds the same expression for the ratio \mathcal{R}_{pA} with both fixed and running coupling, namely:

$$\mathcal{R}_{pA}(k_\perp) \approx z \Gamma(0, z) \rho_A \quad \text{for} \quad k_\perp \sim Q_s(A). \quad (2.22)$$

This is of the form anticipated in Eq. (2.21), and thus is of order ρ_A when $z \sim 1$ ($\Gamma(0, 1) = 0.219\dots$). It can be checked that the function $f(z) \equiv z \Gamma(0, z)$ has a maximum at $z_0 \approx 0.435$, with the peak value $f(z_0) \approx 0.281$. Moreover, this peak is very pronounced, since $f(z)$ is almost linearly increasing below the peak, but exponentially decreasing above it.

It is then straightforward to add the contribution of the twist terms in Eq. (2.15) or (2.17), and compute their effect on the location and the magnitude of the peak in an expansion in powers of $1/\rho_A$. One finds (with $\mathcal{R}_{\text{max}}(A) \equiv \mathcal{R}_{pA}(z_0)$) :

$$\begin{aligned} z_0 &= 0.435 + \frac{0.882}{\rho_A} + \frac{2.122}{\rho_A^2} + \mathcal{O}(\rho_A^{-3}), \\ \mathcal{R}_{\text{max}}(A) &= 0.281 \rho_A + 0.300 + \frac{0.294}{\rho_A} + \mathcal{O}(\rho_A^{-2}), \end{aligned} \quad (2.23)$$

in fixed coupling case, and respectively

$$\begin{aligned} z_0 &= 0.435 + \frac{1.382}{\rho_A} + \frac{2.038}{\rho_A^2} + \mathcal{O}(\rho_A^{-3}), \\ \mathcal{R}_{\text{max}}(A) &= 0.281 \rho_A + 0.524 + \frac{0.804}{\rho_A} + \mathcal{O}(\rho_A^{-2}), \end{aligned} \quad (2.24)$$

in the running coupling case.

Finally, for both fixed and running coupling one can compare the results obtained above in the $1/\rho_A$ expansion to the corresponding exact results, and the agreement is good even

for $\rho_A = 4$ (which, we recall, is a realistic value at RHIC). For example, with such a value for ρ_A , and for running coupling, one finds $z_0 = 0.89$ and $\mathcal{R}_{\max} = 1.85$, while Eq. (2.24) would give $z_0 = 0.91$ and $\mathcal{R}_{\max} = 1.85$.

In Fig. 4, where we show the Cronin ratio in the MV model with both fixed and running coupling, we also represent the individual contributions separated in the r.h.s. of Eq. (2.13) (or (2.17)), to better emphasize that the ‘twist’ effects give only a small contribution in the region of the peak. As obvious on this figure, the effect of the twist corrections is to flatten the peak a little bit, and also to move it towards larger momenta. Still, a well pronounced peak emerges because, even for ρ_A as small as 4, the dominant contribution to $\varphi_A(k_\perp)$ for k_\perp around $Q_s(A)$ is still given by the compact, ‘saturating’, piece φ_A^{sat} . Accordingly, the nuclear occupation factor shows an exponential fall-off for momenta just above $Q_s(A)$. It can be easily checked that the behavior changes from an exponential to a power law around $z \sim \ln \rho_A$.

2.4 A sum rule in the MV model and its consequences

In this subsection we shall discuss an alternative, global, argument in favor of the existence of the Cronin peak in the MV model, which sheds more light on the role of non-linear effects in the nuclear gluon distribution. This argument, due Kharzeev, Kovchegov, and Tuchin [22], is specific to the MV model — it is based on a sum-rule which reflects the basic property of this model that color sources are uncorrelated —, and cannot be extended to $y > 0$ (since the quantum evolution introduces correlations among the color sources; see below). But even within the MV model, the use of this argument is quite subtle, because of possible complications with ultraviolet divergences. In fact, as we shall explain below, the original formulation of the relevant sum-rule in Ref. [22] is not mathematically rigorous, which may have given rise to confusion (especially, in relation with the generalization of this sum-rule to $y > 0$; see the discussion in Ref. [23]). In what follows, we shall properly restate this argument, and then present a stronger version of it, based on partial sum-rules, which provides a more detailed information on the distribution of gluon at saturation.

Specifically, the argument in Ref. [22] is based on the following ‘sum-rule’ (the IR cutoff Λ is strictly needed only for the proton) :

$$\int_{\Lambda^2} \frac{d^2 k_\perp}{\pi} \left\{ \varphi_A(k_\perp) - A^{1/3} \varphi_p(k_\perp) \right\} = 0, \quad (2.25)$$

which holds indeed within the MV model, for both fixed and running coupling, as we shall demonstrate shortly. From this relation, one can infer the existence of a Cronin peak

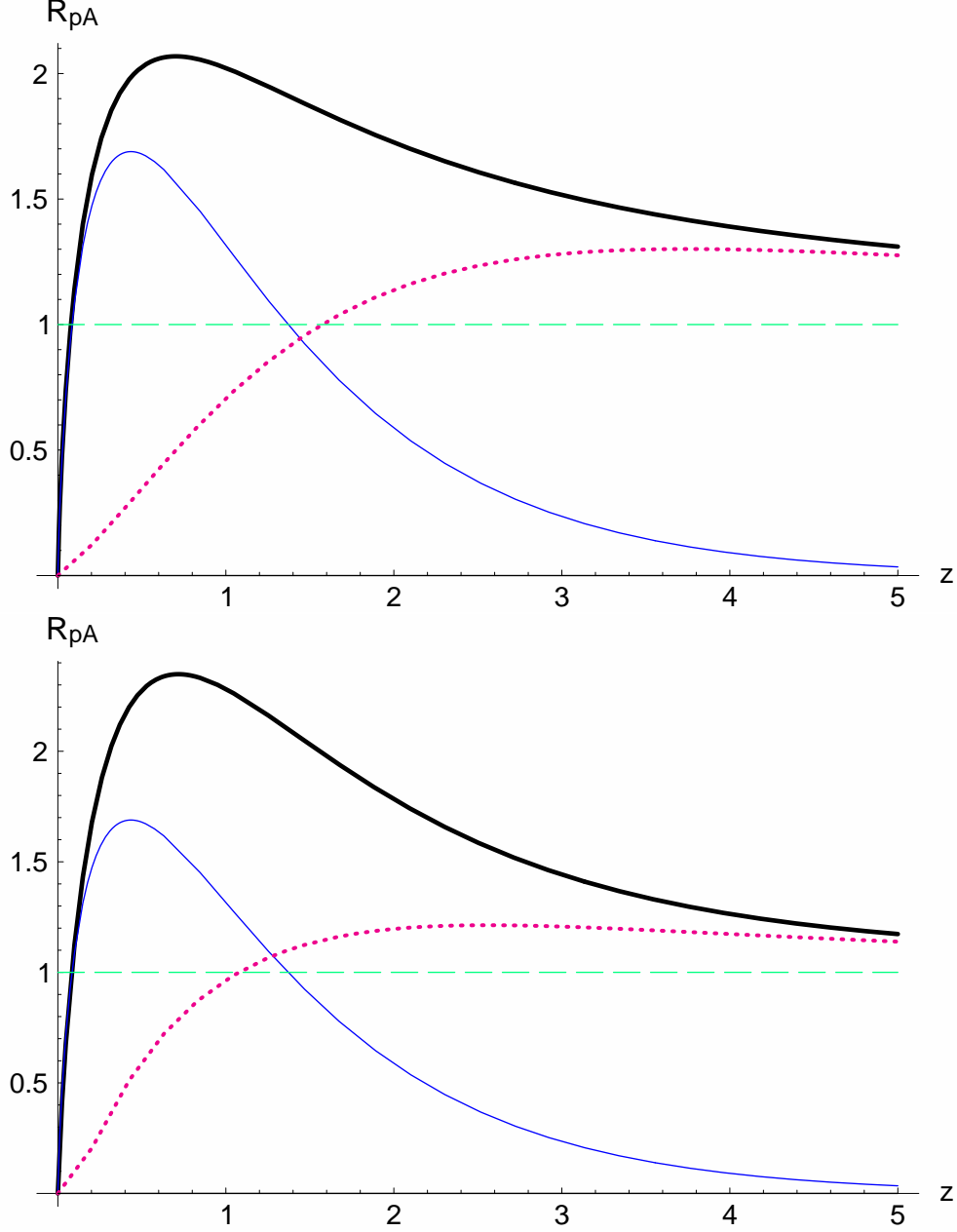


Fig. 4. The Cronin ratio $\mathcal{R}_{pA}(z)$ as a function of the scaled momentum variable $z = k^2/Q_s^2(A)$ in fixed and running coupling McLerran-Venugopalan model for $\rho_A = 6$. The black (thick) line corresponds to the ratio $\mathcal{R}_{pA}(z)$; the blue (solid) line shows the saturation contribution $\mathcal{R}_{pA}^{\text{sat}}(z)$; the magenta (dotted) line shows the twist contribution $\mathcal{R}_{pA}^{\text{twist}}(z)$.

through the following reasoning: Since at low momenta $k_\perp \ll Q_s(A)$ we have $\varphi_A(k_\perp) < A^{1/3}\varphi_p(k_\perp)$ due to gluon saturation in the nucleus, whereas at large momenta $k_\perp \gg Q_s(A)$ the two functions approach the same limit, one concludes that $\varphi_A(k_\perp)$ must be larger than $A^{1/3}\varphi_p(k_\perp)$ at some intermediate momenta, in order to give rise to the same integrated

distribution. One reason for the debate around this argument in the literature [23] is that in Ref. [22] the sum–rule has been abusively written as:

$$\int_{\Lambda^2} \frac{d^2 k_{\perp}}{\pi} \varphi_A(k_{\perp}) = A^{1/3} \int_{\Lambda^2} \frac{d^2 k_{\perp}}{\pi} \varphi_p(k_{\perp}). \quad (2.26)$$

At a first sight, this might look identical to Eq. (2.25), but in reality Eq. (2.26) is meaningless, since the expressions on both sides are logarithmically divergent in the ultraviolet. If, moreover, one introduces an upper cutoff Q^2 to eliminate these divergences, then the ensuing, finite, expressions do not coincide with each other for any finite Q^2 (see below). The would–be divergent pieces (i.e., the contributions proportional to $\ln Q^2$) are indeed the same for both integrals — because $\varphi_A(k_{\perp}) \simeq A^{1/3} \varphi_p(k_{\perp})$ for large $k_{\perp} \gg Q_s(A)$ —, but by itself this property only tells us that the integral in the left hand side of Eq. (2.25) is well defined, but not also that the value of this integral is actually zero. In other terms, the equality of the divergent pieces in Eq. (2.26) carries no information about the behavior of the integrands at intermediate momenta, and thus cannot guarantee the existence of the Cronin peak [23].

Still, as we shall prove below, the difference $\mathcal{G}_A(Q^2) - A^{1/3} \mathcal{G}_p(Q^2)$ vanishes like $1/Q^2$ when $Q^2 \rightarrow \infty$, so the sum–rule (2.25) holds indeed as written. We have defined here:

$$\mathcal{G}_A(Q^2) \equiv \int_{\Lambda^2} \frac{d^2 k_{\perp}}{\pi} \varphi_A(k_{\perp}), \quad (2.27)$$

(together with a similar expression for the proton) which, up to a global factor $\pi R_A^2 \times (N_c^2 - 1)/(2\pi)^2$ (cf. Eq. (2.1)), is the integrated gluon distribution in the MV model, i.e., the total number of gluons having a transverse area $1/Q^2$.

Our proof of Eq. (2.25) is very similar to the original one in Ref. [22], namely it uses the Fourier representation of the integrand (cf. Eqs. (2.4)–(2.5)) to easily perform the integral over k_{\perp} , and thus produce a δ –function $\delta^{(2)}(r_{\perp})$. Then, the sum–rule immediately follows because the integrand vanishes when $r_{\perp} \rightarrow 0$. For instance, in the case of a running coupling, Eq. (2.5), we write (we omit unnecessary constant factors) :

$$\begin{aligned} & \int \frac{d^2 k_{\perp}}{\pi} \int d^2 r_{\perp} e^{-i k_{\perp} \cdot r_{\perp}} \left\{ \frac{1 - e^{-\frac{1}{4} r_{\perp}^2 Q_A^2}}{r_{\perp}^2} - \frac{Q_A^2}{4} \right\} \ln \frac{4}{r_{\perp}^2 \Lambda^2} \\ & \propto \lim_{r_{\perp} \rightarrow 0} \left\{ \frac{1 - e^{-\frac{1}{4} r_{\perp}^2 Q_A^2}}{r_{\perp}^2} - \frac{Q_A^2}{4} \right\} \ln \frac{4}{r_{\perp}^2 \Lambda^2} = 0, \end{aligned} \quad (2.28)$$

which vanishes as $r_{\perp}^2 \ln r_{\perp}^2$ when $r_{\perp} \rightarrow 0$.

If the above integral over k_\perp is restricted to some finite, but large Q^2 , with $Q^2 \gg Q_A^2$, then instead of the δ -function $\delta^{(2)}(r_\perp)$ one generates a smooth distribution in r_\perp which is peaked at $r_\perp = 0$, with the peak height proportional to Q^2 , and the width of the peak of order $1/Q^2$. When integrated over such a distribution, the ‘higher-twist’ terms in Eq. (2.28) (i.e., the higher order terms in the expansion of the exponential) give contributions which vanish as powers of $1/Q^2$ (up to factors of $\ln(Q^2/\Lambda^2)$) when $Q^2 \rightarrow \infty$. The dominant higher-twist contribution, of order $1/Q^2$, turns out to be **negative** (this is explicitly computed in the Appendix). Thus, for a finite, but large, Q^2 , the total number of gluons with transverse area $1/Q^2$ is **smaller** in the MV spectrum of a nucleus than in the corresponding bremsstrahlung spectrum (i.e., than it would be in the absence of non-linear effects). Specifically, one can use the results in the Appendix to deduce that

$$\mathcal{G}_A(Q^2) - \mathcal{G}_{BS}(Q^2) \simeq -\frac{Q_s^4(A)}{2Q^2} \quad \text{for} \quad Q^2 \gg Q_s^2(A), \quad (2.29)$$

with $\mathcal{G}_{BS}(Q^2) \equiv A^{1/3}\mathcal{G}_p(Q^2)$. This is illustrated in Fig. 5.

The sum-rule (2.25) can be understood as the consequence of two basic properties, out of which one is generic — the fact that the non-linear effects fall off as inverse powers of k_\perp^2 in the high-momentum limit —, and the other one is specific to the MV model: the fact that the color sources (here, the valence quarks) are **uncorrelated**. Specifically, for high momenta $k_\perp \gg Q_s$, the unintegrated gluon distribution $\pi R_A^2 \varphi_A(k_\perp)$ is simply proportional to the correlator $\langle \rho_a(k_\perp) \rho_a(-k_\perp) \rangle_A$ of the color charge density in the nucleus (see [12] for details). In the MV model, this correlator is equal to the total color charge squared in the nucleus, which in turn is the same as A times the color charge squared of a single proton (since the color charges of the valence quarks sum up incoherently). This explains why the terms proportional to $\ln Q^2$ in the integrals in Eq. (2.26) are necessarily the same. Moreover, the difference between the respective integrands at finite, but large ($k_\perp \gg Q_s(A)$), momenta falls off as $1/k_\perp^2$, which then explains Eq. (2.29), and thus the sum-rule in Eq. (2.25).

The considerations above also help understanding why the sum rule is bound to fail after taking the quantum evolution with y into account: At $y > 0$, the color sources are predominantly gluons which are themselves products of radiation, and thus are correlated with each other (unlike the valence quarks) even in the leading-twist approximation. Because of that, the gluon occupation factors in the nucleus and in the proton are not simply proportional to each other, not even at high k_\perp . This can be easily verified on Eqs. (3.51) and (3.62), which give the dominant behavior at large momenta. For instance, for fixed coupling, Eq. (3.51) implies (we omit the trivial factor $1/\alpha_s N_c$) :

$$\begin{aligned}
\varphi_A(k_\perp, y) - A^{1/3}\varphi_p(k_\perp, y) &\approx \frac{Q_A^2}{k_\perp^2} \left\{ e^{\sqrt{4\bar{\alpha}_s y \rho(A, k_\perp)}} - e^{\sqrt{4\bar{\alpha}_s y \rho(p, k_\perp)}} \right\} \\
&\approx -\rho_A \frac{Q_A^2}{k_\perp^2} \sqrt{\frac{\bar{\alpha}_s y}{\rho(A, k_\perp)}} e^{\sqrt{4\bar{\alpha}_s y \rho(A, k_\perp)}} \quad \text{for } k_\perp \gg Q_s(A, y),
\end{aligned} \tag{2.30}$$

where the second line has been obtained by writing $\rho(p, k_\perp) \equiv \ln k_\perp^2/Q_p^2 = \rho(A, k_\perp) + \rho_A$, and keeping only the leading term at large $\rho(A, k_\perp)$. Although the expression above does vanish as $k_\perp \rightarrow \infty$, it is clear that it is not integrable in the sense of Eq. (2.25). The very fact that the sum–rule fails to apply at $y > 0$ does not preclude the existence of the Cronin peak: The sum–rule is only a **sufficient** condition for the existence of the peak, but not also a **necessary** one. And indeed the peak does persist (although its height is rapidly decreasing) in the early stages of the evolution, as we shall show in Sect. 5. This is also seen in the numerical results in Ref. [23].

If the difference in Eq. (2.30) is integrated up to some large momentum Q^2 , the result is clearly negative⁴, and divergent as $Q^2 \rightarrow \infty$. This is, of course, consistent with the high- k_\perp suppression of the ratio \mathcal{R}_{pA} at $y > 0$, to be discussed in the next section.

Returning to the MV model, where the sum–rule (2.25) is valid, it is instructive to understand its physical implications in more detail: Eq. (2.25) tells us that the net result of the non–linear effects in the gluon dynamics is merely a **redistribution** of the gluons in the transverse momentum space. As it should be clear from the previous arguments, and also from the plot in Fig. 3, this redistribution is associated with repulsive interactions which push the gluons towards the modes with larger momenta. In Fig. 3 one can see that, whereas at low momenta $k_\perp < Q_c(A)$ the gluon occupation factor is larger for the bremsstrahlung spectrum than for the MV spectrum, at higher momenta $k_\perp > Q_c(A)$ the opposite situation occurs. Here, $Q_c(A)$ is defined by⁵ (see Eq. (2.9)):

$$\frac{Q_A^2}{k_\perp^2} \sim \ln \frac{Q_s^2(A)}{k_\perp^2} \quad \text{for } k_\perp \sim Q_c(A), \tag{2.31}$$

which implies :

$$Q_c^2(A) \simeq \frac{Q_A^2}{\ln \frac{Q_s^2(A)}{Q_c^2(A)}} \simeq \frac{Q_A^2}{\ln \frac{Q_s^2(A)}{Q_A^2}} \simeq \frac{Q_s^2(A)}{\rho_A \ln \rho_A}, \tag{2.32}$$

⁴ The fact that this is negative has nothing to do with the shadowing by higher twist effects (as was the case for the MV model; see Eq. (2.29)). Rather, it is again the property that the proton evolves faster than the nucleus, as explained in Sect. 4.

⁵ The subsequent formulae in this subsection are written for the case of a fixed coupling, for definiteness. It can be easily checked that analog formulae, leading to similar conclusions, apply also for the MV model with a running coupling.

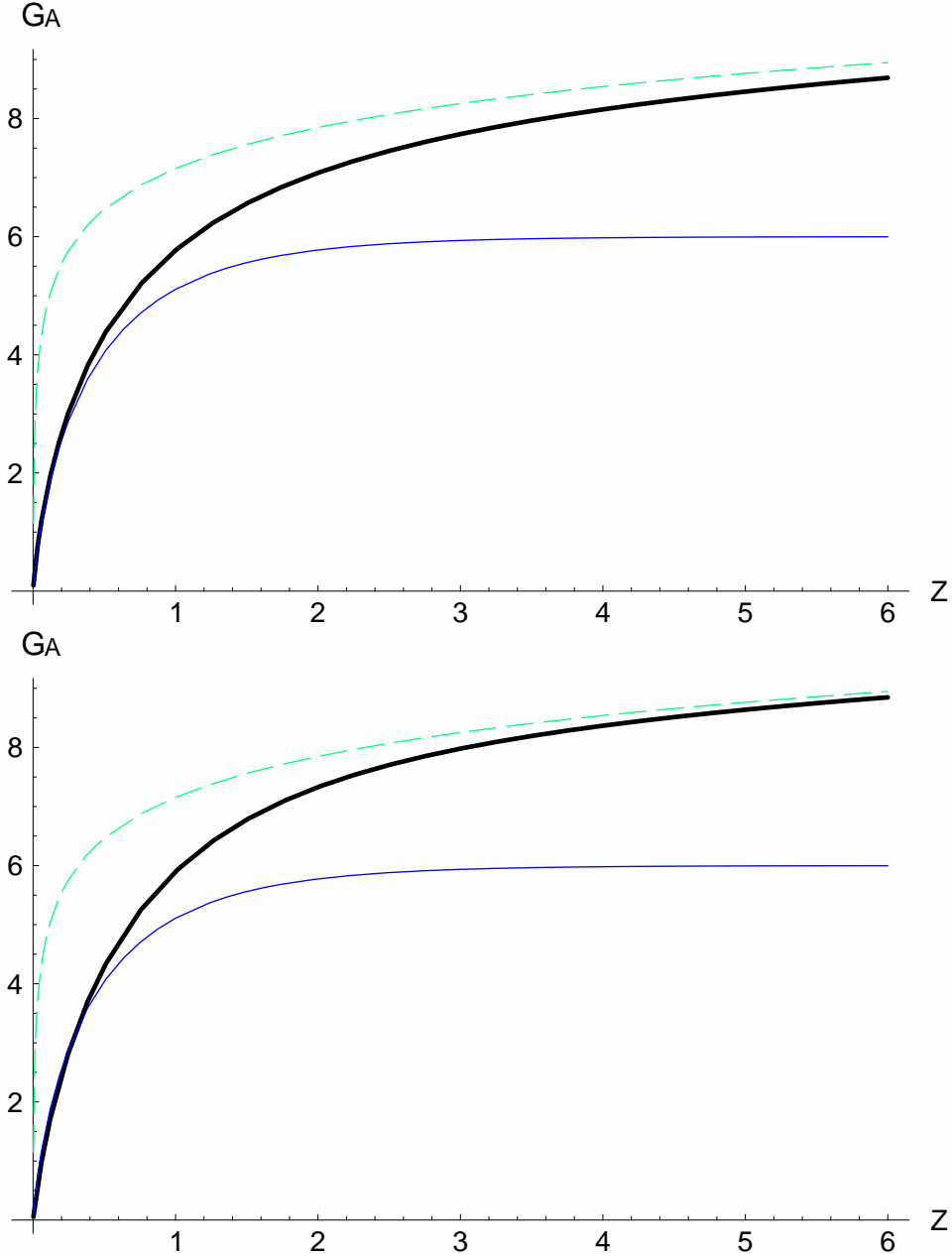


Fig. 5. The integrated gluon distribution function $\mathcal{G}_A(Z)$ as a function of the scaled momentum variable $Z = Q^2/Q_s^2(A)$ in fixed and running coupling McLerran-Venugopalan model for $\rho_A = 6$. The black (thick) line corresponds to the integrated gluon distribution function $\mathcal{G}_A(Z)$; the blue (solid) line shows the saturation contribution $\mathcal{G}_A^{\text{sat}}(Z)$; the green (dashed) line represents the bremsstrahlung distribution function.

where we have also used $Q_s^2(A) = Q_A^2 \rho_A$, cf. Eq. (2.7). It is easily checked that $\Lambda^2 \ll Q_c^2(A) \ll Q_s^2(A)$ (since $\rho_A \gg 1$).

Thus, the effect of the interactions is to move the gluons up in transverse momentum, from below to above $Q_c(A)$. This explains, in particular, why when counting the gluons up to a finite (large) Q^2 , one necessarily finds a smaller number for the MV spectrum than for the bremsstrahlung one, cf. Eq. (2.29). But as we shall explain now, at large $k_\perp \gg Q_s(A)$ the effects of this redistribution are only tiny: **Most of the gluons which are in excess in the bremsstrahlung spectrum at $k_\perp < Q_c(A)$ are found in the MV spectrum in the saturation region at $k_\perp \lesssim Q_s(A)$.** In particular, the enhancement factor $1/\alpha_s \sim \rho_A$ characteristic of saturation finds its origin in the phase-space for bremsstrahlung radiation at momenta $\Lambda < k_\perp < Q_c(A)$. This factor is large because of the infrared sensitivity of the bremsstrahlung spectrum.

A simple way to see this is to notice that the total number of gluons in the region $\Lambda < k_\perp < Q_s(A)$ is essentially the same for both the bremsstrahlung spectrum and the MV spectrum, which shows that the bremsstrahlung gluons in excess at $k_\perp < Q_c(A)$ have been redistributed in the MV spectrum within the range $Q_c(A) < k_\perp < Q_s(A)$. Indeed, we have first :

$$\mathcal{G}_{BS}(Q_s^2(A)) = \int_{\Lambda^2}^{Q_s^2(A)} \frac{d^2 k_\perp}{\pi} \frac{1}{\alpha_s N_c} \frac{Q_A^2}{k_\perp^2} = \frac{Q_A^2}{\alpha_s N_c} \ln \frac{Q_s^2(A)}{\Lambda^2} = \frac{Q_s^2(A)}{\alpha_s N_c}, \quad (2.33)$$

where the saturation momentum $Q_s(A)$ has been reconstructed as $Q_s^2(A) = Q_A^2 \rho_A$, cf. Eq. (2.7). Note that the large factor $\rho_A = \ln Q_s^2(A)/\Lambda^2$ has been generated from the phase-space for the bremsstrahlung gluons at $\Lambda < k_\perp < Q_s(A)$. For the MV spectrum, we shall define $\mathcal{G}_A(Q_s^2(A))$ as the total number of gluons contained in the saturating component of the spectrum $\varphi_A^{\text{sat}}(k_\perp)$. This is appropriate since $\varphi_A(k_\perp) \approx \varphi_A^{\text{sat}}(k_\perp)$ for any $k_\perp < Q_s(A)$, whereas at larger momenta $\varphi_A^{\text{sat}}(k_\perp)$ falls off exponentially. One then obtains:

$$\mathcal{G}_A(Q_s^2(A)) = \int \frac{d^2 k_\perp}{\pi} \frac{1}{\alpha_s N_c} \Gamma(0, k_\perp^2/Q_s^2(A)) = \frac{Q_s^2(A)}{\alpha_s N_c}. \quad (2.34)$$

(The simplest way to obtain this result is to notice that the unrestricted integral of $\varphi_A^{\text{sat}}(k_\perp)$ is tantamount to letting $r_\perp \rightarrow 0$ in the integral representation of $\varphi_A^{\text{sat}}(k_\perp)$ in Eq. (2.15).) As anticipated, the final expressions in Eqs. (2.33) and (2.34) are identical. But, of course, although the total number of gluons at $\Lambda < k_\perp < Q_s(A)$ is the same in both spectra, the way how these gluons are distributed in k_\perp is very different in the two cases: For the bremsstrahlung spectrum, which is infrared divergent, most of these gluons are located at low momenta $k_\perp < Q_c(A)$, while for the MV spectrum they are rather uniformly distributed at all momenta up to $Q_s(A)$. For instance (see Eq. (2.32)):

$$\mathcal{G}_{BS}(Q_c^2(A)) = \int_{\Lambda^2}^{Q_c^2(A)} \frac{d^2 k_\perp}{\pi} \frac{1}{\alpha_s N_c} \frac{Q_A^2}{k_\perp^2} = \frac{Q_A^2}{\alpha_s N_c} \ln \frac{Q_c^2(A)}{\Lambda^2} \approx \frac{Q_A^2}{\alpha_s N_c} (\rho_A - \ln \rho_A), \quad (2.35)$$

is almost the same as the result in Eq. (2.33) (in particular, it includes already the enhancement factor ρ_A due to the logarithmic phase-space⁶).

The above considerations together with the sum-rule (2.25) tell us that also the total number of gluons **above** $Q_s(A)$ must be the same in both spectra. More precisely, with a large upper cutoff Q^2 , we have (cf. the Appendix)

$$\frac{Q_A^2}{\alpha_s N_c} \ln \frac{Q^2}{Q_s^2(A)} = \int^{Q^2} \frac{d^2 k_\perp}{\pi} \varphi_A^{\text{twist}}(k_\perp) + \frac{1}{\alpha_s N_c} \frac{Q_A^4}{Q^2} \ln \frac{Q^2}{Q_s^2(A)}, \quad (2.36)$$

where the expression in the l.h.s. is the number of bremsstrahlung gluons with momenta in the range $Q_s(A) < k_\perp < Q$, while in the r.h.s. we have the ‘twist’ distribution in the MV spectrum integrated up to Q^2 .

3 Non-linear gluon evolution in the Color Glass Condensate

Within the effective theory for the CGC [24], the evolution of the gluon distribution with y is not described by a single, closed, equation, but rather by an infinite hierarchy of coupled equations, which relate n -point functions with arbitrary $n \geq 2$ (by itself, $\varphi(k_\perp, y)$ corresponds to a 2-point function), and are compactly summarized in a *functional* evolution equation, the JIMWLK equation. Fortunately, this complicated evolution simplifies considerably in interesting limiting cases, which are tractable through analytic approximations [33, 34].

At low momenta $k_\perp \lesssim Q_s(A, y)$, the gluons form a condensate with occupation factors of order $1/\alpha_s$, and the dynamics is highly non-linear. Still, one can rely on mean field approximations to deduce a formula for $\varphi(k_\perp, y)$ valid in the low momentum limit $k_\perp \ll Q_s(A, y)$ [33–35, 56], which will be presented in Sect. 3.1 below.

At high momenta $k_\perp \gg Q_s(A, y)$, the gluon density is low, and non-linear effects in the evolution become negligible. Then, to lowest order in α_s , the general equations for the evolution of the gluon distribution boil down to a single, linear, equation: the BFKL equation [41]. The latter controls also the approach towards saturation from the above (at least, approximately), and thus determines the saturation momentum $Q_s(A, y)$ [7, 36–39].

⁶ Although $Q_c^2(A) \approx Q_s^2(A)/\rho_A \ll Q_s^2(A)$, the logarithmic phase-space at $\Lambda < k_\perp < Q_c(A)$ (namely $\rho_A - \ln \rho_A$) is almost the same as that for the whole interval $\Lambda < k_\perp < Q_s(A)$ (which is equal to ρ_A).

To obtain analytic formulae, we shall consider the solution to the BFKL equation in the saddle point approximation and with saturation boundary conditions, as constructed in Refs. [36–39] (see however [46]). Although the detailed construction of this solution can be found in the original papers, we shall nevertheless outline a few steps in its derivation, in Sect. 3.2, in order to emphasize a subtle point — namely, the fact that it is the saturation scale in the initial conditions, $Q_s(A)$, which sets the infrared cutoff for the transverse phase-space available for evolution [40] —, and also to prepare the ground for a general discussion of high- k_\perp suppression through quantum evolution, to be presented in Sect. 4.

Within the general saddle point approximation, we shall distinguish between two physical regimes, which are controlled by different saddle points : the (more standard) ‘DLA regime’ at very high momenta, and a ‘BFKL regime’ at intermediate momenta (k_\perp above, but not far above, $Q_s(A, y)$), which is the linear regime precursory of saturation. Strictly speaking, the transition between these two regimes is not analytically under control, but an approximate matching will be performed in the case of a fixed coupling.

The BFKL solution will be presented with both fixed and running coupling, with the scale for running set either by the momentum k_\perp of the gluon (in the DLA regime), or by the saturation momentum (in the BFKL regime).

3.1 *Non-linear evolution at low k_\perp : Saturation and universality*

In the high density regime deeply at saturation ($k_\perp \ll Q_s(A, y)$), the color fields are strong ($A^i \sim 1/g$) and the dynamics is fully non-linear, which makes it difficult to use standard perturbative techniques. On the other hand, these conditions are favorable to the use of mean field approximations [33, 34], which enable us to determine the y - and k_\perp -dependencies of the gluon occupation factor. Similar results are obtained also from studies of the unitarization effects in dipole-hadron scattering [35, 56].

Remarkably, it turns out that the functional form of the gluon occupation factor at saturation is **universal** [33]: For $k_\perp \ll Q_s(A, y)$, $\varphi_A(k_\perp, y)$ is independent of either the initial condition at $y = 0$, or the details of the evolution leading to saturation, except for the corresponding dependencies of the saturation scale itself. Moreover, this universal form happens to be the same as in the MV model (cf. the expressions in the second lines of Eqs. (2.9) and (2.10)), which is quite non-trivial, and to some extent surprising, since the physical conditions leading to this functional form are very different in the two cases: Whereas in the MV model the color sources are uncorrelated, and the logarithmic behavior at low k_\perp is merely the result of non-linear effects in the classical equations of motions for the color fields [12, 28], in the effective theory at small x the color sources are strongly correlated, in such a way to ensure color neutrality over a transverse size $\sim 1/Q_s(A, y)$ [33, 34, 56], and the logarithmic behavior at low k_\perp is already encoded in the correlations

of the color sources (i.e., it holds independently of the presence of non-linear terms in the classical field equations; the latter affect only the overall normalization of the gluon distribution, which in this non-linear regime is anyway not under control).

Specifically, for fixed coupling, one finds [33–35] :

$$\varphi_A(k_\perp, y) \approx \frac{a_0}{\alpha_s N_c} \ln \frac{Q_s^2(A, y)}{k_\perp^2}, \quad (\text{fixed coupling}), \quad (3.37)$$

whereas for running coupling (with the scale for running set by the gluon momentum k_\perp) one obtains [12, 56].

$$\varphi_A(k_\perp, y) \approx \frac{a_0}{N_c} \left\langle \frac{1}{\alpha_s} \right\rangle \ln \frac{Q_s^2(A, y)}{k_\perp^2}, \quad (\text{running coupling}), \quad (3.38)$$

with (compare to Eq. (2.11)) :

$$\left\langle \frac{1}{\alpha_s} \right\rangle \equiv \frac{1}{2b_0} \left\{ \ln \frac{Q_s^2(A, y)}{\Lambda^2} + \ln \frac{k_\perp^2}{\Lambda^2} \right\}. \quad (3.39)$$

The overall factor a_0 in these equations is a number of order one which cannot be computed analytically (and which needs not be the same for fixed and running coupling).

Note that, in the fixed coupling case, the gluon distribution at saturation depends upon the two kinematical variables k_\perp and y only via the ratio $z \equiv k_\perp^2/Q_s^2(A, y)$. This property, known as **geometric scaling** [49], reflects the fact that the saturation momentum is the only intrinsic scale at saturation. As manifest on Eq. (3.38), the running of the coupling introduces a second intrinsic scale, namely Λ , and this is a source of geometric scaling violations, which are however under control.

3.2 Linear evolution at high k_\perp : Fixed coupling

In the low density regime at high momenta $k_\perp \gg Q_s(A, y)$, the dynamics is linear, and the nuclear gluon occupation factor can be obtained (to the present accuracy) by solving the BFKL equation [41] with initial conditions at $y = 0$ provided by the MV model (cf. Eq. (2.4)–(2.5)) and with an ‘absorptive’ boundary condition at $k_\perp \sim Q_s(A, y)$ [37, 38] which mimics the non-linear effects in the approach towards saturation. (Similar results have been recently obtained [39] through direct studies of the non-linear Kovchegov equation [30, 31].) In particular, the saturation scale itself is obtained by requiring $\varphi_A(k_\perp, y)$ to become of order $1/\alpha_s$ at saturation (up to subleading terms of $\mathcal{O}(1)$) :

$$\varphi_A(k_\perp, y) \simeq \frac{\kappa}{\alpha_s(Q_s^2(A, y))N_c} \quad \text{for} \quad k_\perp \sim Q_s(A, y). \quad (3.40)$$

(κ is a number of order one.)

When y and/or k_\perp are relatively large (see below), an approximate analytic solution can be obtained, via a saddle point approximation. Here we shall outline only a few steps in the construction of this solution (see Refs. [36, 37] for details).

For fixed coupling, the solution to the BFKL equation for $\varphi_A(k_\perp, y)$ can be written in Mellin form as:

$$\varphi_A(k_\perp, y) = \int_C \frac{d\gamma}{2\pi i} \left(\frac{Q_0^2}{k_\perp^2} \right)^\gamma e^{\bar{\alpha}_s y \chi(\gamma)} \widetilde{\varphi}_A(\gamma; Q_0), \quad (3.41)$$

where $\bar{\alpha}_s = \alpha_s N_c / \pi$, $\chi(\gamma) = 2\psi(1) - \psi(\gamma) - \psi(1 - \gamma)$ with $\psi(\gamma) \equiv d \ln \Gamma(\gamma) / d\gamma$ and complex γ is the eigenvalue of the BFKL kernel, $\widetilde{\varphi}_A(\gamma; Q_0)$ is the Mellin transform of the initial condition $\varphi_A(k_\perp)$, Eq. (2.4):

$$\widetilde{\varphi}_A(\gamma; Q_0) = \int_0^\infty \frac{dk_\perp^2}{k_\perp^2} \left(\frac{k_\perp^2}{Q_0^2} \right)^\gamma \varphi_A(k_\perp), \quad (3.42)$$

and Q_0 is an arbitrary reference scale introduced for dimensional reasons, and which drops out in the complete result, as obvious on the above equations. Given the behavior of the initial distribution $\varphi_A(k_\perp)$ in various limits, cf. Eq. (2.9), it can be checked that the integral over k_\perp^2 in Eq. (3.42) is absolutely convergent for $0 < \text{Re } \gamma < 1$. Thus the contour for the complex integration in Eq. (3.41) can be chosen as $C = \{\gamma = \gamma_1 + i\gamma_2; -\infty < \gamma_2 < \infty\}$, with a fixed γ_1 in the range $0 < \gamma_1 < 1$.

The same study of the convergence properties of the integral in Eq. (3.42) tells us that this integral is dominated by momenta of the order of the initial saturation momentum $Q_s(A)$: Indeed, for large $k_\perp \gg Q_s(A)$, $\varphi_A(k_\perp) \propto 1/k_\perp^2$, and the integral is saturated by momenta of the order of the lower cutoff $Q_s(A)$. Furthermore, for low momenta $k_\perp \ll Q_s(A)$, the initial distribution saturates: $\varphi_A(k_\perp) \propto \ln(Q_s^2/k_\perp^2)$, so the integral is now dominated by momenta near the upper cutoff, i.e., by $k_\perp \sim Q_s(A)$ once again. Thus, after performing the integral over k_\perp , $Q_s(A)$ replaces Q_0 as the natural reference scale in the Mellin representation of the solution $\varphi_A(k_\perp, y)$. Then, Eq. (3.41) can be rewritten as:

$$\varphi_A(k_\perp, y) = \frac{1}{\alpha_s N_c} \int_C \frac{d\gamma}{2\pi i} \left(\frac{Q_s^2(A)}{k_\perp^2} \right)^\gamma e^{\bar{\alpha}_s y \chi(\gamma)} \widetilde{\varphi}_A(\gamma; \rho_A), \quad (3.43)$$

where any reference to the arbitrary scale Q_0 has disappeared. Note that, for more clarity, we have extracted a factor $1/\alpha_s N_c$ out of the (Mellin transform of) the initial condition $\widetilde{\varphi}_A(\gamma; \rho_A)$. The latter still depends upon $Q_s(A)$, but only logarithmically, via $\rho_A \equiv \ln(Q_s^2(A)/\Lambda^2)$. The precise form of the function $\widetilde{\varphi}_A(\gamma; \rho_A)$ will not be needed in

what follows. Rather, we shall use its approximate form which is obtained when $\varphi_A(k_\perp)$ in Eq. (3.42) is replaced by the simplest interpolation between the asymptotic behaviors shown in Eq. (2.9). This reads :

$$\widetilde{\varphi}_A(\gamma; \rho_A) \approx \frac{1}{\rho_A} \frac{1}{1-\gamma} + \frac{1}{\gamma^2}. \quad (3.44)$$

The first term, which has a pole at $\gamma = 1$ and is suppressed as $1/\rho_A$, comes from the high- k_\perp behavior (the bremsstrahlung spectrum in Eqs. (2.9)), while the second term, with a double pole at $\gamma = 0$, comes from the saturating behavior at low k_\perp .

3.2.1 The saddle point approximation

At this stage, it becomes natural to introduce the logarithmic momentum variable $\rho \equiv \ln(k_\perp^2/Q_s^2(A)) = \rho(A, k_\perp)$, and notice that, when either $\bar{\alpha}_s y$, or ρ , or both, are large, the integral in Eq. (3.43) can be evaluated via a saddle point approximation. Specifically, if one writes:

$$\varphi_A(k_\perp, y) = \frac{1}{\alpha_s N_c} \int_C \frac{d\gamma}{2\pi i} e^{\bar{\alpha}_s y F(\gamma, r)} \widetilde{\varphi}_A(\gamma; \rho_A), \quad (3.45)$$

where:

$$r \equiv \frac{\rho}{\bar{\alpha}_s y}, \quad F(\gamma, r) = -\gamma r + \chi(\gamma), \quad (3.46)$$

then the saddle point $\gamma_0 \equiv \gamma_0(r)$ satisfies the condition:

$$\left. \frac{\partial F}{\partial \gamma}(\gamma, r) \right|_{\gamma=\gamma_0(r)} = -r + \chi'(\gamma_0(r)) = 0, \quad (3.47)$$

which shows that $\gamma_0(r)$ is a real number, in between 0 and 1. The behavior of the function $\chi(\gamma)$ in this range is illustrated in Fig. 6.

After expanding around the saddle point and performing the Gaussian integral over the small fluctuations, one obtains :

$$\varphi_A(k_\perp, y) \approx \frac{1}{\alpha_s N_c} \frac{e^{\bar{\alpha}_s y F(\gamma_0, r)}}{\sqrt{2\pi \bar{\alpha}_s y \chi''(\gamma_0)}} \widetilde{\varphi}_A(\gamma_0; \rho_A). \quad (3.48)$$

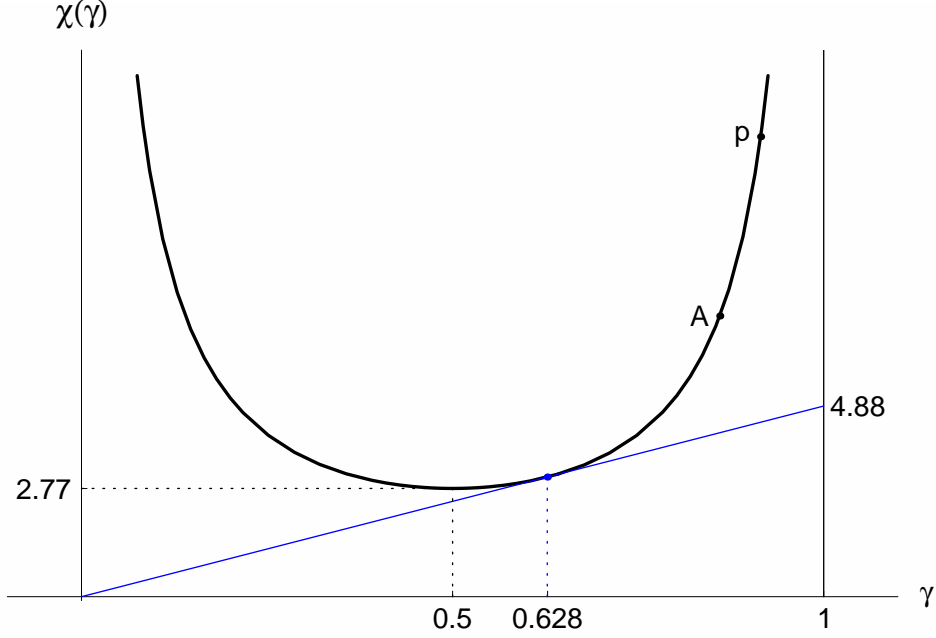


Fig. 6. The BFKL eigenvalue $\chi(\gamma)$ and the graphical solution to the saturation problem. The value $\gamma_s = 0.628$ corresponds to the saturation saddle point and the value $\chi(\gamma_s)/\gamma_s = 4.88$ determines the asymptotic energy dependence of the saturation momentum (for comparison, the “hard pomeron” saddle point $\gamma_{\mathbb{P}} = 1/2$ and its intercept $\omega_{\mathbb{P}} = 4 \ln 2 = 2.77$ are shown). The points \mathbb{p} and \mathbb{A} correspond to the proton and the nucleus respectively, for the same transverse momentum and rapidity, when they are far above the saturation scale.

This is a reasonable approximation to Eq. (3.43) provided $\bar{\alpha}_s y \gtrsim 1$, $\rho \gtrsim 1$, and at least one of these quantities is much larger than one.

When r varies from 0 to ∞ , the function $\gamma_0(r)$ is monotonously increasing, and spans the range from $\gamma_0(0) = 1/2$ to $\gamma_0(\infty) = 1$. Note, however, that physically the ratio r cannot be smaller than the value $r_s \equiv \rho_s(y)/\bar{\alpha}_s y$ (with $\rho_s(y) \equiv \ln[Q_s^2(A, y)/Q_s^2(A)]$) which corresponds to the saturation momentum. Indeed, the linear approximation is justified only as long as $k_{\perp} \gg Q_s(A, y)$, or $\rho > \rho_s(y)$.

To compute the saturation momentum, and the corresponding saddle point $\gamma_s \equiv \gamma_0(r_s)$, we shall use the saturation boundary condition (3.40), together with the approximation (3.48) for $\varphi_A(k_{\perp}, y)$, which for this purpose is extrapolated down to $k_{\perp} \sim Q_s(A, y)$. It can be justified that this is a legitimate procedure for the calculation of the energy dependence of $Q_s(A, y)$, although not necessarily also for its absolute normalization [36, 37]. To the accuracy of interest here, Eqs. (3.48) and (3.40) imply just that the exponent in Eq. (3.48) must vanish on the saturation line:

$$F(\gamma_0(r), r) \Big|_{r=r_s} \equiv -\gamma_s r_s + \chi(\gamma_s) = 0, \quad (3.49)$$

which shows that r_s is a pure number, to be denoted as c in what follows. This number together with γ_s are determined by Eqs. (3.47) and (3.49) as: $\gamma_s = \chi(\gamma_s)/\chi'(\gamma_s) = 0.627\dots$ and $c \equiv r_s = \chi'(\gamma_s) = 4.883\dots$ [7, 35–37].

Note that in writing the saturation condition in the form (3.49) we have neglected the effect of the Gaussian fluctuations around the saddle point. The reason is that this effect is modified by the absorptive boundary condition at saturation [37] (that we neglect here), and thus cannot be correctly computed in the present approximations. As a general rule, we shall always ignore such slowly varying prefactors, but only include the dominant behavior at high energy. To the same accuracy, the nuclear saturation momentum reads:

$$Q_s^2(A, y) \simeq Q_s^2(A) e^{c\bar{\alpha}_s y}, \quad c = 4.883\dots \quad (3.50)$$

This expression appears to satisfy the initial condition $Q_s^2(A, y = 0) = Q_s^2(A)$, but this is only formal, since the calculation above is valid only for relatively large y , with $\alpha_s y > 1$, so the extrapolation to $y \rightarrow 0$ is not justified. In fact, the energy dependence of $Q_s^2(A, y)$ displayed in Eq. (3.50) is only the first term in an asymptotic expansion at large y , out of which also the second term [37, 38] and the third one [39] are presently known.

For practical purposes, the saddle point approximation (3.48) is still quite involved, since the function $\gamma_0(r)$ is known only implicitly, as the solution to Eq. (3.47). However, important simplifications leading to fully explicit formulae can be performed either for very large momenta, $\rho \gg \bar{\alpha}_s y$ — this corresponds to the so-called “double-logarithmic accuracy”, or DLA, regime —, or for momenta above, but relatively close to the saturation scale, where one can expand Eq. (3.48) around the saturation saddle point. Below, we shall refer to the latter regime as the “BFKL regime”⁷.

Let us briefly describe here the modifications which should be brought into the previous formulae in order to adapt them to the case of a proton. Recall that there is no saturation scale (i.e., no analog of the nuclear scale $Q_s(A)$) in the proton at $y = 0$. The infrared cutoff is rather set by the scale Q_p which is soft and reflects non-perturbative physics (cf. Eq. (2.18)). This is therefore also the scale which enters the formulae for the linear evolution of $\varphi_p(k_\perp, y)$ with increasing y . E.g., the proton analog of Eq. (3.43) is obtained by replacing $Q_s(A) \rightarrow Q_p$ and taking an initial condition $\widetilde{\varphi}_p(\gamma) = 1/(1 - \gamma)$ (compare to Eq. (3.44)). In particular, the variable ρ for the proton is defined as $\rho(p, k_\perp) \equiv \ln(k_\perp^2/Q_p^2)$. Of course, for sufficiently large y , the gluon density in the proton will become large, and a (hard) saturation scale $Q_s(p, y)$ will be eventually generated. The dominant y -dependence

⁷ Note that this is not the usual BFKL regime associated with the saddle point $\gamma_{\mathbb{P}} = 1/2$ and corresponding to the high energy limit $\alpha_s y \gg \rho$. Whereas $\gamma_{\mathbb{P}} = 1/2$ describes the evolution with y at fixed (and relatively low) k_\perp , $\gamma_s = 0.63$ corresponds rather to an evolution where, when increasing y , k_\perp is correspondingly increased, in such a way that the condition $k_\perp^2 > Q_s^2(A, Y)$ (or $\rho > \rho_s(Y)$) remains satisfied.

of this scale at large y is described again by Eq. (3.50), but with $Q_s(A) \rightarrow Q_p$. More generally, all the formulae to be obtained below in this section can be translated to the case of a proton by replacing everywhere $Q_s(A) \rightarrow Q_p$.

3.2.2 DLA regime

If $\rho \gg \alpha_s y$, the saddle point is close to one, and only the first term (the one having a pole at $\gamma = 1$) must be retained in the initial condition (3.44). A straightforward calculation yields $\gamma_0(r) \approx 1 - 1/\sqrt{r}$, and :

$$\varphi_A(k_\perp, y) \simeq \frac{1}{\alpha_s N_c} \frac{Q_A^2}{k_\perp^2} \frac{e^{\sqrt{4\bar{\alpha}_s y \rho}}}{\sqrt{2\pi\sqrt{4\bar{\alpha}_s y \rho}}}, \quad (3.51)$$

where the factor Q_A^2 has been reconstructed as $Q_s^2(A)/\rho_A$. This approximation is valid for $\bar{\alpha}_s y \rho \gg 1$, and as long as this condition is satisfied, Eq. (3.51) can be even used for relatively small y , with $\bar{\alpha}_s y \ll 1$. Indeed, in this regime Eq. (3.51) can be obtained from the DGLAP equation [57], which provides a resummation based on the assumptions that $\alpha_s \rho \geq 1$, but $\alpha_s y \ll 1$.

3.2.3 BFKL regime: weak universality and approximate scaling

When ρ is larger than $\rho_s(y) \equiv \ln(Q_s^2(A, y)/Q_s^2(A)) = c\bar{\alpha}_s y$, but not **much** larger, one can obtain an explicit form for $\varphi_A(k_\perp, y)$ by expanding the general saddle point approximation, Eq. (3.48), in powers of $r - r_s$ (or, equivalently, in powers of $(\rho - \rho_s)/\rho_s$). To second order in this expansion, one obtains [36–39]

$$\varphi_A(k_\perp, y) \approx \frac{\kappa_0}{\alpha_s N_c} \left\{ \rho - \rho_s + \frac{1}{\Delta} \right\} e^{-\gamma_s(\rho - \rho_s)} \exp \left\{ -\frac{(\rho - \rho_s)^2}{2\beta\bar{\alpha}_s y} \right\}, \quad (3.52)$$

or, more explicitly [recall that $\rho - \rho_s = \ln(k_\perp^2/Q_s^2(A, y))$] :

$$\varphi_A(k_\perp, y) \approx \frac{\kappa_0}{\alpha_s N_c} \left\{ \ln \frac{k_\perp^2}{Q_s^2(A, y)} + \frac{1}{\Delta} \right\} \left(\frac{Q_s^2(A, y)}{k_\perp^2} \right)^{\gamma_s} \exp \left\{ -\frac{1}{2\beta\bar{\alpha}_s y} \ln^2 \frac{k_\perp^2}{Q_s^2(A, y)} \right\} \quad (3.53)$$

In these equations, $\gamma_s \simeq 0.63$ appears as an “anomalous dimension” (recall that, at very high k_\perp , the actual power of $1/k_\perp^2$ was one, both in the initial condition at $y = 0$, and in the DLA approximation (3.51) at $y > 0$). Furthermore, $\beta \equiv \chi''(\gamma_s) = 48.518\dots$ plays the role of a diffusion coefficient for the diffusion in $\ln(k_\perp^2/Q_s^2)$. The constant numbers κ_0 and Δ are not known, as they depend upon the detailed matching onto the (unknown)

solution in the transition region around $Q_s(A, y)$. Thus, it makes no sense, for instance, to try and match Eqs. (3.53) and (3.40). Still, it seems natural to impose $\Delta \leq \gamma$, to avoid that Eq. (3.53) become a decreasing function of $1/k_{\perp}^2$ when approaching $Q_s(A, y)$ from the above.

An important property of Eq. (3.53), that we shall refer to as **weak universality** (as opposed to the **strong universality** that has been found at saturation [33]) is the fact that the functional form of this expression, seen as a function of $z \equiv k_{\perp}^2/Q_s^2(A, y)$ and y , is independent of the initial condition at $y = 0$, but rather is fully determined by the quantum (BFKL) evolution together with the saturation boundary condition. The initial condition affects only the value of the saturation momentum, cf. Eq. (3.50) [40].

The factor linear in $\rho - \rho_s$ in the right hand side of Eq. (3.52), or (3.53), does not come from the expansion of Eq. (3.48), but rather from the absorptive boundary condition at saturation [37, 39], that we have ignored so far. The reason why this factor cannot be neglected (in contrast, e.g., with the prefactor in the expression (3.50) for the saturation scale) is that this factor is not suppressed at large y , and thus must be treated as a leading-order effect. The other factors in Eq. (3.52), which involve $\rho - \rho_s$ in the exponent, do come from the expansion of Eq. (3.48). A priori, one would expect this expansion to be valid so long as $(\rho - \rho_s)/\rho_s \ll 1$, since this is the “small parameter”. However, since β is a relatively large number, the second order term in the expansion, quadratic in $\rho - \rho_s$, remains small as compared to the linear term even for $\rho - \rho_s \sim \rho_s$. We conclude that Eq. (3.52) (or (3.53)) is a good approximation for any ρ within the following range [36] :

$$0 < \rho - \rho_s(y) \simeq \rho_s(y), \tag{3.54}$$

often referred to as the “extended scaling window”, since within this range the BFKL solution approximately preserves the geometric scaling property characteristic of saturation [36, 37]: More precisely, Eq. (3.52) shows scaling so long as $\rho - \rho_s(y) \ll \sqrt{2\beta\bar{\alpha}_s y}$, whereas for larger ρ , the scaling is violated by the diffusion term. Both the scaling property, and its violation, seem to be necessary to understand the small- x data at HERA [49, 58, 59].

3.2.4 The geometric scaling line : Approximately matching BFKL and DLA

The approximate solutions that we have found so far apply in different kinematical regions — $\rho \gg \alpha_s y$ for the DLA formula (3.51), and $\rho - \rho_s \lesssim \rho_s$ for the BFKL expression (3.52) —, which have no overlap with each other. So, a priori, there seems to be no reason why these expressions could be matched onto each other. Still, if one chooses $\rho = 2\rho_s(y) = 2c\bar{\alpha}_s y$, and one estimates both the DLA and the BFKL expressions along this line, then one finds that the dominant (exponential) behavior in y is very similar, although not exactly the same, for both approximations. This is in agreement with an observation [36] that

the **geometric scaling line** $\rho = 2\rho_s(y)$ is approximately the borderline between the regions dominated by the saturation saddle point and, respectively, by the DLA saddle point in the $y - \ln k_\perp^2$ plane.

This opens the possibility to achieve at least an **approximate matching** between the two limiting expressions, by appropriately tuning the borderline between these two regime. Of course, there is no fundamental reason in favor of this matching, but this will be convenient in practice, as it will allow us to avoid exponentially large discontinuities when studying the ratio \mathcal{R}_{pA} in different regimes. Specifically, we shall tune the upper limit in the window (3.54) in such a way that the leading, exponential, behavior along that line be exactly the same for the DLA and BFKL approximations with fixed coupling. A straightforward calculation shows that Eq. (3.54) must be replaced by

$$0 < \rho - \rho_s(y) \leq \nu\rho_s(y), \quad (3.55)$$

or, equivalently,

$$Q_s^2(A, y) \ll k_\perp^2 < Q_g^2(A, y) \equiv Q_s^2(A, y) \left(\frac{Q_s^2(A, y)}{Q_s^2(A)} \right)^\nu, \quad (3.56)$$

with $\nu \approx 1.647$ determined by solving the following equation:

$$c[(1 - \gamma_s)\nu + 1] - \sqrt{4c(\nu + 1)} - \frac{(\nu c)^2}{2\beta} = 0. \quad (3.57)$$

As anticipated, ν is a number of order one.

3.3 Linear evolution at high k_\perp : Running coupling

Since the (leading-order) BFKL equation corresponds to a fixed-coupling approximation, the inclusion of running is a priori ambiguous. Physical arguments, together with recent experience [38, 43] with the next-to-leading order BFKL equation [42], suggest that it should be appropriate to use a coupling which is running with the transverse momentum k_\perp of the gluon [i.e., $\alpha_s(k_\perp^2)$]. This running has been already used in obtaining Eq. (3.38).

Since the running is only logarithmic, one expects that, for momenta within the scaling window (3.56), there should be also possible to use the running with the saturation momentum [i.e., $\alpha_s(Q_s^2(A, y))$]. This is confirmed by the analyses in Refs. [36–38] which show that both types of running yield the same **dominant** behavior in the high-energy limit (defined here as the limit in which, with increasing y , ρ is increased as well, in such a

way that one remains in the linear regime at $\rho > \rho_s(y)$). The **subleading** terms, on the other hand, so like the “prefactors” that we ignore here anyway, depend upon the specific choice for the running.

In what follows, we shall adopt the running with k_{\perp}^2 in the DLA regime at high momenta, but we shall rather use the running with the saturation momentum $Q_s^2(A, y)$ for the BFKL regime defined by Eq. (3.56), since the corresponding calculations are considerably simpler (compare, in this respect, the developments in Refs. [36] and respectively [37, 38]). But one should stress that, except for the diffusion term in the expression for the gluon distribution (see Eq. (3.63) below) — which is indeed a subleading effect at high energy —, all the formulae to be obtained below are valid for either running.

With a one-loop running coupling:

$$\bar{\alpha}_s(Q_s^2(A, y)) = \frac{b}{\ln(Q_s^2(A, y)/\Lambda^2)}, \quad b = b_0 N_c / \pi = (11N_c - 2N_f) / 12N_c, \quad (3.58)$$

the only modification in the previous calculations of the BFKL solution consists in the replacement $\bar{\alpha}_s y \rightarrow \tau_A(y)$ in the exponent of the integrand in Eq. (3.41) (and correspondingly in all the subsequent formulae). Here, $\tau_A(y)$ is defined as the solution to $d\tau_A/dy = \alpha_s(Q_s^2(A, y))$ with $\tau_A(0) = 0$. Then calculations entirely similar to those described in the previous subsection lead to the condition $c\tau_A(y) = \rho_s(y) \equiv \ln(Q_s^2(A, y)/Q_s^2(A))$, which can be solved together with the equation defining $\tau_A(y)$, to give [36, 37, 40]:

$$Q_s^2(A, y) \simeq Q_A^2 e^{c\tau_A}, \quad \tau_A \equiv \frac{1}{c} \left(\sqrt{2cby + \rho_A^2} - \rho_A \right), \quad (3.59)$$

where $c \simeq 4.88$ is the same number as in Eq. (3.50).

The function $\tau_A(y)$ is such that, for $2cby \ll \rho_A^2$, $\tau_A(y) \simeq by/\rho_A = \bar{\alpha}_s(Q_A^2)y$, and one recovers the same behavior as for fixed coupling, cf. Eq. (3.50), but with α_s evaluated at the initial saturation scale $Q_s(A) = Q_A$. On the other hand, with increasing y , the dependence on A becomes weaker and weaker [40]:

$$Q_s^2(A, y) \simeq \Lambda^2 e^{\sqrt{2cby}} \exp \left\{ \frac{\rho_A^2}{2\sqrt{2cby}} \right\} \quad \text{for} \quad 2cby \gg \rho_A^2. \quad (3.60)$$

By using similar formulae (with $\rho_A \rightarrow \rho_p \sim 1$) also for the proton, it becomes clear that, unlike what happens in the fixed coupling case, where the ratio $Q_s^2(A, y)/Q_s^2(p, y) = Q_s^2(A)/Q_s^2(p)$ is independent of y and thus fixed by the initial conditions, in the case of a running coupling, this ratio decreases with y , and converges to one for sufficiently large y [40]:

$$\frac{Q_s^2(A, y)}{Q_s^2(p, y)} \simeq \exp \left\{ \frac{\rho_A^2 - \rho_p^2}{2\sqrt{2cby}} \right\} \sim 1 \quad \text{for} \quad 2cby \gtrsim \rho_A^4. \quad (3.61)$$

Thus, due to running coupling effects in the evolution, the initial difference between the proton and the nucleus is washed out after a rapidity evolution $cby \sim \rho_A^4$.

3.3.1 DLA regime

In the case of a fixed coupling, it has been possible to obtain the solution corresponding to the high k_\perp^2 regime by appropriate simplifications in the general solution to the BFKL equation. With a running coupling, however, the BFKL equation is notoriously difficult, so it is a better strategy to simplify this equation first, and solve it only after. The simplified equation valid at high k_\perp^2 , known as the DLA equation, is actually a common limit of the BFKL and DGLAP equations, and its solution is well known (even exactly). For consistency with the other approximations that we have considered so far, we shall only use the saddle point approximation to this solution, valid when $4by\eta \gg 1$, with $\eta \sim \ln \rho$ (see below for a precise definition). This approximate solution reads:

$$\varphi_A(k_\perp, y) \simeq \frac{1}{b_0 N_c} \frac{Q_A^2}{k_\perp^2} \frac{e^{\sqrt{4by\eta}}}{\sqrt{2\pi\sqrt{4by\eta}}}, \quad \eta \equiv \ln \left[\frac{\ln \frac{k_\perp^2}{\Lambda^2}}{\ln \frac{Q_A^2}{\Lambda^2}} \right]. \quad (3.62)$$

3.3.2 BFKL regime

With a running coupling $\alpha_s(Q_s^2(A, y))$, and for momenta within the scaling window (3.56), the gluon occupation factor takes the same form as for fixed coupling, Eq. (3.52), but with $\bar{\alpha}_s y \rightarrow \tau_A$. Specifically:

$$\varphi_A(k_\perp, y) \approx \frac{\kappa_0}{\alpha_s(Q_s^2(A, y)) N_c} \left\{ \rho - \rho_s + \frac{1}{\Delta} \right\} e^{-\gamma(\rho - \rho_s)} \exp \left\{ -\frac{(\rho - \rho_s)^2}{2\beta\tau_A} \right\}, \quad (3.63)$$

where $\rho_s \equiv \ln(Q_s^2(A, y)/Q_A^2) = c\tau_A(y)$. Note that, in this case, ρ_s depends also upon A , in contrast to the fixed coupling case, where $\rho_s = c\bar{\alpha}_s y$. As manifest on Eq. (3.63), the running of the coupling represents an additional source of violation for geometric scaling.

Another difference with respect to the case of a fixed coupling is that, for a running coupling, there seems not to be possible to perform even an approximate matching between the solutions in the BFKL and DLA regimes. For instance, if we define the geometric scaling line by analogy with the fixed coupling case, namely: $Q_g^2(A, y) \equiv Q_s^2(A, y) e^{\nu c\tau_A} = Q_A^2 e^{(1+\nu)c\tau_A}$ with $\nu = \mathcal{O}(1)$, then this scale is a good estimate for the upper bound of

the validity range of the BFKL approximation (3.63), but is probably still far below the kinematical range where the DLA approximation (3.62) starts to apply. Indeed, when evaluated along this line, the expression in Eq. (3.62) grows faster than that in Eq. (3.63).

4 High- k_\perp suppression from quantum evolution: The general argument

Before we embark ourselves in a systematic analysis of the ratio $\mathcal{R}_{pA}(k_\perp, y)$, let us present here a general argument explaining why the quantum evolution leads to a suppression in this ratio at generic momenta. The argument can be succinctly formulated as follows⁸: The suppression of the ratio $\mathcal{R}_{pA}(k_\perp, y)$ with increasing y is due to the different evolution rates for the gluon distribution in the nucleus and in the proton: the one in the proton evolves faster because (a) the corresponding saturation momentum in the initial conditions is much smaller ($Q_p \ll Q_s(A)$), and (b) the convexity of the function $\chi(\gamma)$ (the eigenvalue of the BFKL kernel) accelerates the evolution with increasing ρ . In particular, the difference between the proton and the nuclear evolution rates is particularly pronounced at small y (when the proton is in the DLA regime for the interesting values of k_\perp), which explains the rapid suppression seen in the early stages of the evolution [23].

Moreover, a similar argument will allow us to conclude that, for any fixed y , such that $\bar{\alpha}_s y \gtrsim 1$, and for transverse momenta in the proton perturbative region ($k_\perp \gg Q_s(p, y)$), the ratio $\mathcal{R}_{pA}(k_\perp, y)$ is a monotonously increasing function of k_\perp , which asymptotically approaches one from the below. In particular, this implies that the Cronin peak has already disappeared for such values of y .

The y -dependence of the ratio in Eq. (1.1) is fully encoded in:

$$\frac{d \ln \mathcal{R}_{pA}}{dy} = \frac{d \ln \varphi_A}{dy} - \frac{d \ln \varphi_p}{dy}. \quad (4.1)$$

We shall assume fixed coupling, for definiteness (the generalization to running coupling will be discussed later), and we shall study separately the linear and the saturation regimes for the nucleus. The proton will be always in the linear regime, as described by the BFKL solution in the saddle point approximation, Eq. (3.48).

4.1 Nucleus in the linear regime ($k_\perp \gg Q_s(A, y)$)

In this regime, both the proton and the nucleus are described by Eq. (3.48), which implies:

⁸ We would like to thank Al Mueller for helping us clarifying this general argument.

$$\ln \varphi_A(k_\perp, y) \approx \bar{\alpha}_s y F(\gamma_0(r_A), r_A), \quad (4.2)$$

where we have neglected the slowly varying prefactors. Here, we have introduced the more specific notation:

$$r_A(k_\perp, y) \equiv \frac{\rho(A, k_\perp)}{\bar{\alpha}_s y} = \frac{\ln k_\perp^2 / Q_s^2(A)}{\bar{\alpha}_s y}, \quad (4.3)$$

(with $Q_s(A) \rightarrow Q_p$ for the proton) to emphasize that quantities like $\rho \equiv \rho(A, k_\perp)$ and r_A are different for the proton and the nucleus, even when considered for the same values of the kinematical variables k_\perp and y . Since $Q_s(A) \gg Q_p$ then, clearly,

$$\rho(A, k_\perp) < \rho(p, k_\perp), \quad \text{and} \quad r_A(k_\perp, y) < r_p(k_\perp, y). \quad (4.4)$$

After taking a total derivative w.r.t. y in Eq. (4.2), and using the saddle point condition, Eq. (3.47), together with the definition (3.46) of the function F , one finds :

$$\frac{d \ln \varphi_A}{dy} \approx \bar{\alpha}_s \chi(\gamma_A), \quad (4.5)$$

(with the simplified notation $\gamma_A \equiv \gamma_0(r_A)$) and therefore:

$$\frac{1}{\bar{\alpha}_s} \frac{d \ln \mathcal{R}_{pA}}{dy} \approx \chi(\gamma_A) - \chi(\gamma_p), \quad (4.6)$$

which is always **negative** (for k_\perp and y within its range of validity), as we show now: Since $\chi(\gamma)$ is a convex function ($\chi''(\gamma) > 0$ for $0 < \gamma < 1$), the function $\gamma_0(r)$ which gives the saddle point is monotonously increasing:

$$\frac{d\gamma_0(r)}{dr} = \frac{1}{\chi''(\gamma_0(r))} > 0, \quad (4.7)$$

(this follows by differentiating the saddle point condition (3.47) w.r.t. r), which together with Eq. (4.4) implies that $\gamma_A < \gamma_p$, from which Eq. (4.6) finally follows because $\chi(\gamma)$ is monotonously increasing for any $\gamma > 1/2$ (recall that $\gamma_A \geq \gamma_s \approx 0.63$). Some of these properties are manifest on Fig. 6.

Moreover, the suppression rate (4.6) is largest in the early stages of the evolution, but decreases with y , and approaches zero (through negative values) when $y \rightarrow \infty$. Indeed, the difference:

$$r_p(k_\perp, y) - r_A(k_\perp, y) = \frac{\rho(p, k_\perp) - \rho(A, k_\perp)}{\bar{\alpha}_s y} = \frac{\ln(Q_s^2(A)/Q_p^2)}{\bar{\alpha}_s y} \approx \frac{\rho_A}{\bar{\alpha}_s y}, \quad (4.8)$$

is independent of k_\perp and largest at small y , but it decreases with y , and vanishes asymptotically at very large y . Therefore, when $y \rightarrow \infty$, we have $\gamma_A - \gamma_p \rightarrow 0$, and thus also $\chi(\gamma_A) - \chi(\gamma_p) \rightarrow 0$.

To be more specific, consider two interesting physical regimes:

a) For very large $k_\perp \gg Q_g(A, y)$, both the proton and the nucleus are in the DLA regime, where $r \gg 1$, $\gamma_0(r) \approx 1 - 1/\sqrt{r}$, $\chi(\gamma_0) \approx \sqrt{r}$, and therefore:

$$\frac{1}{\bar{\alpha}_s} \frac{d \ln \mathcal{R}_{pA}}{dy} \approx \sqrt{\frac{\rho(A, k_\perp)}{\bar{\alpha}_s y}} - \sqrt{\frac{\rho(p, k_\perp)}{\bar{\alpha}_s y}}, \quad (4.9)$$

which confirms that the rate of variation is largest in the early stages of the evolution (although Eq. (4.9) cannot be trusted, strictly speaking, when $y \rightarrow 0$).

b) For k_\perp and y such that both the nucleus and the proton are in the BFKL regime (this assumes the existence of a common window for extended geometric scaling, which in turn requires y to be large enough for $Q_g(p, y) > Q_s(A, y)$; see Sect. 6 for details), then one can expand both $\chi(\gamma_A)$ and $\chi(\gamma_p)$ around $\gamma_s \approx 0.63$. This is entirely similar to the expansion leading from Eq. (3.48) to Eq. (3.52), and gives:

$$\frac{1}{\bar{\alpha}_s} \frac{d \ln \mathcal{R}_{pA}}{dy} \approx -\frac{c\rho_A}{\beta\bar{\alpha}_s y} \left\{ 1 + \frac{1}{c\bar{\alpha}_s y} \left(\ln \frac{k_\perp^2}{Q_s^2(A, y)} + \frac{\rho_A}{2} \right) \right\}, \quad (4.10)$$

which shows that, when increasing y and k_\perp in such a way that $\ln(k_\perp^2/Q_s^2(A, y)) \sim \text{const.}$, the rate eventually becomes independent of k_\perp , and vanishes as $1/y$.

4.2 Nucleus in the saturation regime ($k_\perp \leq Q_s(A, y)$)

All that we need to know about this regime for the present purposes is that the nuclear gluon distribution at saturation is only a function of $z \equiv k_\perp^2/Q_s^2(A, y)$. The most interesting evolution is the one in which y and k_\perp are simultaneously increased along a line parallel to the nuclear saturation line (i.e., the evolution at fixed z). For instance, this is the evolution relevant for the study of the Cronin peak (see Sect. 5). Proceeding as before, we have:

$$\ln \mathcal{R}_{pA}(z, y) \approx \ln \varphi_A(z) - \bar{\alpha}_s y \chi(\gamma_p) + \gamma_p \ln \frac{z Q_s^2(A, y)}{Q_p^2}, \quad (4.11)$$

where the proton saddle point γ_p is now determined by (cf. Eq. (3.47)) :

$$\chi'(\gamma_p) = \frac{\ln[z Q_s^2(A, y)/Q_p^2]}{\bar{\alpha}_s y} = \frac{\ln[z Q_s^2(A)/Q_p^2]}{\bar{\alpha}_s y} + \chi'(\gamma_s). \quad (4.12)$$

In the above equation, the second equality follows after using Eq. (3.50) for the saturation momentum and recalling that $c = \chi'(\gamma_s) \approx 4.88$ with $\gamma_s \approx 0.63$. Taking a derivative w.r.t. y in Eq. (4.11) and using Eq. (4.12) yields:

$$\frac{1}{\bar{\alpha}_s} \frac{d \ln \mathcal{R}_{pA}}{dy} \approx \gamma_p \chi'(\gamma_s) - \chi(\gamma_p), \quad (4.13)$$

which is negative for any y , as is quite obvious by inspection of Fig. 6 (the straightline $f(\gamma_p) \equiv \gamma_p \chi'(\gamma_s)$ is precisely the line which is tangent to $\chi(\gamma_p)$ at $\gamma_p = \gamma_s$), and we formally prove now: From Eq. (4.12) it is clear that $\gamma_p(y)$ is a monotonously decreasing function of y , with $\gamma_p(y) \rightarrow 1$ as $y \rightarrow 0$, and $\gamma_p(y) \rightarrow \gamma_s$ when $y \rightarrow \infty$. Since $\chi(\gamma)$ is an increasing function for $\gamma \geq \gamma_s$, it is easily checked that the r.h.s. of Eq. (4.13) is always negative, and approaches zero when $y \rightarrow \infty$ (recall that $\gamma_s \chi'(\gamma_s) = \chi(\gamma_s)$). Moreover, the suppression rate is very large at small y , since $\chi(\gamma_p) \rightarrow \infty$ as $\gamma_p \rightarrow 1$. We conclude that the ratio $\mathcal{R}_{pA}(z, y)$ is rapidly decreasing with y in the early stages of the evolution, and approaches a constant value for very large y .

4.3 A general argument on the k_\perp -dependence

We now present a mathematically similar argument which allows us to characterize the k_\perp dependence of the ratio $\mathcal{R}_{pA}(k_\perp, y)$. We would like to show that, for a fixed rapidity y with $\bar{\alpha}_s y \gtrsim 1$ (such that the saddle point approximation (3.48) applies), and for all momenta $k_\perp \gg Q_s(p, y)$ (where the proton is in a linear regime), the function $\mathcal{R}_{pA}(k_\perp, y)$ is monotonously increasing with k_\perp .

Consider first the linear regime for the nucleus, at $k_\perp \gg Q_s(A, y)$. Using Eq. (4.2) and the saddle point condition, Eq. (3.47), one obtains (e.g., for the proton),

$$\frac{d \ln \varphi_p}{d \ln(k_\perp^2/\Lambda^2)} \approx -\gamma_p, \quad (4.14)$$

together with a similar formula for the nucleus, and therefore:

$$\frac{d \ln \mathcal{R}_{pA}}{d \ln(k_{\perp}^2/\Lambda^2)} \approx \gamma_p - \gamma_A, \quad (4.15)$$

which by the previous arguments is strictly positive and vanishes asymptotically when $k_{\perp} \rightarrow \infty$. Thus, in this regime, the function $\mathcal{R}_{pA}(k_{\perp}, y)$ is strictly increasing with k_{\perp} for any fixed y , and saturates to a constant value when $k_{\perp} \rightarrow \infty$. As it will be checked in Sect. 6, this limiting value is one.

Consider also the case where the nucleus is saturation. Then, as already argued, φ_A is only slowly, logarithmically, decreasing with $z \equiv k_{\perp}^2/Q_s^2(A, y)$ (see Eq. (3.37)), while according to Eq. (4.14), the proton distribution φ_p has a faster, power-like, decrease, with “anomalous dimension” $\gamma_p \geq \gamma_s \simeq 0.63$. Therefore, also in this range, the function $\mathcal{R}_{pA}(k_{\perp}, y)$ is still increasing with k_{\perp} .

These qualitative features will be confirmed by the more systematic analysis of the ratio $\mathcal{R}_{pA}(k_{\perp}, y)$ in the forthcoming sections, where all the possible kinematical regimes will be investigated, for both fixed and running coupling.

To conclude this section, let us briefly discuss the extension of these general arguments to the case of a running coupling. Since, in that case, we have treated differently the DLA and the BFKL (scaling) regimes (in particular, we have used different runnings in the two regimes), we cannot construct a general argument valid in the whole perturbative region. But all the general conclusions about the y - and k_{\perp} -dependencies of the ratio $\mathcal{R}_{pA}(k_{\perp}, y)$ that we have found above remain true also for a running coupling, as we shall check via explicit calculations in Sect. 6. Moreover, if one excludes the DLA region (for both the proton and the nucleus), i.e., if we restrict ourselves to momenta $k_{\perp} < Q_g(p, y)$, then all the previous manipulations in this section can be extended to the case of a running coupling by simply replacing $\bar{\alpha}_s y$ with $\tau_A(y)$ for the nucleus, and with $\tau_p(y)$ for the proton (e.g., $r_A(k_{\perp}, y) = \rho(A, k_{\perp})/\tau_A(y)$, etc.). Since $\tau_A(y) > \tau_p(y)$ for any y , and $d\tau_A(y)/dy > 0$, it is clear that all the previous inequalities are still valid (e.g., $r_A(k_{\perp}, y) < r_p(k_{\perp}, y)$), and therefore so are also our conclusions.

5 The evolution of the Cronin peak with increasing y

The problem of the evolution of the Cronin peak with increasing y is a delicate one, as it involves the nuclear transition region towards saturation, on which we have little analytic control at $y > 0$. Moreover, the experience with the MV model suggests that the existence of the peak and its properties are tributary to the actual behavior of the nuclear gluon distribution $\varphi_A(k_{\perp}, y)$ at momenta just above the saturation scale: If the distribution is rapidly decreasing with k_{\perp} (say, according to an exponential law), then a pronounced peak exists; but if its decrease is only power-like, then there is at most a very

flat peak, if any. In the MV model, the gluon distribution above $Q_s(A)$ has been found to be the superposition between an exponential and a power-law tail, with the exponential being the dominant contribution though, since parametrically enhanced at large A . As we shall see below in this section, the effect of the evolution is to enhance the power-law contributions, which for $\alpha_s y \sim 1$ become as large as the exponential one (for momenta just above $Q_s(A)$). When this happens, the Cronin peak has completely flattened out.

In order to study this flattening, one needs a more accurate calculation which follows the non-linear evolution of the nucleus in the saturation region. To achieve the necessary accuracy while still preserving an analytic control, we shall perform just one step in the evolution of the MV model according to the non-linear Kovchegov equation [31]. Strictly speaking, this calculation applies only for rapidities $\alpha_s y \ll 1$, but as we shall see in Sect. 5.3, this is enough to reveal the mechanism responsible for the flattening of the peak. By extrapolation, we shall then conclude that the peak disappears after an evolution $\alpha_s y \sim 1$.

Whereas the flattening of the peak is a rather subtle effect which has to do with the nuclear evolution, the rapid decrease in the height of the peak, on the other hand, is a more robust phenomenon, and also easier to calculate, since this is due solely to the perturbative evolution of the proton. Because of that, we shall begin our analysis in this section with a study of the evolution of the magnitude of the peak with increasing y . Since we expect the peak to follow the nuclear saturation momentum, we shall consider the evolution of the ratio $\mathcal{R}_{pA}(k_\perp, y)$ along the nuclear saturation line $k_\perp = Q_s(A, y)$. This is possible within the present approximation because, along this particular line, the nuclear gluon distribution is known, cf. Eq. (3.40). By itself, this calculation cannot tell us whether a peak actually exists or not; but so long as the peak exists, it provides us with a correct estimate for the magnitude of the peak and its parametric dependencies upon A and y . Although, as we shall argue later, the peak disappears already when $\alpha_s y \sim 1$, in Sects. 5.1 and 5.2 we shall follow the evolution along the nuclear saturation line up to very large y . This will reveal the basic features of the high- k_\perp suppression, to be more systematically analyzed in Sect. 6.

5.1 *The suppression of the peak: Fixed coupling*

In this subsection and the following one, we shall need only the (proton and nuclear) gluon distributions along the nuclear saturation line $k_\perp = Q_s(A, y)$. For the nucleus, this is simply a constant times $1/\alpha_s$, cf. Eq. (3.40). For the proton, the corresponding distribution is in a linear regime, which can be either DLA, or BFKL, depending upon the value of y : With increasing y , the proton geometric scale $Q_g(p, y_c)$ rises faster than the nuclear saturation momentum, so the corresponding evolution lines in the plane $y - \ln k_\perp^2$ cross each other at some rapidity y_c (see Fig. 1), where the proton changes from the DLA to the BFKL regime. The condition $Q_s(A, y_c) = Q_g(p, y_c)$ together with Eqs. (3.50) and

(3.56) imply :

$$c\bar{\alpha}_s y_c \simeq \frac{1}{\nu} \ln \frac{Q_s^2(A)}{Q_p^2} \simeq \frac{\rho_A}{\nu}. \quad (5.1)$$

5.1.1 $y < y_c$: Proton in the DLA regime

For $y < y_c$, but such that $\bar{\alpha}_s y \rho > 1$, one can use Eq. (3.51) with $Q_s(A) \rightarrow Q_p$ to deduce :

$$\begin{aligned} \mathcal{R}_{sat}(A, y) \equiv \mathcal{R}_{pA}(k_{\perp} = Q_s(A, y), y) &\sim \frac{Q_s^2(A, y)}{A^{1/3} Q_p^2} e^{-\sqrt{4\bar{\alpha}_s y \rho}} \\ &\sim \rho_A \exp\left\{c\bar{\alpha}_s y - \sqrt{4\bar{\alpha}_s y(\rho_A + c\bar{\alpha}_s y)}\right\}, \end{aligned} \quad (5.2)$$

where we have used Eqs. (2.7), (2.19) and (3.50) to write:

$$\frac{Q_s^2(A, y)}{A^{1/3} Q_p^2} = \frac{Q_s^2(A, y)}{Q_A^2} = e^{c\bar{\alpha}_s y} \frac{Q_s^2(A)}{Q_A^2} = e^{c\bar{\alpha}_s y} \rho_A, \quad (5.3)$$

and also (recall that $Q_p^2 \sim \Lambda^2$) :

$$\rho \equiv \ln \frac{Q_s^2(A, y)}{Q_p^2} = c\bar{\alpha}_s y + \ln \frac{Q_s^2(A)}{Q_p^2} \simeq c\bar{\alpha}_s y + \rho_A. \quad (5.4)$$

Note that, in writing Eq. (5.2), we have ignored the slowly varying prefactor in Eq. (3.51), since presently we are only interested in the dominant parametric dependencies upon A and y . When $y \rightarrow 0$, Eq. (5.2) is formally consistent with the corresponding result in the MV model, Eq. (2.22), but one should keep in mind that the results obtained here cannot be used for very small values of y .

Eq. (5.2) offers, in particular, an estimate for the magnitude of the Cronin peak; indeed, for as long as it survives, the peak should be located in the vicinity of $Q_s(A, y)$. Note that, for any $0 < y \leq y_c$, the expression within the exponent in Eq. (5.2) is negative, showing that the magnitude of the peak is rapidly decreasing with y . Since the initial maximum at $y = 0$ was relatively large ($\mathcal{R}_{max}(A) \sim \rho_A$, cf. Eq. (2.23)), it is interesting to check how fast is the height of the peak decreasing to a value which is parametrically of order one. The condition $\mathcal{R}_{sat}(A, y) \sim 1$ for $y \sim y_0$ implies:

$$\bar{\alpha}_s y_0 \sim \frac{\ln^2 \rho_A}{4\rho_A} \sim \frac{(\ln \ln A^{1/3})^2}{\ln A^{1/3}} \ll \bar{\alpha}_s y_c. \quad (5.5)$$

This is a small rapidity interval, but is still within the reach of the saddle point approximation (3.51), since $\rho_A \bar{\alpha}_s y_0 \sim \ln^2 \rho_A > 1$. In fact, for such a short evolution in y , one can ignore the evolution of the nucleus in the vicinity of the peak, i.e., one can neglect $c\bar{\alpha}_s y \ll 1$ next to ρ_A within Eq. (5.2). This is reassuring since, when $\alpha_s y \ll 1$, one cannot really trust the BFKL approximation (3.50) for the saturation scale of the nucleus.

In view of this, it is possible to obtain a more accurate estimate for the rapidity y_0 by using the MV model for the gluon distribution of the nucleus together with the more complete DLA expression (3.51) for the proton distribution, including the prefactor. This yields:

$$\bar{\alpha}_s y_0 = \frac{1}{4\rho_A} \ln^2 \left[a\rho_A \sqrt{\ln(a\rho_A)} \right], \quad a \equiv \sqrt{2\pi} z_0 \Gamma(0, z_0). \quad (5.6)$$

Eq. (5.2) also shows that, after a very short rapidity evolution $\bar{\alpha}_s y \sim 1/\rho_A$, the magnitude of the Cronin peak becomes a **decreasing** function of ρ_A (and thus of A), in sharp contrast with the corresponding behavior at $y = 0$, cf. Eq. (2.23). This is in qualitative agreement with the experimental observation at RHIC that, in dA collisions at forward rapidities, the value of the (experimentally measured) \mathcal{R}_{pA} ratio decreases for more central collisions.

As anticipated, the rapid decrease in the height of the Cronin peak during the early stages of the evolution is to be attributed solely to the fast evolution of the proton. For larger rapidities, $y \gg y_0$, the evolution of the nucleus starts to matter as well (and Eq. (3.50) can be trusted), but as long as $y \leq y_c$ the proton evolution is still faster, so \mathcal{R}_{sat} keeps decreasing with y , as manifest on Eq. (5.2). In particular, for $y = y_c$ one has:

$$\mathcal{R}_{sat}(A, y_c) \sim \rho_A e^{-\kappa\rho_A} \sim \frac{\ln A^{1/3}}{A^{\kappa/3}} \ll 1, \quad \kappa = \frac{1}{\nu} \left(\sqrt{4(1+\nu)/c} - 1 \right) \approx 0.29. \quad (5.7)$$

For even larger y , Eq. (5.2) would predict an **increase** of the peak with y , but this is incorrect, since for $y > y_c$ this equation does not apply any longer.

5.1.2 $y > y_c$: Proton in the BFKL regime

For $y > y_c$, the proton enters the scaling window (3.56), where Eq. (3.53) becomes appropriate. We shall shortly argue that, when this happens, the Cronin peak has already disappeared; but it is still interesting to follow the ratio $\mathcal{R}_{pA}(k_\perp, y)$ further up along the

nuclear saturation line. By using Eq. (3.53) with $Q_s(A, y) \rightarrow Q_s(p, y)$, together with the relations:

$$\frac{Q_s^2(A, y)}{Q_s^2(p, y)} = \frac{Q_s^2(A)}{Q_p^2} = A^{1/3} \rho_A, \quad \ln(A^{1/3} \rho_A) \simeq \rho_A, \quad (5.8)$$

one finds (with the simpler notation $\gamma \equiv \gamma_s$):

$$\mathcal{R}_{sat}(A, y) \sim \frac{1}{A^{\frac{1-\gamma}{3}}} \frac{1}{\rho_A^{1-\gamma}} \exp \left\{ \frac{\rho_A^2}{2\beta\bar{\alpha}_s y} \right\} \ll 1. \quad (5.9)$$

Note the emergence of the power of A in the denominator, which provides a strong suppression factor which is independent of y . This power was missing in the DLA (compare to Eq. (5.2)), but appears here as a consequence of the ‘anomalous dimension’ $\gamma < 1$ characteristic of the BFKL solution in the vicinity of the saturation line [36, 37].

Note furthermore that Eq. (5.9) shows only a weak dependence on y , coming from the ‘diffusion term’ in Eq. (3.53): the dominant dependencies, which are exponential, have cancelled in the ratio between the nuclear and the proton saturation momenta, cf. Eq. (5.8). Thus, as compared to the DLA regime at $y < y_c$, where $\mathcal{R}_{sat}(A, y)$ is rapidly decreasing with y , in the BFKL regime at $y > y_c$ this ratio almost stabilizes at a very small value, proportional to an inverse power of A .

In particular, when approaching y_c from the above, one finds:

$$\mathcal{R}_{sat}(A, y_c) \sim \frac{1}{(A^{1/3} \rho_A)^\kappa} \sim \frac{1}{(A^{1/3} \ln A^{1/3})^\kappa}, \quad (5.10)$$

which by construction involves the same power of A as Eq. (5.7) (because of our matching between the DLA and BFKL approximations along the geometric scaling line). The sub-leading dependencies on A , which are logarithmic, are different in Eqs. (5.7) and (5.10), but this difference merely reflects our imperfect matching.

Furthermore, for very large y , such that $2\beta\bar{\alpha}_s y \gg \rho_A^2$ (in practice, this limit is approached very fast, since $2\beta \approx 97$ is a large number), the ratio becomes independent of y :

$$\mathcal{R}_{sat}(A, y) \sim \frac{1}{(A^{1/3} \rho_A)^{1-\gamma}} \sim \frac{1}{(A^{1/3} \ln A^{1/3})^{1-\gamma}} \quad \text{for} \quad 2\beta\bar{\alpha}_s y \gg \rho_A^2. \quad (5.11)$$

5.2 The suppression of the peak: Running coupling

With running coupling, the rapidity y_c separating between the DLA and BFKL regimes is not so well under control, because for running coupling we have not been able to perform a matching between these two regimes. As an estimate for y_c , we shall take the rapidity at which the BFKL approximation starts to apply for a proton with $k_\perp \sim Q_s(A, y)$. This is determined again by the condition $Q_s(A, y_c) \sim Q_g(p, y_c)$, but now with the expression (3.59) for the saturation momentum. This yields :

$$2cby_c \sim \rho_A^2/3, \quad (5.12)$$

where the factor 1/3 in the r.h.s. comes out when using $\nu = 1$ in Eq. (3.56); but this factor is not really under control, and is given here only indicatively.

Note the different scaling of y_c with ρ_A in Eq. (5.12) as compared to the fixed coupling result, Eq. (5.1). This is only one of the numerous differences between the fixed and running coupling scenarios that we shall encounter in the subsequent analysis. Another such a difference is the fact that, for running coupling, one cannot use the linear (BFKL) approximation for the proton up to arbitrarily large y , even though k_\perp is let to increase along the nuclear saturation line $k_\perp \sim Q_s(A, y)$. Indeed, for y so large that $2cby \gtrsim \rho_A^4$, the proton saturation momentum catches up with that of nucleus, cf. Eq. (3.61), so the proton too enters the non-linear regime. Needless to say, the Cronin peak flattens out already long before this degenerate regime is reached.

5.2.1 $y < y_c$: Proton in the DLA regime

In this regime, the proton is described by Eq. (3.62) where, for $k_\perp^2 = Q_s^2(A, y)$, the variable η can be evaluated as (see also Eq. (3.59)):

$$\eta = \ln \ln \frac{Q_s^2(A, y)}{\Lambda^2} - \ln \ln \frac{Q_p^2}{\Lambda^2} \simeq \ln(c\tau_A + \rho_A). \quad (5.13)$$

One finds then:

$$\mathcal{R}_{sat}(A, y) \sim (c\tau_A + \rho_A) \exp\left\{c\tau_A - \sqrt{4by \ln(c\tau_A + \rho_A)}\right\}, \quad (5.14)$$

which for $y < y_c$ decreases rapidly with y , and becomes of order one after a small rapidity evolution y_0 , with:

$$y_0 \simeq \frac{1}{4b} \ln \rho_A \sim \ln A^{1/3}. \quad (5.15)$$

The saddle point approximation for $\varphi_p(k_\perp, y)$, Eq. (3.62), is justified for $y \sim y_0$ since $\sqrt{4by_0\eta} \simeq \sqrt{4by_0 \ln \rho_A} = \ln \rho_A > 1$. We find a situation similar to the fixed coupling case (cf. Eq. (5.5)), namely, y_0 is so small that the corresponding evolution of the nucleus can be neglected: $c\tau_A(y_0) \sim \ln \rho_A/\rho_A \ll 1$, and therefore $Q_s^2(A, y) \simeq Q_A^2$ for $y \leq y_0$.

When comparing Eqs. (5.5) and (5.15), it appears that the running coupling estimate for y_0 is parametrically larger than the fixed coupling one in the limit where A is large. This seems to indicate that the running effects slow down the evolution. However, one should keep in mind that the rapidity is naturally measured in units of $1/\alpha_s$, and whereas $\alpha_s y_0 \sim \ln^2 \rho_A/\rho_A$ for fixed coupling, we also have $\alpha_s(Q_A^2) y_0 \sim \ln \rho_A/\rho_A$ for running coupling. Thus, when expressed in natural units, the two values are rather close to each other, and the fixed coupling estimate could be even slightly larger.

Finally, if one extrapolates the DLA result (5.14) up to $y \sim y_c$, cf. Eq. (5.12), one finds (with the factor $1/3$ in Eq. (5.12) replaced by some value $\delta = \mathcal{O}(1)$) :

$$\mathcal{R}_{max}(A, y_c) \sim \rho_A e^{-\kappa(\ln \rho_A)\rho_A}, \quad \kappa(\ln \rho_A) \simeq 1 - \sqrt{1 + \delta} + \sqrt{(2\delta/c) \ln \rho_A}, \quad (5.16)$$

which shows a somehow stronger suppression than the corresponding result in the fixed coupling case, Eq. (5.7).

5.2.2 $y > y_c$: Proton in the BFKL regime

For rapidities y within the range $\rho_A^2 < 2cby \ll \rho_A^4$, the proton saturation momentum remains considerably smaller than the nuclear one, so the proton with $k_\perp \sim Q_s(A, y)$ is in the scaling window (3.56), where Eq. (3.63) applies. Using the latter (with $A \rightarrow p$) together with Eq. (3.40), one finds:

$$\mathcal{R}_{sat}(A, y) \sim \frac{1}{A^{1/3}} \frac{\xi_A}{\xi_p} \frac{1}{\xi_A - \xi_p + 1/\Delta} \exp \left\{ \gamma(\xi_A - \xi_p) + \frac{(\xi_A - \xi_p)^2}{2\beta\tau_p} \right\}, \quad (5.17)$$

where we have denoted: $\xi_A \equiv c\tau_A + \rho_A = \ln(Q_s^2(A, y)/\Lambda^2)$ (and similarly for the proton). The main difference with respect to the fixed coupling case discussed previously (cf. Eq. (5.9)) is that for running coupling the dominant dependencies upon y did not compensate in the ratio $Q_s^2(A, y)/Q_s^2(p, y)$. Thus, at least for not so large values of y , Eq. (5.17) preserves a relatively fast decrease with increasing y , which is quite similar to that encountered in the DLA regime at $y < y_c$ (compare to Eq. (5.14)). It is only when y becomes so large that $2cby \gg \rho_A^2$ that the suppression rate slows down (cf. Eq. (3.61)) :

$$\mathcal{R}_{sat}(A, y) \approx \frac{1}{A^{1/3}} \exp \left\{ \frac{\gamma}{2} \frac{\rho_A^2}{\sqrt{2cby}} \right\}. \quad (5.18)$$

Finally, for even larger y , such that $2cby \gg \rho_A^4$, the ratio stabilizes at a very small value:

$$\mathcal{R}_{sat}(A, y) \simeq \frac{1}{A^{1/3}} \quad \text{for} \quad 2cby \gg \rho_A^4. \quad (5.19)$$

Strictly speaking, the BFKL calculation ceases to be valid for such a large y , but the result (5.19) is nevertheless correct since, in this limit, the nuclear and proton saturation scales coincide with each other, cf. Eq. (3.61), so the corresponding occupation factors at $k_\perp \sim Q_s(A, y)$ coincide as well. Moreover, by the same argument, it is clear that for $2cby \gg \rho_A^4$, the limiting value $\mathcal{R}_{pA} = 1/A^{1/3}$ is reached for any $k_\perp \leq Q_g(A, y)$ — this includes the saturation region, and also the window for geometric scaling above saturation, cf. Eq. (3.56) — since in this whole range of momenta the gluon distribution is **universal**, i.e., it depends upon the specific properties of the hadron at hand only via its saturation momentum (cf. Sect. 3). This will be further discussed in Sect. 6.

Let us finally compare the asymptotic regimes for fixed and running coupling: By inspection of Eqs. (5.11) and (5.19), it becomes clear that the ultimate value of \mathcal{R}_{sat} is much smaller for fixed coupling, and it is reached after a much longer evolution. Note, however, that if one measures the rapidity in units of $1/\alpha_s$, with α_s evaluated at the nuclear saturation scale $Q_s(A, y)$ as natural, then for large y :

$$\bar{\alpha}_s(Q_s^2(A, y)) \equiv \frac{b}{\ln(Q_s^2(A, y)/\Lambda^2)} \simeq \frac{b}{\sqrt{2cby}} \quad \text{for} \quad 2cby \gg \rho_A^2, \quad (5.20)$$

and the asymptotic regime in Eq. (5.19) corresponds to $\bar{\alpha}_s y \gg \rho_A^2$. This is parametrically of the same order in A as the evolution required to reach the limit (5.11) in the fixed coupling case. Still, the presence of the large factor $\beta \approx 48$ in the fixed coupling condition $\beta \bar{\alpha}_s y \gg \rho_A^2$ makes that, in practice, the lowest value of \mathcal{R}_{sat} is reached considerably faster with fixed coupling evolution than with running coupling. In this sense, the running coupling evolution is slower.

5.3 The flattening of the Cronin peak

Since restricted to momenta along the saturation line $k_\perp = Q_s(A, y)$, the previous analysis could not tell us whether a maximum actually exists or not, neither describe its detailed properties, like the position of the peak and its actual shape. To study this, we need the nuclear gluon distribution for $y > 0$ and generic momenta around $Q_s(A, y)$, that we shall

compute in this section to lowest non-trivial order in $\bar{\alpha}_s y$, that is, after a single step in the quantum evolution. Since, as we shall see, the quantum evolution and the twist expansion interfere with each other, it is convenient to choose the same “small parameter”, namely $1/\rho_A \ll 1$, to control both of them. If $\Delta Y \equiv \bar{\alpha}_s y$ denotes the rapidity increment that we shall consider (this satisfies $\Delta Y \ll 1$), then our objective in what follows will be to construct the nuclear gluon distribution $\varphi_A(k_\perp, \Delta Y)$ in such a way that, for $\Delta Y \sim 1/\rho_A$ and $k_\perp \lesssim Q_s(A, y)$, all the terms to order $1/\rho_A$ are correctly included. This means that when we use this result to construct the \mathcal{R}_{p_A} -ratio (and therefore we multiply by ρ_A ; see e.g. Eq. (2.22)), we just lose contributions that vanish when $\rho_A \gg 1$.

This implies, in particular, that only the terms of $\mathcal{O}(1)$ and of $\mathcal{O}(1/\rho_A)$ need to be kept in the initial condition $\varphi_{\text{in}} \equiv \varphi_A(k_\perp, Y = 0)$. (Throughout this subsection, we shall often omit the subscript A on the various formulae, to simplify writing.) We thus write:

$$\varphi_{\text{in}} = \varphi_0 + \frac{1}{\rho_A} \varphi_1 + \mathcal{O}(\rho_A^{-2}), \quad (5.21)$$

where φ_0 is the same as the saturating piece in Eq. (2.22) (i.e., the piece involving the function $\Gamma(0, z)$), which is of $\mathcal{O}(1)$, while φ_1 is the term with $n = 1$ in the twist expansion shown in that equation (which, we recall, includes the bremsstrahlung spectrum together with higher twist effects to all orders in $1/z$), and is of $\mathcal{O}(1/\rho_A)$.

To study the non-linear evolution with y , it is convenient to use the Kovchegov equation [31], since this is a closed equation. This can be written both in momentum space, i.e., as an equation for $\varphi(k_\perp, Y)$, and in coordinate space, as an equation for the dipole scattering amplitude which appears in Eq. (5.22). In what follows, both forms of this equation will be used, for convenience. We start by rewriting Eq. (2.2) as:

$$\varphi(k_\perp, Y) = \frac{1}{\alpha_s N_c} \int \frac{d^2 r_\perp}{\pi r_\perp^2} e^{-ik_\perp \cdot r_\perp} \mathcal{N}(r_\perp, Y) = \frac{2}{\alpha_s N_c} \int \frac{dr}{r} J_0(kr) \mathcal{N}(r, Y). \quad (5.22)$$

In the following we shall omit the overall factor $1/\alpha_s N_c$, which we can restore at the end. In terms of $\mathcal{N}(r, Y) \equiv \mathcal{N}_{xy}(Y)$ (with $r_\perp = x_\perp - y_\perp$), the Kovchegov equation reads:

$$\frac{\partial \mathcal{N}_{xy}}{\partial Y} = \int \frac{d^2 z_\perp}{2\pi} \mathcal{K}_{xyz} (\mathcal{N}_{xz} + \mathcal{N}_{zy} - \mathcal{N}_{xy} - \mathcal{N}_{xz} \mathcal{N}_{zy}), \quad (5.23)$$

where \mathcal{K}_{xyz} is the dipole emission kernel :

$$\mathcal{K}_{xyz} \equiv \frac{(x_\perp - y_\perp)^2}{(x_\perp - z_\perp)^2 (z_\perp - y_\perp)^2}. \quad (5.24)$$

One can transform the above integration over z_\perp into an integration over the sizes of the

emitted dipoles r_1 and r_2 :

$$\begin{aligned} \frac{\partial \mathcal{N}(r)}{\partial Y} &= \int \frac{dr_1}{r_1} \frac{dr_2}{r_2} r^2 \ell d\ell J_0(\ell r_1) J_0(\ell r_2) J_0(\ell r) \\ &\times [\mathcal{N}(r_1) + \mathcal{N}(r_2) - \mathcal{N}(r) - \mathcal{N}(r_1)\mathcal{N}(r_2)]. \end{aligned} \quad (5.25)$$

Through Eq. (5.22), this gives a non-linear equation for $\varphi(k_\perp, Y)$, in which the structure of the non-linear term is actually simpler [31, 36] :

$$\frac{\partial \varphi}{\partial Y} = \mathcal{K} \otimes \varphi - \frac{1}{2} \varphi^2, \quad (5.26)$$

where now \mathcal{K} is an operator with the BFKL eigenvalue spectrum, but for our current purposes we prefer to view it as a multiple integration determined from Eqs. (5.22) and (5.25), that is :

$$\begin{aligned} \mathcal{K} \otimes \varphi &= 2 \int \frac{dr_1}{r_1} \frac{dr_2}{r_2} r dr \ell d\ell J_0(\ell r_1) J_0(\ell r_2) J_0(\ell r) J_0(kr) \\ &\times [\mathcal{N}(r_1) + \mathcal{N}(r_2) - \mathcal{N}(r)]. \end{aligned} \quad (5.27)$$

To obtain the change $\Delta\varphi$ in φ after a small step in rapidity $\Delta Y \ll 1$, it is enough to iterate the evolution equation only once. This gives:

$$\Delta\varphi = \Delta Y \left(\mathcal{K} \otimes \varphi_{\text{in}} - \frac{\varphi_{\text{in}}^2}{2} \right) + \mathcal{O}((\Delta Y)^2), \quad (5.28)$$

with φ_{in} the initial condition. To keep the discussion simple, we shall imagine that $\Delta Y \sim 1/\rho_A$, which is the amount of rapidity (up to $\ln \rho_A$ factors) that gives a suppression of the Cronin peak to a value of order $\mathcal{O}(1)$, due to the fast evolution of the proton (cf. Eq. (5.5)). Then we have:

$$\Delta\varphi = \Delta Y \left(\mathcal{K} \otimes \varphi_0 - \frac{1}{2} \varphi_0^2 \right) + \mathcal{O}\left(\frac{\Delta Y}{\rho_A}, (\Delta Y)^2\right), \quad (5.29)$$

and therefore the evolved gluon distribution is finally written as

$$\varphi = \varphi_0 + \frac{1}{\rho_A} \varphi_1 + \Delta Y \tilde{\varphi}_0 + \mathcal{O}\left(\frac{1}{\rho_A^2}, \frac{\Delta Y}{\rho_A}, (\Delta Y)^2\right), \quad (5.30)$$

where we have introduced the shorthand notation

$$\tilde{\varphi}_0 = \mathcal{K} \otimes \varphi_0 - \frac{1}{2} \varphi_0^2. \quad (5.31)$$

Eq. (5.30) fulfills our objective in that all the neglected terms there become of order $1/\rho_A^2$ when $\Delta Y \sim 1/\rho_A$ (for generic momenta $k_\perp \sim Q_s(A, y)$).

To compute the action of the BFKL operator on φ_0 we shall use Eq. (5.27) in which $\mathcal{N} \rightarrow \mathcal{N}_0 \equiv 1 - \exp(-r^2 Q_s^2/4)$. Since the three separate integrations (corresponding to the three terms in the square bracket) in (5.27) are individually ultraviolet divergent (the divergences only cancel in their sum), we shall regulate the $r_{1,2}$ integrations by letting

$$\int \frac{dr_1}{r_1} \frac{dr_2}{r_2} \rightarrow \lim_{\epsilon \rightarrow 0^+} \int \frac{dr_1}{r_1^{1-2\epsilon}} \frac{dr_2}{r_2^{1-2\epsilon}}, \quad (5.32)$$

with the limit to be taken at the end of the calculation. After performing each of the three (multiple) integrations separately, and adding the respective results, we obtain :

$$\begin{aligned} \mathcal{K} \otimes \varphi_0 = & \lim_{\epsilon \rightarrow 0^+} \frac{1}{2} \frac{\Gamma^2(\epsilon)}{\Gamma^2(1-\epsilon)} \left(\frac{z}{4}\right)^{-2\epsilon} \\ & \times \left[1 - 2 z^\epsilon \Gamma(1-\epsilon) \Phi(\epsilon, 1, -z) + z^{2\epsilon} \Gamma(1-2\epsilon) \Phi(2\epsilon, 1, -z) \right], \end{aligned} \quad (5.33)$$

where, as usual, we have used the scaled momentum variable $z = k^2/Q_s^2(A)$. The limit in this last expression is finite. After also combining this with the non-linear contribution, which reads simply $-(1/2)\Gamma^2(0, z)$, we finally find :

$$\tilde{\varphi}_0 = \frac{\pi^2}{12} - \frac{1}{2} [\gamma_E + \ln z + \Gamma(0, z)]^2 + \frac{1}{2} \Phi^{200}(0, 1, -z), \quad (5.34)$$

where $\gamma_E = 0.577$ is the Euler–Mascheroni constant, and $\Phi^{200}(0, 1, -z)$ is a particular derivative of the confluent hypergeometric function, to be defined in the Appendix. It is illuminating to study the small- and large- z limits of $\tilde{\varphi}_0$, which are given by

$$\tilde{\varphi}_0 = \begin{cases} \frac{\pi^2}{12} - \frac{z^2}{4} + \dots & \text{if } z \ll 1 \\ \frac{1}{z} + \frac{1}{2z^2} + \dots & \text{if } z \gg 1. \end{cases} \quad (5.35)$$

When z is small, we simply obtain a constant correction. This is consistent with the fact that the low- k_\perp limit of φ is not affected by the evolution — this is rather fixed by Eq. (5.22) as $\varphi(k, Y) \rightarrow \ln k_\perp^2$ when $k_\perp \rightarrow 0$ —, but it is only the scale in this logarithm which changes with y : this is the saturation momentum $Q_s(A, y)$, since this is the scale at which the dipole starts to be completely absorbed: $\mathcal{N}(r, Y) \simeq 1$ for $r \gtrsim 1/Q_s(A, y)$. This discussion suggests that the term $(\pi^2/12) \Delta Y$ coming from the one-step evolution could be interpreted as the first contribution to the evolution of the saturation scale.

The crucial point about the correction induced by evolution, as displayed in Eqs. (5.34)–(5.35), is that this contains **power-law** tails at large z , despite the fact that it has been generated by evolving the **compact** (saturating) part of the initial distribution alone. This is due to the fact that the (perturbative) gluon interactions — as encoded in the BFKL kernel — are long-ranged, in both the momentum and the coordinate space (see Eq. (5.24)).

A similar phenomenon is the generation of power-law tails in impact parameter space when solving the Kovchegov equation (5.23), as found in Ref. [60].

Thus, in addition to the original “twist” contributions encoded in the function φ_1 , which are parametrically suppressed at large A , the evolved gluon distribution in Eq. (5.30) contains other power-law contributions **which are not parametrically suppressed**, because they are generated by the evolution of the gluons which were originally at saturation. φ_0 and $\tilde{\varphi}_0$ are parametrically of the same order, and the induced piece $\Delta\varphi = \Delta Y \tilde{\varphi}_0$ is small only as long as ΔY itself is small. But although we cannot rely on the previous approximation to go up to larger values of $\bar{\alpha}_s y = Y$, it is clear that, when $\bar{\alpha}_s y \sim 1$, the twist effects induced by the evolution become comparable to the original distribution at momenta just above the saturation scale. (Incidentally, this justifies the fact that, for $\bar{\alpha}_s y \gtrsim 1$, we can rely on the linear, BFKL, evolution to approach the saturation region from the above.)

We are now in a position to explain the rapid flattening of the Cronin peak, as seen in the numerical simulations in Ref. [23]. We have already noticed, in the analysis of the Cronin peak in the MV model in Sect. 2.3, that the presence of long-range tails has the effect to flatten the peak, and to push it towards larger values of k_\perp . At $y = 0$ and for a large value of A , a well pronounced peak exists just because the compact contribution to the gluon distribution due to the saturated gluons (i.e., φ_0) is the dominant contribution at $k_\perp \lesssim Q_s(A)$ (see Figs. 2 and Figs. 4). However, with increasing y , the power-law tails are enhanced, and the effect of this enhancement is particularly pronounced in the early stages of the evolution ($\bar{\alpha}_s y \ll 1$), when the high- k_\perp modes receives large contributions from the evolution of the gluons which were originally at saturation. In this way, the exponential tail in the saturating distribution at $y = 0$ is rapidly washed out, and replaced by a power law tail all the way down to $Q_s(A, y)$. When this happens the peak in the ratio \mathcal{R}_{pA} flattens out completely and disappears. In view of the previous estimates, we expect a complete flattening for $\bar{\alpha}_s y \sim 1$. But the effect shows up already for smaller rapidities, where our one-step evolution is a good approximation.

To illustrate this, we have represented in Fig. 7 the ratio \mathcal{R}_{pA} (for $\rho_A = 6$) obtained by using the result in Eq. (5.30) for the nuclear gluon distribution together with the DLA approximation for the proton distribution⁹. For comparison, we have also represented on the same plot the ratio which is obtained when the non-evolved, MV model, distribution is used for the nucleus. The rapid suppression of the peak, due to the fast rise in the proton distribution, is clearly seen in both cases. But in the absence of nuclear evolution the peak

⁹ To be able to perform this calculation also for very small values of Y , where the saddle point approximation is not appropriate anymore, we have used the exact solution to the DLA equation, which is well known to read (compare to Eq. (3.51)) : $\varphi_p(k_\perp, y) = \frac{1}{\alpha_s N_c} \frac{Q_p^2}{k_\perp^2} I_0(\sqrt{4\bar{\alpha}_s y \rho})$, with $\rho = \ln(k_\perp^2/Q_p^2)$ and $I_0(z)$ the modified Bessel function of the first kind.

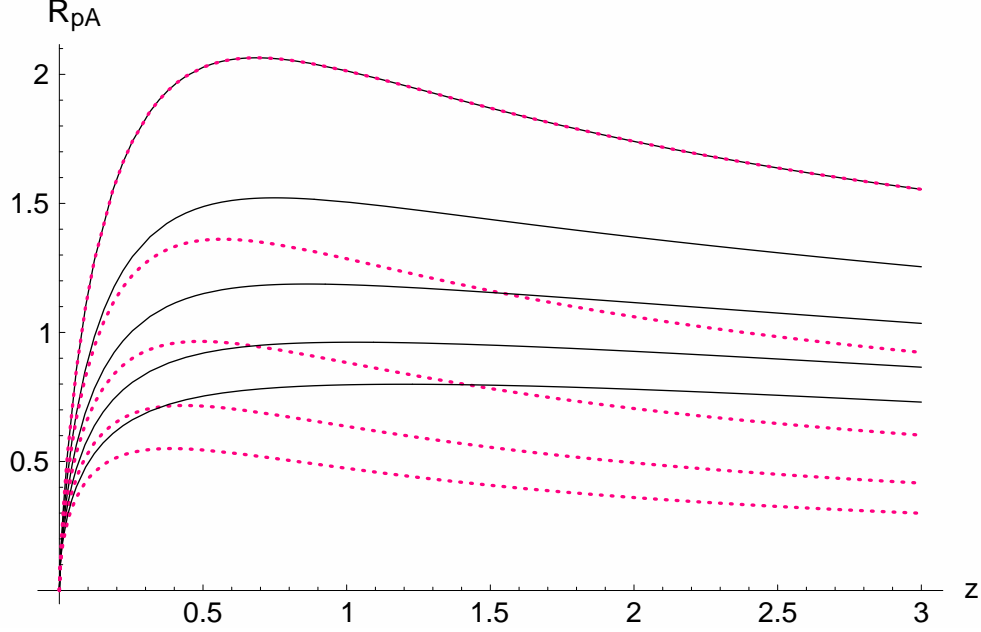


Fig. 7. The Cronin ratio $\mathcal{R}_{pA}(z)$ below and near the saturation scale for $\rho_A = 6$. The black (solid) lines correspond to an evolved nuclear wavefunction by $\Delta Y \ll 1$. The red (dotted) lines correspond to an unevolved one (MV). The proton wavefunction is always given by the full DLA solution. The curves, from top to bottom, correspond to $\Delta Y = n/(2\rho_A)$ with $n = 0, 1, \dots, 4$

is always there; just its amplitude gets smaller and smaller. By contrast, when using the evolved nucleus distribution from Eq. (5.30) the flattening of the peak is manifest, and in fact the maximum has almost disappeared after an evolution $\Delta Y = 2/\rho_A \approx 0.3$.

It is also visible on Fig. 7 that with increasing y , the position of the peak moves towards larger momenta — in agreement with our expectation that the peak should follow the nuclear saturation momentum —, but it does that only *very slowly*. This is so slow because, first, the nucleus evolves only little for such a small rapidity increment, and, second, there is an opposite effect due to the DLA evolution of the proton, which for the small values of Y of interest here is almost compensating the evolution towards larger k_\perp due to the nucleus. Using Eq. (5.30) for the nuclear distribution, together with the DLA approximation (the full Bessel function) for the proton, we have been able to compute analytically the position of the peak for very small values of y . The result reads (compare to Eq. (2.23)) :

$$z_0(Y) \approx 0.435 + \frac{0.882}{\rho_A} + 0.862Y - 0.769\sqrt{\frac{Y}{\rho_A}}, \quad (5.36)$$

where the neglected terms are such that, when $Y \sim 1/\rho_A$, they are all of $\mathcal{O}(\rho_A^{-2})$.

To summarize the previous considerations, the ratio (1.1) can be suggestively rewritten

as follows:

$$\begin{aligned}\mathcal{R}_{pA}(k_{\perp}, y) &\equiv \frac{\varphi_A(k_{\perp}, y)}{A^{1/3} \varphi_p(k_{\perp}, y)} = \frac{\Phi_A(k_{\perp}, y)}{\Phi_p(k_{\perp}, y)} \mathcal{R}_{pA}(k_{\perp}, y = 0), \\ \Phi_A(k_{\perp}, y) &\equiv \frac{\varphi_A(k_{\perp}, y)}{\varphi_A(k_{\perp}, y = 0)}, \quad \Phi_p(k_{\perp}, y) \equiv \frac{\varphi_p(k_{\perp}, y)}{\varphi_p(k_{\perp}, y = 0)}.\end{aligned}\tag{5.37}$$

The ratios Φ_A and Φ_p , which describe the relative evolutions of the nucleus and of the proton, respectively, play very different roles for the evolution at small y and momenta around $Q_s(A, y)$: Φ_p rises very fast with y , and is responsible for the rapid suppression of \mathcal{R}_{pA} at generic momenta. However, this factor varies only slowly with k_{\perp} , and thus cannot be responsible for the flattening of the peak. Φ_A , on the other hand, rises only slowly with y , but its evolution is quite asymmetric around $Q_s(A, y)$: the (relative) evolution is substantially larger at momenta above $Q_s(A, y)$ than below it, and because of this asymmetry, the peak gets progressively tilted (its ‘upper’ side at larger k_{\perp} rises faster than the lower one) and also flattens, until it eventually disappears.

6 High- k_{\perp} suppression in the nuclear gluon distribution at small x

In this section we shall extend our analysis of the evolution of the ratio $\mathcal{R}_{pA}(k_{\perp}, y)$ with increasing y to arbitrary values of the transverse momentum k_{\perp} . The various regimes of evolution in the $\ln k_{\perp}^2 - y$ plane are illustrated in Figs. 1 and 10 for fixed and running coupling, respectively. In Sect. 5, we have followed the nuclear saturation line $k_{\perp} = Q_s(A, y)$ in this plane. Below, we shall focus mostly on the high momentum region $k_{\perp} \gg Q_s(A, y)$ where the nucleus is in a linear regime (either BFKL, or DLA, depending upon the value of k_{\perp}). This is the interesting region for understanding the disappearance of the Cronin peak and also the phenomenon of “high- k_{\perp} suppression”, which is perhaps relevant for the phenomenology at RHIC.

In performing this analysis, it is useful to keep in mind the limitations of the analytic approximations that we shall use for the solution to BFKL equation: The transition regions from saturation to BFKL, and also from BFKL to DLA, are not analytically under control, nor are the very early stages of the evolution. In fact, in the BFKL regime where $\bar{\alpha}_s y \sim \rho$ (with $\rho_s(A, y) < \rho < \rho_g(A, y)$), the saddle point approximation is justified only when $\alpha_s y \geq 1$, while for the DLA regime at $\rho \gg \alpha_s y$, the corresponding condition reads $\alpha_s y \rho \gg 1$. We recall that $\rho \equiv \rho(A, k_{\perp}) = \ln k_{\perp}^2 / Q_s^2(A)$ is much larger for the proton than for the nucleus (for the same value of k_{\perp}). This enables us to study the early evolution of the proton (which is described by DLA), but not also that of the nucleus (unless k_{\perp} is so large that the nucleus itself enters the DLA regime).

The natural way to follow this evolution is to increase simultaneously y and k_\perp , in such a way that the ratio $z \equiv k_\perp^2/Q_s^2(A, y)$ remains constant. This ensures that, with increasing y , the nucleus remains in the same physical regime, which could be either the saturation regime (for $z < 1$), or the (nuclear) BFKL regime (for $z > 1$).

The analysis performed in this section is to confirm the previous general arguments in Sect. 4 about the dependencies of the ratio \mathcal{R}_{pA} upon y and k_\perp . There, it was argued that in the linear regime for both the proton and the nucleus, the ratio decreases with increasing y at fixed k_\perp , while it increases with increasing k_\perp at fixed y . We are going to show that this is indeed the case in all the linear regimes in Figs. 1 and 10. Furthermore, we shall compute the limiting values of the ratio at large y and/or large k_\perp , which was not available from the general argument in Sect. 4.

It is convenient to summarize here the results that we shall obtain below in this section: The Cronin peak flattens out completely already in the early stages of the evolution. (When the nucleus starts to be described by the BFKL saddle point, the peak has already disappeared, see Sect. 5.3.) For any fixed y such that $\alpha_s y \geq 1$ (for the present approximations to apply) the ratio $\mathcal{R}_{pA}(k_\perp, y)$ is smaller than one at any k_\perp . It is furthermore a monotonously increasing function of k_\perp which asymptotically approaches one from the below, in accordance with the general argument for both the fixed and running coupling. Finally, for a fixed k_\perp , the ratio is rapidly decreasing with y , and approaches quite fast a very small limiting value which is independent of both y and k_\perp , but is different for fixed or running coupling. In fact, for sufficiently large y we recover the same scenario as in the previous section, where we have focused on $k_\perp \sim Q_s(A, y)$: In the fixed coupling case, most of the suppression takes place very early, when the proton is still in the DLA regime; the corresponding limiting value is of order $1/(A^{1/3}\rho_A)^{1-\gamma}$. For a running coupling, the rapid suppression is pursued in the proton BFKL regime, because of the evolution of the proton and nuclear saturation scales towards each other. This gives an ultimate suppression factor equal to $1/A^{1/3}$, which is achieved when, for a given k_\perp , there is no difference in between the nuclear and proton gluon distributions anymore.

6.1 Fixed coupling

In this section we shall explore the various regimes for the fixed coupling evolution exhibited in Fig. 1, and study the variation of the ratio $\mathcal{R}_{pA}(k_\perp, y)$ with y and k_\perp , as well as its parametric dependence upon A .

6.1.1 $k_{\perp} < Q_s(A, y)$: The nuclear saturation region

The nuclear distribution at saturation is not explicitly known (except for very small momenta $k_{\perp} \ll Q_s(A, y)$, where Eq. (3.37) applies), but this is some slowly varying function of $z \equiv k_{\perp}^2/Q_s^2(A, y)$ (because of geometric scaling), which moreover is simply a constant when the evolution is performed along a line parallel to the saturation line (which is the most interesting case). As for the proton, this can be either at saturation, or in the linear regime above saturation, depending upon the value of k_{\perp} .

(I) $k_{\perp} < Q_s(p, y)$: Proton at saturation

In this regime, the gluon distributions both in the proton and in the nucleus are universal functions of $k_{\perp}^2/Q_s^2(A, y)$ (with $Q_s(A, y) \rightarrow Q_s(p, y)$ in the case of the proton), which are rather slowly varying with both y and k_{\perp} . Thus, clearly, the ratio (1.1) is of order $1/A^{1/3}$, and has only weak, logarithmic, dependencies upon A , y and k_{\perp} . This becomes explicit for sufficiently low momenta, $k_{\perp} \ll Q_s(p, y)$, where one can use Eq. (3.37) both for the nucleus and for the proton. One then finds that the ratio is monotonously increasing with k_{\perp} , and slowly, but monotonously, decreasing with y at fixed k_{\perp} . In particular, along the proton saturation line $k_{\perp} = Q_s(p, y)$, which defines the upper boundary of this region, one finds:

$$\mathcal{R}_{pA}(k_{\perp} = Q_s(p, y), y) \sim \frac{\rho_A}{A^{1/3}} \quad (\text{independent of } y). \quad (6.1)$$

(II) $Q_s(p, y) < k_{\perp} < Q_s(A, y)$: Proton in the linear regime

The corresponding analysis is very similar to that of the evolution along the nuclear saturation line, as discussed in Sect. 5. For $y < y_c$, cf. Eq. (5.1), the proton can be either in the DLA, or in the BFKL, regime (depending upon to the value of k_{\perp}), while for larger y , it is always in the BFKL regime (see Fig. 1).

A straightforward analysis shows that the ratio is rapidly decreasing with y at any fixed k_{\perp} , due to the fast evolution of the proton. Moreover, the discussion in Sect. 5 shows that the ratio is also decreasing if y and k_{\perp} are simultaneously increased, along any line parallel to the (proton or nucleus) saturation line. To be more specific, let us just consider the large y behavior at fixed z . Then, the proton is in the BFKL regime, so using Eq. (3.53) (with $Q_s(A, y) \rightarrow Q_s(p, y)$) and writing $\varphi_A(k_{\perp}, y) = (1/\alpha_s N_c) \bar{\varphi}_0(z)$, one obtains (with $\gamma \equiv \gamma_s \simeq 0.63$ from now on) :

$$\begin{aligned}
\mathcal{R}_{pA}(k_\perp, y) &\sim \frac{\rho_A^\gamma}{A^{\frac{1-\gamma}{3}}} \frac{z^\gamma \bar{\varphi}_0(z)}{\rho_A - \ln 1/z + 1/\Delta} \exp \left\{ \frac{(\rho_A + \ln z)^2}{2\beta\bar{\alpha}_s y} \right\} \\
&\rightarrow \frac{\rho_A^\gamma}{A^{\frac{1-\gamma}{3}}} \frac{z^\gamma \bar{\varphi}_0(z)}{\rho_A - \ln 1/z}, \quad \text{for } 2\beta\bar{\alpha}_s y \gg \rho_A^2,
\end{aligned} \tag{6.2}$$

(in this regime $\rho_A > \ln 1/z$), which is indeed consistent with the previous result (5.11) on the nuclear saturation line $z = 1$.

6.1.2 $Q_s(A, y) < k_\perp < Q_g(A, y)$: The nuclear BFKL region

For $y < y_c$, the proton is in the DLA regime for any k_\perp , while for $y > y_c$, it can be either in the BFKL, or in the DLA regime, according to the value of k_\perp .

(I) $y < y_c$: Proton in the DLA regime

In this region, the ratio \mathcal{R}_{pA} is formed by using Eq. (3.53) for the nucleus and Eq. (3.51) for the proton. After straightforward manipulations, similar to those leading to Eq. (5.2), the result can be cast into the form:

$$\mathcal{R}_{pA}(z, Y) \sim \rho_A z^{1-\gamma} \left(\ln z + \frac{1}{\Delta} \right) \exp \left\{ cY - \sqrt{4Y(\ln z + cY + \rho_A)} - \frac{\ln^2 z}{2\beta Y} \right\}, \tag{6.3}$$

with the compact notations: $z \equiv k_\perp^2/Q_s^2(A, y)$, and $Y \equiv \bar{\alpha}_s y$. Note that the overall normalization is not under control. Eq. (6.3) applies for k_\perp in the nuclear scaling window (3.56), that is:

$$0 < \ln z < \ln \left[Q_g^2(A, y)/Q_s^2(A, y) \right] = \nu cY, \quad \text{and} \quad 1 \lesssim Y < Y_c \equiv \rho_A/\nu c. \tag{6.4}$$

It can be checked that, within this physical range¹⁰ the function $\mathcal{R}_{pA}(z, Y)$ is monotonously increasing with z , and also rapidly decreasing with Y at any fixed z . This behavior is in agreement with the general results in Sect. 4, and is illustrated in Fig. 8.

It is interesting to use Eq. (6.3) in order to check our previous finding that the Cronin peak must have disappeared when $Y \gtrsim 1$. To that aim, one has to approach the nuclear saturation line $k_\perp = Q_s(A, y)$ from the above. Even without doing any calculation, it is quite clear that, in this limit, Eq. (6.3) will yield the same function of Y and A as we have found before, in Eq. (5.2). Indeed, for $k_\perp \rightarrow Q_s(A, y)$, the BFKL approximation (3.53) reduces to a constant times $1/\alpha_s$, in agreement (up to the overall normalization) with the saturation condition (3.40) that we have used in deriving Eq. (5.2). This shows that, for

¹⁰ The function in Eq. (6.3) develops a maximum at very large z , well outside the window (6.4). This is, of course, unphysical.

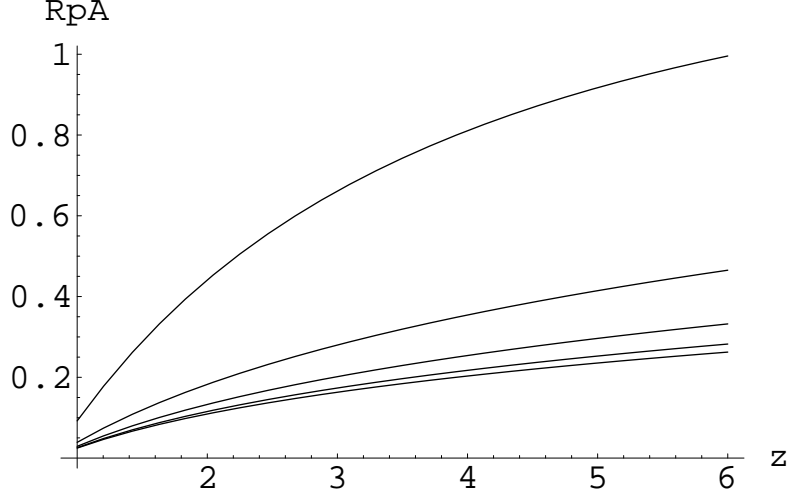


Fig. 8. The ratio $\mathcal{R}_{pA}(z, Y)$ as a function of $z = k_{\perp}^2/Q_s^2(A, y)$ for $\rho_A = 10$ (i.e., $Y_c \approx 1.24$) and rapidities $Y = 0.1 + 0.3n$, with $n = 0, 1, \dots, 4$, from top to bottom. The bottom line corresponds to $Y = 1.3 \simeq Y_c$. The ratio \mathcal{R}_{pA} is measured in arbitrary units, since the normalization of Eq. (6.3) is not under control. Note the rapid decrease with increasing Y in the early stages of the evolution.

$Y \gtrsim 1$, there is no parametric enhancement for the ratio \mathcal{R}_{pA} along the saturation line, or for momenta well above it, where the BFKL approximation applies. Moreover, when increasing k_{\perp} above $Q_s(A, y)$, the ratio is monotonously increasing, as mentioned. Thus, clearly, there is no local maximum around $Q_s(A, y)$.

(II) $y > y_c$ & $Q_s(A, y) < k_{\perp} < Q_g(p, y)$: Double-scaling regime

This region is interesting in that the proton and the nucleus are both in the same physical regime, namely in the window (3.56) for (approximate) geometric scaling, so they are described by the same approximation — the BFKL expression (3.53) —, and the normalization ambiguities cancel in the ratio \mathcal{R}_{pA} . Thus, in this regime, one can also predict the **amplitude** of this ratio, and not only its functional dependencies. Besides, this is also the regime for which the quantum evolution above the saturation line has been originally invoked, by Kharzeev, Levin and McLerran [16], as a possible mechanism to explain the high- k_{\perp} suppression observed in the RHIC data.

Using Eq. (3.53) both for the nucleus and for the proton, one finds :

$$\mathcal{R}_{pA}(k_{\perp}, y) \simeq \frac{\rho_A^{\gamma}}{A^{\frac{1-\gamma}{3}}} \frac{\ln z + \frac{1}{\Delta}}{\ln z + \rho_A + \frac{1}{\Delta}} \exp \left[\frac{\rho_A}{2\beta Y} (2 \ln z + \rho_A) \right], \quad (6.5)$$

where we have used the same notations as in Eq. (6.3), together with the relation $\ln[k_{\perp}^2/Q_s^2(p, y)] \simeq$

$\ln z + \rho_A$. This expression holds within the range:

$$0 < \ln z < \nu c Y - \rho_A \quad \text{and} \quad Y > Y_c \equiv \rho_A / \nu c. \quad (6.6)$$

As anticipated in the Introduction, the dominant y -dependencies of the nuclear and proton distributions, as encoded in the respective saturation momenta, have cancelled in the ratio $Q_s^2(A, y) / Q_s^2(p, y) = Q_s^2(A) / Q_p^2 \simeq A^{1/3} \rho_A$. The remaining dependence on y in Eq. (6.5) comes from the diffusion terms, and is rather weak. (This is also in agreement with the discussion in Sect. 4; see especially Eq. (4.10).) Thus, for $Y > Y_c$, the suppression slows down, and for sufficiently large Y (such that the exponent in the second line of Eq. (6.5) becomes negligible), \mathcal{R}_{pA} stabilizes at a small value which depends upon z :

$$\mathcal{R}_{pA}(z, Y \rightarrow \infty) \simeq \frac{\rho_A}{(A^{1/3} \rho_A)^{1-\gamma}} \frac{\ln z + \frac{1}{\Delta}}{\ln z + \rho_A + \frac{1}{\Delta}}. \quad (6.7)$$

It can be verified that most of this suppression has been achieved already in the early stages of the evolution, while the proton was still in the DLA regime.

It is easily checked that the ratio (6.5) is an **increasing** function of z for arbitrary Y , and a **decreasing** function of Y for arbitrary $z > 1$. This behavior is illustrated in Fig. 9.

When approaching the nuclear saturation line from the above, Eq. (6.5) yields:

$$\mathcal{R}_{pA}(z \rightarrow 1, Y) \simeq \frac{1}{(A^{1/3} \rho_A)^{1-\gamma}} e^{\frac{\rho_A^2}{2\beta Y}} \xrightarrow{Y \rightarrow \infty} \frac{1}{(A^{1/3} \rho_A)^{1-\gamma}}. \quad (6.8)$$

As expected, this is the same function of A and y as obtained when approaching the saturation line from the below, cf. Eq. (5.9), with the noticeable difference that, now, also the **normalization** of this result is under control.

It is finally interesting to also evaluate the ratio (6.5) on the proton geometric line (i.e., $k_\perp = Q_g(p, y)$, or $\ln z = \nu c Y - \rho_A$), which is the upper boundary for the double-scaling regime considered here. In the large Y limit, one obtains:

$$\lim_{y \rightarrow \infty} \mathcal{R}_{pA}(k_\perp \sim Q_g(p, y), y) = \frac{\rho_A}{(A^{1/3} \rho_A)^\delta}, \quad \delta = 1 - \gamma - \frac{\nu c}{\beta} \simeq 0.21. \quad (6.9)$$

The dominant power of $1/A^{1/3}$ is lower on the upper boundary than on the lower one ($\delta \approx 0.21$ as compared to $1 - \gamma \approx 0.37$), since at fixed Y the ratio is increasing with z .

(III) $y > y_c$ & $Q_g(p, y) < k_\perp < Q_g(A, y)$: Proton in the DLA regime

In this regime, the ratio $\mathcal{R}_{pA}(z, Y)$ is given again by Eq. (6.3), but which now applies to a different kinematical range : $\nu c Y - \rho_A < \ln z < \nu c Y$ and $Y > Y_c$.

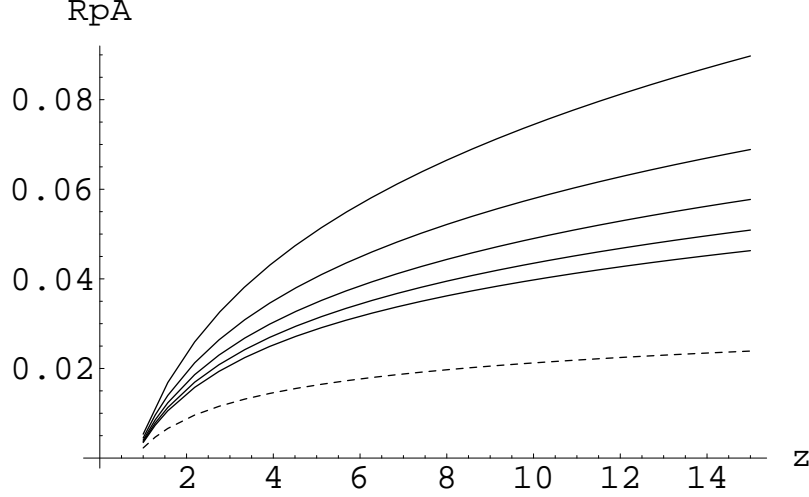


Fig. 9. The ratio $\mathcal{R}_{pA}(z, Y)$ in the double scaling window for $\rho_A = 10$ as a function of z at different $Y \gtrsim Y_c \approx 1.2$. Each solid line corresponds $Y = 1.2 + 0.3n$, with $n = 0, \dots, 4$ from top to bottom. The dashed line is the asymptotic ($Y \rightarrow \infty$) profile in Eq. (6.7). The upper limit of the double scaling window $z_{\max} = \exp\{\nu c(Y - Y_c)\}$ rapidly increases with increasing Y . For instance, $z_{\max} \approx 7.81$ for $Y = 1.5$ ($n = 1$), and $z_{\max} \approx 87.12$ for $Y = 1.8$ ($n = 2$).

6.1.3 $k_{\perp} > Q_g(A, y)$: The nuclear DLA region

This is the high momentum limit, in which both the proton and nucleus are in the DLA (or, more properly, DGLAP) regime, so the ratio can be again computed without uncertainties related to the normalization. One finds:

$$\mathcal{R}_{pA}(k_{\perp}, y) = \exp \left[\sqrt{4Y(\ln z + cY)} - \sqrt{4Y(\ln z + cY + \rho_A)} \right], \quad (6.10)$$

valid for $\ln z > \nu cY$. It is clear that the extra term ρ_A in the exponential comes from the difference between two saturation scales. It is easy to check analytically that the ratio is an increasing function of z for any Y , but a decreasing function of Y for any fixed z . In particular, at very large z such that $\ln z \gg cY + \rho_A$, one obtains

$$\mathcal{R}_{pA} \simeq e^{-\rho_A} \sqrt{Y/\ln z}. \quad (6.11)$$

Therefore, when $z \rightarrow \infty$ the ratio approaches one from below. This completes the confirmation of the general arguments in Sect. 4 for the fixed coupling case.

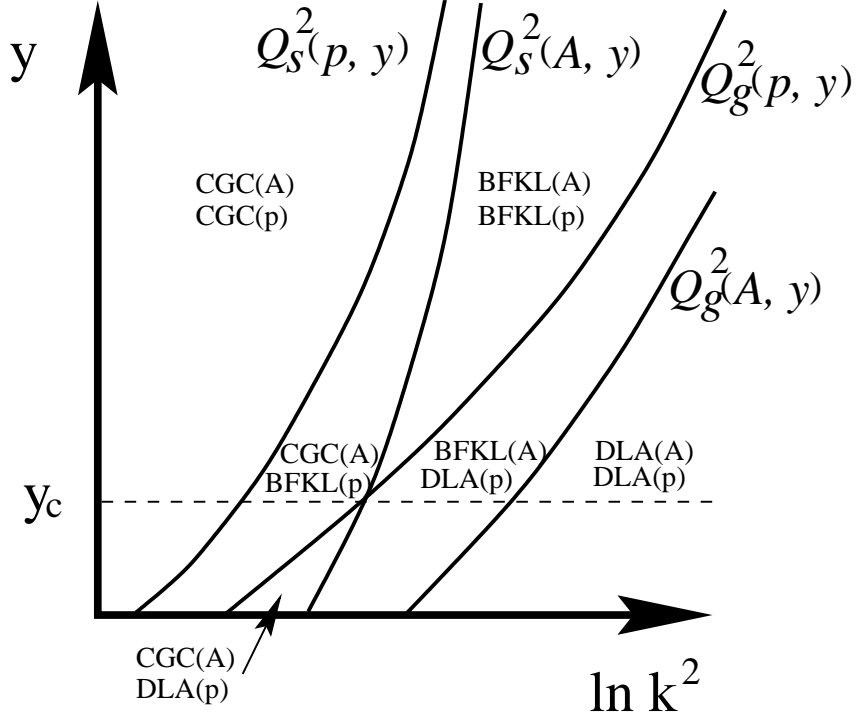


Fig. 10. Various regimes of evolution for running coupling.

6.2 Running coupling

The physical regions for evolution with running coupling are exhibited in Fig. 10. The main differences with respect to the fixed coupling case are related to the fact that the two saturation scales evolve differently with y (that for the proton growing faster) until they reach a common limit, independent of A , for very large y (cf. Eqs. (3.59)–(3.61)). As manifest on Fig. 10, this has interesting consequences: some of the physical domains get squeezed in between the proton and nucleus saturation lines (or in between the respective scales for geometric scaling) when increasing y .

Also, as already discussed in Sects. 3.3 and 5.2, the transition from the BFKL to the DLA behaviors is even less under control than it was for fixed coupling. This affects in particular the determination of the rapidity y_c beyond which the interesting double scaling regime starts to exist. As shown in Sect. 5.2, y_c is estimated as $2cb y_c \sim \rho_A^2/3$ if one uses $\nu = 1$ (see Eq. (5.12)). The factor $1/3$ changes if one takes a different value for ν , and thus is not under control.

6.2.1 $k_\perp < Q_s(A, y)$: The nuclear saturation region

(I) $k_\perp < Q_s(p, y)$: Proton at saturation

The general behavior of the ratio \mathcal{R}_{pA} with y and k_\perp is the same as in the corresponding regime at fixed coupling. In particular, along the proton saturation line $k_\perp = Q_s(p, y)$ one finds (with $\xi_A \equiv c\tau_A + \rho_A = \ln(Q_s^2(A, y)/\Lambda^2) = \sqrt{2cby + \rho_A^2}$, and similarly for the proton):

$$\mathcal{R}_{pA}(k_\perp = Q_s(p, y), y) \sim \frac{1}{A^{1/3}} \frac{(\xi_A + \xi_p)(\xi_A - \xi_p)}{2\xi_p}. \quad (6.12)$$

So long as $2cby \ll \rho_A^4$, the ratio keeps decreasing with y . For instance, within the range $\rho_A^2 \ll 2cby \ll \rho_A^4$, one finds:

$$\mathcal{R}_{pA}(k_\perp = Q_s(p, y), y) \sim \frac{1}{A^{1/3}} \frac{\rho_A^2}{2\sqrt{2cby}}. \quad (6.13)$$

But for larger y , such that $2cby \gg \rho_A^4$, the nuclear and proton saturation momenta converge to a common value, and the ratio \mathcal{R}_{pA} approaches an universal constant, as expected from the discussion in Sect. 5.2 :

$$\mathcal{R}_{pA}(k_\perp = Q_s(p, y), y) \sim \frac{1}{A^{1/3}}. \quad (6.14)$$

(II) $Q_s(p, y) < k_\perp < Q_s(A, y)$: Proton in the linear regime

The analysis is almost the same as for the evolution along the nuclear saturation line, previously discussed in Sect. 5.2.

6.2.2 $Q_s(A, y) < k_\perp < Q_g(A, y)$: The nuclear BFKL region

For $y < y_c$, the proton is in the DLA regime for any k_\perp , while for $y > y_c$, it can be either in the BFKL, or in the DLA regime, according to the value of k_\perp .

(I) $y < y_c$: Proton in the DLA regime

After straightforward manipulations, one finds:

$$\mathcal{R}_{pA}(z, y) = \kappa_0 \xi_A z^{1-\gamma} \left(\ln z + \frac{1}{\Delta} \right) \exp \left\{ c\tau_A - \sqrt{4by \ln(\ln z + \xi_A)} - \frac{\ln^2 z}{2\beta\tau_A} \right\}, \quad (6.15)$$

with the same notation as before.

Eq. (6.15) applies for k_\perp in the nuclear scaling window (3.56), that is: $0 < \ln z < \ln \left[Q_g^2(A, y)/Q_s^2(A, y) \right] = \nu c \tau_A$. It can be checked that, within this physical range, the ratio $\mathcal{R}_{pA}(z, y)$ is monotonously increasing with z , and also rapidly decreasing with y at any fixed z .

The ratio at nuclear saturation scale is given by the same function as in Eq. (5.14) (up to the overall (uncontrollable) factor). This is because the BFKL solution is just a constant at the saturation line which is the common property of the BFKL solution irrespective of the coupling being fixed or running. Therefore, the parametric dependence of the ratio upon A for $y = y_c$ is the same as before (Eq. (5.16)).

(II) $y > y_c$ & $Q_s(A, y) < k_\perp < Q_g(p, y)$: Double-scaling regime

In this regime, since the overall uncontrollable factors cancel out between the proton and the nucleus, one can predict the **amplitude** of this ratio, as well as its functional dependencies.

Using Eq. (3.63) both for the nucleus and for the proton, one finds :

$$\mathcal{R}_{pA}(k_\perp, y) \simeq \frac{1}{A^{1/3}} \left(\frac{\xi_A}{\xi_p} \right) \frac{\ln z + \frac{1}{\Delta}}{\ln z + \xi_A - \xi_p + \frac{1}{\Delta}} \exp \left[\gamma(\xi_A - \xi_p) + \frac{(\ln z + \xi_A - \xi_p)^2}{2\beta\tau_p} - \frac{(\ln z)^2}{2\beta\tau_A} \right]. \quad (6.16)$$

This expression holds within the range: $0 < \ln z < \nu c \tau_A - (\xi_A - \xi_p)$. The difference from the corresponding result in the fixed coupling case comes from the saturation scales and the overall running coupling constant $1/\alpha_s(Q_s)$ in Eq. (3.63).

It can be checked that, within the physical regime, the ratio (6.16) is an **increasing** function of z , and a **decreasing** function of Y .

When approaching the nuclear saturation line from the above (this corresponds to $z = 1$), Eq. (6.16) reduces to:

$$\mathcal{R}_{pA}(z = 1, y) \simeq \frac{1}{A^{1/3}} \frac{\xi_A}{\xi_p} \frac{\frac{1}{\Delta}}{\xi_A - \xi_p + \frac{1}{\Delta}} e^{\gamma(\xi_A - \xi_p) + \frac{(\xi_A - \xi_p)^2}{2\beta\tau_p}}. \quad (6.17)$$

For large y , such that $2cby \gg \rho_A^2$, one finds:

$$\mathcal{R}_{pA}(z = 1, y) \sim \frac{1}{A^{1/3}} \exp \left\{ \frac{\gamma}{2} \frac{\rho_A^2}{\sqrt{2cby}} \right\} \xrightarrow{y \rightarrow \infty} \frac{1}{A^{1/3}}, \quad (6.18)$$

which is again the same result as that of the Cronin peak (see Eqs. (5.18) and (5.19)).

(III) $y > y_c$ & $Q_g(p, y) < k_\perp < Q_g(A, y)$: Proton in the DLA regime

In this regime, the ratio $\mathcal{R}_{pA}(z, y)$ is given again by Eq. (6.15), but which now applies to a different kinematical range : $\nu c\tau_A - (\xi_A - \xi_p) < \ln z < \nu c\tau_A$.

6.2.3 $k_\perp > Q_g(A, y)$: The nuclear DLA region

Since both the proton and the nucleus are in the same DLA regime, one can compute the ratio without uncertainties. One obtains:

$$\mathcal{R}_{pA}(z, y) = \exp \left[\sqrt{4by \{ \ln(\ln z + \xi_A) - \ln \rho_A \}} - \sqrt{4by \{ \ln(\ln z + \xi_A) - \ln \rho_p \}} \right], \quad (6.19)$$

which is valid for $\ln z > \nu c\tau_A$. It is easy to check analytically that the ratio is an increasing function of z for any y . Also, it can be (so far numerically) checked for $\ln z > \nu c\tau_A$ that it is an decreasing function of y .

At very large z such that $\ln z \gg \xi_A$, one obtains

$$\mathcal{R}_{pA} \simeq e^{-\ln \frac{\rho_A}{\rho_p}} \sqrt{Y/\ln \ln z}. \quad (6.20)$$

Thus, when $z \rightarrow \infty$ the ratio approaches one from below.

We have now finished the explicit calculations of the ratio $\mathcal{R}_{pA}(k_\perp, y)$ for both the fixed and running coupling in all the possible kinematical regimes, and found that when the proton and the nucleus are in the linear regime, the ratio indeed shows the behaviors which are predicted by the general arguments given in Sect. 4.

Acknowledgments

We are particularly grateful to Al Mueller for his careful and repeated reading of this manuscript, and many useful suggestions. During the elaboration of this work, we have benefited from vivid discussions, incisive questions, and insightful remarks from Jean-Paul Blaizot, François Gelis, Larry McLerran, and Stephane Munier.

A Appendix

Here we study in more detail the gluon occupation factor φ_A and the integrated gluon distribution function \mathcal{G}_A in the McLerran-Venugopalan model, both for fixed and running coupling. We first deal with the running coupling case, which turns out to be simpler, and then we continue with the fixed coupling one. At the end of the appendix we present some useful properties of the confluent hypergeometric function.

The Running Coupling Case

The twist contribution to the gluon occupation factor, as given in Eq. (2.17), and with the constant factor $1/(b_0 N_c)$ omitted since it can be restored at the end of the calculation, reads

$$\varphi_A^{\text{twist}} = \int_0^\infty dt J_0(\sqrt{4zt}) \frac{1 - e^{-t}}{t} \ln \frac{1}{t}. \quad (\text{A.1})$$

In principle, one should integrate up to $\sim t_{\text{max}} = e^{\rho_A}$, which corresponds to a dipole size $\sim r_{\text{max}} = 2/\Lambda$. However, it is harmless to extend the integration to infinity, so long as we are interested in momenta $k \gg \Lambda \Leftrightarrow z \gg e^{-\rho_A}$. We can do the above integration by replacing $\ln(1/t) \rightarrow t^{-a}$. Then we obtain an expression involving the confluent hypergeometric function ${}_1F_1(-a, 1, -z) \equiv \Phi(-a, 1, -z)$. Finally we take the derivative with respect to a at $a = 0$ to recover the quantity in Eq. (A.1), and we obtain

$$\varphi_A^{\text{twist}} = -\frac{1}{2} \ln^2 z - \gamma \ln z + \gamma \Gamma(0, z) + \frac{\pi^2}{12} - \frac{\gamma^2}{2} + \frac{1}{2} \Phi^{200}(0, 1, -z), \quad (\text{A.2})$$

where $\gamma \equiv \gamma_E = 0.577$ denotes the Euler–Mascheroni constant throughout this Appendix. In the small- z limit the hypergeometric term vanishes and one is left with

$$\varphi_A^{\text{twist}} = -\frac{1}{2} \ln^2 z - 2\gamma \ln z + \frac{\pi^2}{12} - \frac{3\gamma^2}{2} + \mathcal{O}(z). \quad (\text{A.3})$$

Notice that this is negative, but it never becomes larger in magnitude than the contribution of the saturation term $\varphi_A^{\text{sat}} = \rho_A \Gamma(0, z)$. Even at $k = \Lambda \Leftrightarrow z = e^{-\rho_A}$, one has

$$\varphi_A^{\text{twist}} \simeq -\frac{1}{2} \rho_A^2 \simeq -\frac{1}{2} \varphi_A^{\text{sat}}. \quad (\text{A.4})$$

and the gluon occupation factor is positive and well defined.

In the large- z region, we can use Eq. (A.21), given at the end of the appendix, to derive the asymptotic expansion of the index-differentiated hypergeometric function. This will

have the form given in Eq.(A.23). It is straightforward to show that

$$\Phi^{200}(0, 1, -z) = \ln^2 z + 2\gamma \ln z + \gamma^2 - \frac{\pi^2}{6} + 2 \sum_{n=1} \frac{\Gamma(n)}{n} \frac{1}{z^n} + \mathcal{O}(e^{-z}). \quad (\text{A.5})$$

Then, Eqs. (A.2) and (A.5) imply that all the logarithmically divergent and constant terms in φ_A cancel, and as expected only the inverse powers of z survive. Therefore one has

$$\varphi_A = \varphi_A^{\text{twist}} = \sum_{n=1} \frac{\Gamma(n)}{n} \frac{1}{z^n} + \mathcal{O}(e^{-z}) = \frac{Q_s^2(A)}{k^2} + \frac{1}{2} \frac{Q_s^4(A)}{k^4} + \frac{2}{3} \frac{Q_s^6(A)}{k^6} + \dots, \quad (\text{A.6})$$

which exhibits the correct bremsstrahlung spectrum, accompanied by power corrections which are all positive.

Now we turn our attention to the integrated gluon distribution function, which we conveniently normalize as

$$\mathcal{G}_A = \int \frac{d^2 k}{\pi Q_s^2(A)} \varphi_A. \quad (\text{A.7})$$

For the saturation term of the gluon occupation factor the integration is trivial, and one obtains

$$\mathcal{G}_A^{\text{sat}} = [1 - e^{-Z} + Z \Gamma(0, Z)] \rho_A. \quad (\text{A.8})$$

In the above we have defined the scaled momentum variable $Z = Q^2/Q_s^2(A)$. For the twist contribution as given in (A.1), one can perform first the integration over k , which simply replaces $J_0(\sqrt{4zt})$ by $\sqrt{Z} J_1(\sqrt{4zt})/\sqrt{t}$. Then the integration over t can be done as before and gives

$$\begin{aligned} \mathcal{G}_A^{\text{twist}} = & -\frac{1}{2} Z \ln^2 Z + (1 - \gamma) Z \ln Z + \left(\frac{\pi^2}{12} - \frac{\gamma^2}{2} + \gamma - 1 \right) Z \\ & + \gamma [1 - e^{-Z} + Z \Gamma(0, Z)] + \frac{1}{2} Z \Phi^{200}(0, 2, -Z). \end{aligned} \quad (\text{A.9})$$

When $Q^2 \gg Q_s^2(A) \Leftrightarrow Z \gg 1$, the last two equations lead to

$$\mathcal{G}_A = \rho_A + \ln Z + 2\gamma - \sum_{n=1} \frac{\Gamma(n)}{n+1} \frac{1}{Z^n} + \mathcal{O}(e^{-Z}), \quad (\text{A.10})$$

where the first term comes from $\mathcal{G}_A^{\text{sat}}$ and the remaining from $\mathcal{G}_A^{\text{twist}}$. One can rewrite the above equation, in a more illuminating way, as

$$\mathcal{G}_A = \ln \frac{Q^2}{\Lambda^2} + 2\gamma - \frac{1}{2} \frac{Q_s^2(A)}{Q^2} - \frac{1}{3} \frac{Q_s^4(A)}{Q^4} + \dots, \quad (\text{A.11})$$

which shows that the higher twist corrections give a small negative contribution (shadowing) to the integrated gluon distribution function.

The Fixed Coupling Case

The twist contribution to the gluon occupation factor as given in Eq. (2.15) and multiplied by the constant factor $\rho_A \alpha_s N_c$, reads

$$\varphi_A^{\text{twist}} = - \int_0^\infty dt J_0(\sqrt{4zt}) e^{-t} \sum_{n=1}^{n_{\text{max}}} \frac{t^{n-1} \ln^n t}{n! \rho_A^{n-1}}. \quad (\text{A.12})$$

The integration in the above equation needs to be cut at $\sim t_{\text{max}} = e^{\rho_A}$ which corresponds to a dipole size $\sim r_{\text{max}} = 2/\Lambda$. However, and in the “worst case” that z is small, each term gets its most contribution from the region $t \approx n$, with the “magnitude” of the n -th term being $\sim (\ln n/\rho_A)^n$. Therefore the integration in the terms with $n \lesssim n_{\text{max}} = e^{\rho_A}$ can be extended to infinity, while terms with $n \gtrsim n_{\text{max}}$ do not contribute, since their peak lies outside the region of integration. Thus, the cutoff in the MV model translates to a cutoff in the series in Eq. (A.12). Furthermore, this (asymptotic) series is rapidly convergent for $\rho_A \gg 1$, since $\ln n/\rho_A < 1$ for $n < e^{\rho_A}$. Thus, it is enough to keep a few terms in (A.12). They can be calculated by the same method we used in the running coupling case. The n -th term, apart from the overall suppressing factor ρ_A^{-n+1} , becomes constant when $z \ll 1$, and falls as z^{-n} (plus all possible higher inverse powers) for $z \gg 1$. The expressions become more and more complicated as n increases, and therefore we shall present only the first two terms. We have

$$\varphi_A^{n=1} = \gamma e^{-z} - \Phi^{100}(1, 1, -z), \quad (\text{A.13})$$

$$\begin{aligned} \varphi_A^{n=2} = & - \frac{1}{\rho_A} \left[\left(\frac{\pi^2}{12} + \frac{\gamma^2}{2} - \gamma \right) (1-z) e^{-z} \right. \\ & \left. + (1-\gamma) \Phi^{100}(2, 1, -z) + \frac{1}{2} \Phi^{200}(2, 1, -z) \right]. \end{aligned} \quad (\text{A.14})$$

Since $\Phi^{n00}(a, 1, -z)$ vanishes at small- z , the limiting value of φ_A^{twist} is finite. One easily finds that

$$\varphi_A^{\text{twist}} = \gamma - \frac{1}{\rho_A} \left(\frac{\pi^2}{12} + \frac{\gamma^2}{2} - \gamma \right) + \mathcal{O}(z). \quad (\text{A.15})$$

In the large- z limit, we need to expand the hypergeometric functions and we obtain

$$\varphi_A = \varphi_A^{\text{twist}} = \frac{Q_s^2(A)}{Q^2} + \frac{Q_s^4(A)}{Q^4} \left[1 + \frac{1}{\rho_A} \left(\ln \frac{Q^2}{Q_s^2(A)} + 2\gamma - 2 \right) \right] + \dots, \quad (\text{A.16})$$

where both the $n = 1$ and $n = 2$ terms contribute to the $1/z^2 = Q_s^4(A)/Q^4$ term. This correction is positive and the same will be true for all the $1/z^n$ ones.

Now let us calculate the integrated gluon distribution function. The saturation contribution is the same as the one we found in the running coupling case and is given in Eq. (A.8). For the twist contributions we shall again present only the first two terms, which are

$$\mathcal{G}_A^{n=1} = \gamma - \gamma e^{-Z} - Z \Phi^{100}(1, 2, -Z) \quad (\text{A.17})$$

$$\begin{aligned} \mathcal{G}_A^{n=2} = & -\frac{1}{\rho_A} Z \left[\left(\frac{\pi^2}{12} + \frac{\gamma^2}{2} - \gamma \right) e^{-Z} \right. \\ & \left. + (1 - \gamma) \Phi^{100}(2, 2, -Z) + \frac{1}{2} \Phi^{200}(2, 2, -Z) \right], \end{aligned} \quad (\text{A.18})$$

and similar, but more complicated expressions can also be obtained for $n \geq 3$. Each term vanishes as Z becomes small, and all terms with $n \geq 2$ approach 0 as Z becomes large. Keeping the $n = 1, 2$ terms, we can obtain the first power law corrections in \mathcal{G}_A in the high momentum limit $Q_s^2(A) \gg Q^2$. We obtain

$$\mathcal{G}_A = \ln \frac{Q^2}{\Lambda^2} + 2\gamma - \frac{Q_s^2(A)}{Q^2} \left[1 + \frac{1}{\rho_A} \left(\ln \frac{Q^2}{Q_s^2(A)} + 2\gamma - 1 \right) \right]. \quad (\text{A.19})$$

As in the running coupling case the higher twist terms give a small negative contribution to the integrated gluon distribution function.

The Confluent Hypergeometric Function $\Phi(a, b, -z)$

Here we give some useful properties of the confluent hypergeometric function ${}_1F_1(a, b, -z) \equiv \Phi(a, b, -z)$. More precisely we examine its n -th derivative with respect to the first argument, that is $\Phi^{n00}(a, b, -z)$. The range of parameters that we are interested in is $a \geq 0$, $b \geq 1$ and $z \geq 0$.

The confluent hypergeometric function is defined as

$$\Phi(a, b, -z) = 1 - \frac{a}{b} z + \frac{1}{2!} \frac{a(a+1)}{b(b+1)} z^2 - \dots, \quad (\text{A.20})$$

and its large- z asymptotic expansion reads

$$\begin{aligned} \Phi(a, b, -z) &= \frac{\Gamma(b)}{\Gamma(b-a)} z^{-a} \\ &\times \left[1 + \frac{a(a-b+1)}{z} + \frac{1}{2!} \frac{a(a+1)(a-b+1)(a-b+2)}{z^2} + \dots \right], \end{aligned} \quad (\text{A.21})$$

where terms that fall as e^{-z} have been neglected.

We can find the behavior of $\Phi^{n00}(a, b, -z)$ in the small- z region from Eq. (A.20) and in the large- z region from Eq. (A.21). We obtain

$$\Phi^{n00}(a, b, -z) = \frac{\Gamma(b)}{\Gamma(b+n)} z^n + \mathcal{O}(z^{n+1}) \quad \text{for } z \ll 1, \quad (\text{A.22})$$

which vanishes when $n \geq 1$, and

$$\Phi^{n00}(a, b, -z) = z^{-a} \left[\sum_{k \geq 0} \frac{c_k}{z^k} \right] \left[\sum_{k=0}^n d_k \ln^k z \right] \quad \text{for } z \gg 1, \quad (\text{A.23})$$

where the coefficients c_k and d_k depend on the set of parameters (n, a, b) and can be determined from Eq. (A.21). The function $\Phi^{n00}(a, b, -z)$ diverges for large- z as a power of $\ln z$ when $a = 0$, while it approaches zero when $a > 0$.

References

- [1] “Quark Matter 2002”, Proceedings of the 16th International Conference on Ultra-Relativistic Nucleus-Nucleus Collisions, (Nantes, France 18-24 July, 2002), Nucl. Phys. A 715 (2003).
- [2] See for example, D. d’Enterria, “*Hard scattering at RHIC: Experimental review,*” arXiv:nucl-ex/0309015 and references therein.
- [3] B. B. Back *et al.* [PHOBOS Collaboration], *Phys. Rev. Lett.* **91** (2003) 072302 [arXiv:nucl-ex/0306025]; S. S. Adler *et al.* [PHENIX Collaboration], *Phys. Rev. Lett.* **91** (2003) 072303 [arXiv:nucl-ex/0306021]; J. Adams *et al.* [STAR Collaboration], *Phys. Rev. Lett.* **91** (2003) 072304 [arXiv:nucl-ex/0306024]; I. Arsene *et al.* [BRAHMS Collaboration], *Phys. Rev. Lett.* **91** (2003) 072305 [arXiv:nucl-ex/0307003].
- [4] I. Arsene [BRAHMS Collaboration], “*On the evolution of the nuclear modification factors with rapidity and centrality in d+Au collisions at $\sqrt{s_{NN}} = 200$ GeV,*” arXiv:nucl-ex/0403005.
- [5] R. Debbe and M. Murray, for the BRAHMS Collaboration, talks given at QM2004, Oakland, USA, January 2004.
- [6] T. Frawley and M. X. Liu, [PHENIX Collaboration], P. Steinberg and R. Nouicer, [PHOBOS Collaboration], and L. Barnby [STAR Collaboration], talks given at QM2004, Oakland, USA, January 2004.
- [7] L.V. Gribov, E.M. Levin, and M.G. Ryskin, *Phys. Rept.* **100** (1983) 1.
- [8] A.H. Mueller and J. Qiu, *Nucl. Phys.* **B268** (1986) 427.
- [9] J.-P. Blaizot and A. H. Mueller, *Nucl. Phys.* **B289** (1987) 847.
- [10] L. McLerran and R. Venugopalan, *Phys. Rev.* **D49** (1994) 2233; *ibid.* **49** (1994) 3352; *ibid.* **50** (1994) 2225.
- [11] A. H. Mueller, *Parton Saturation—An Overview*, hep-ph/0111244. Published in *QCD Perspectives on Hot and Dense Matter*, Eds. J.-P. Blaizot and E. Iancu, NATO Science Series, Kluwer, 2002.
- [12] E. Iancu, A. Leonidov and L. McLerran, *The Colour Glass Condensate: An Introduction*, hep-ph/0202270. Published in *QCD Perspectives on Hot and Dense Matter*, Eds. J.-P. Blaizot and E. Iancu, NATO Science Series, Kluwer, 2002;
E. Iancu and R. Venugopalan, *The Color Glass Condensate and High Energy Scattering in QCD*, hep-ph/0303204. Published in *Quark-Gluon Plasma 3*, Eds. R. C. Hwa and X.-N. Wang, World Scientific, 2003.
- [13] J. W. Cronin, et al. *Phys. Rev.* **D11** (1975) 3105; D. Antreasyan, et al. *Phys. Rev. Lett.* **38** (1977) 112; D. Antreasyan, et al. *Phys. Rev.* **D19** (1979) 764.
- [14] Yu.V. Kovchegov and A.H. Mueller, *Nucl. Phys.* **B529** (1998), 451.

- [15] A. Accardi and M. Gyulassy, “*Cronin effect vs. geometrical shadowing in $d + Au$ collisions at RHIC,*” arXiv:nucl-th/0308029.
- [16] D. E. Kharzeev, E. Levin, and L. McLerran, *Phys. Lett.* **B561** (2003) 93.
- [17] B.Z. Kopeliovich, J. Nemchik, A. Schafer, and A.V. Tarasov, *Phys. Rev. Lett.* **88** (2002) 232303. A. Accardi, arXiv:hep-ph/0212148; I. Vitev, *Phys. Lett.* **B562** (2003) 36 [arXiv:nucl-th/0302002].
- [18] For a review, see M. Gyulassy, I. Vitev, X. N. Wang and B. W. Zhang, “*Jet quenching and radiative energy loss in dense nuclear matter,*” arXiv:nucl-th/0302077. Published in *Quark Gluon Plasma 3*, editors: R.C. Hwa and X.N. Wang, World Scientific, Singapore.
- [19] M. Braun, *Eur. Phys. J.* **C16** (2000) 337; *Phys. Lett.* **B483** (2000) 105.
- [20] Yu. V. Kovchegov and K. Tuchin, *Phys. Rev.* **D65** (2002) 074026.
- [21] J.P. Blaizot, F. Gelis, R. Venugopalan, hep-ph/0402256; hep-ph/0402257.
- [22] D. Kharzeev, Yu. V. Kovchegov, and K. Tuchin, *Phys. Rev.* **D66** (2003) 094013.
- [23] J. L. Albacete, et al. *Phys. Rev. Lett.* **92** (2004) 082001 [arXiv:hep-ph/0307179].
- [24] E. Iancu, A. Leonidov and L. McLerran, *Nucl. Phys.* **A692** (2001), 583; *Phys. Lett.* **B510** (2001) 133; E. Ferreiro, E. Iancu, A. Leonidov and L. McLerran, *Nucl. Phys.* **A703** (2002) 489.
- [25] D. Kharzeev, E. Levin and M. Nardi, *Nucl. Phys. A* **730** (2004) 448, erratum in arXiv:hep-ph/0212316.
- [26] J. Jalilian-Marian, “*Forward Rapidity Hadron Production in Deuteron Gold Collisions from Valence Quarks,*” arXiv:nucl-th/0402080.
- [27] Yu.V. Kovchegov, *Phys. Rev.* **D54** (1996), 5463; *Phys. Rev.* **D55** (1997), 5445.
- [28] J. Jalilian-Marian, A. Kovner, L. McLerran, H. Weigert, *Phys. Rev.* **D55** (1997) 5414.
- [29] J. Jalilian-Marian, A. Kovner, A. Leonidov and H. Weigert, *Nucl. Phys.* **B504** (1997) 415; *Phys. Rev.* **D59** (1999) 014014.
- [30] I. Balitsky, *Nucl. Phys.* **B463** (1996) 99; *Phys. Rev. Lett.* **81** (1998) 2024; *Phys. Lett.* **B518** (2001) 235; *High-energy QCD and Wilson lines*, hep-ph/0101042.
- [31] Yu. V. Kovchegov, *Phys. Rev.* **D60** (1999), 034008; *ibid.* **D61** (2000) 074018.
- [32] H. Weigert, *Nucl. Phys.* **A703** (2002) 823.
- [33] E. Iancu and L. McLerran, *Phys. Lett.* **B510** (2001) 145.
- [34] E. Iancu, K. Itakura and L. McLerran, *Nucl. Phys.* **A724** (2003) 181.
- [35] A. H. Mueller, *Nucl. Phys.* **B558** (1999) 285.

- [36] E. Iancu, K. Itakura, and L. McLerran, *Nucl. Phys.* **A708** (2002) 327.
- [37] A. H. Mueller and D.N. Triantafyllopoulos, *Nucl. Phys.* **B640** (2002) 331.
- [38] D.N. Triantafyllopoulos, *Nucl. Phys.* **B648** (2003) 293.
- [39] S. Munier and R. Peschanski, *Phys. Rev. Lett.* **91** (2003) 232001; hep-ph/0310357; hep-ph/0401215.
- [40] A. H. Mueller, *Nucl. Phys.* **A724** (2003) 223.
- [41] L.N. Lipatov, *Sov. J. Nucl. Phys.* **23** (1976) 338; E.A. Kuraev, L.N. Lipatov and V.S. Fadin, *Zh. Eksp. Teor. Fiz* **72**, 3 (1977) (*Sov. Phys. JETP* **45** (1977) 199); Ya.Ya. Balitsky and L.N. Lipatov, *Sov. J. Nucl. Phys.* **28** (1978) 822.
- [42] V.S. Fadin and L.N. Lipatov, *Phys. Lett.* **B429** (1998) 127; G. Camici and M. Ciafaloni, *Phys. Lett.* **B430** (1998) 349.
- [43] G.P. Salam, *JHEP* **9807** (1998) 19; M. Ciafaloni, D. Colferai, *Phys. Lett.* **B452** (1999) 372; M. Ciafaloni, D. Colferai, and G.P. Salam, *Phys. Rev.* **D60** (1999) 114036.
- [44] K. Rummukainen and H. Weigert, hep-ph/0309306.
- [45] E. Iancu and A.H. Mueller, *Nucl. Phys.* **A730** (2004) 494.
- [46] A.H. Mueller and A.I. Shoshi, hep-ph/0402193.
- [47] F. Gelis and J. Jalilian-Marian, *Phys. Rev.* **D67** (2003) 074019 [arXiv:hep-ph/0211363].
- [48] J. Jalilian-Marian, Y. Nara and R. Venugopalan, *Phys. Lett.* **B577** (2003) 54 [arXiv:nucl-th/0307022].
- [49] A.M. Staśto, K. Golec-Biernat, and J. Kwieciński, *Phys. Rev. Lett.* **86** (2001) 596.
- [50] N. Armesto and M. Braun, *Eur. Phys. J.* **C20** (2001) 517; *ibid.* **C22** (2001) 351.
- [51] K. Golec-Biernat, L. Motyka, and A.M. Staśto, *Phys. Rev.* **D65** (2002) 074037.
- [52] E. Levin and M. Lublinsky, *Phys. Lett.* **B521** (2001) 233; *Eur. Phys. J.* **C22** (2002) 647; M. Lublinsky, *Eur. Phys. J.* **C21** (2001) 513.
- [53] A. Dumitru and L. McLerran, *Nucl. Phys.* **A700** (2002) 492.
- [54] F. Gelis and J. Jalilian-Marian, *Phys. Rev.* **D66** (2002) 014021; *ibid.* 094014.
- [55] D. Kharzeev and M. Nardi, *Phys. Lett.* **B507** (2001) 121; D. E. Kharzeev and E. Levin, *Phys. Lett.* **B523** (2001) 79.
- [56] A. H. Mueller, *Nucl. Phys.* **B643** (2002) 501.
- [57] V.N. Gribov and L.N. Lipatov, *Sov. Journ. Nucl. Phys.* **15** (1972) 438; G. Altarelli and G. Parisi, *Nucl. Phys.* **B126** (1977) 298; Yu. L. Dokshitzer, *Sov. Phys. JETP* **46** (1977) 641.

- [58] K. Golec-Biernat and M. Wüsthoff, *Phys. Rev.* **D59** (1999) 014017; *ibid.* **D60** (1999) 114023.
- [59] E. Iancu, K. Itakura and S. Munier, arXiv:hep-ph/0310338, to appear in *Phys. Lett. B*.
- [60] K. Golec-Biernat and A.M. Stasto, *Nucl. Phys.* **B668** (2003) 345.